1   **Convergence of multiple RNA-silencing pathways on GW182/TNRC6**

2   Thomas Welte[1,2,#], Alison Goulois[1], Michael B. Stadler[1,3,4], Daniel Hess[1], Charlotte

3   Soneson[1,3], Anca Neagu[1], Chiara Azzi[1], Marlena J. Lübke[1,4], Jan Seebacher[1], Isabel

4   Schmidt[5], David Estoppey[5], Florian Nigsch[5], John Reece-Hoyes[6], Dominic Hoepfner[5],

5   Helge Großhans[1,4,#]

6

7   [1] Friedrich Miescher Institute for Biomedical Research, Basel, Switzerland.

8   [2] Department of Medicine IV, Medical Center, Faculty of Medicine, University of

9   Freiburg, Freiburg, Germany.

10   [3] SIB Swiss Institute of Bioinformatics, Basel, Switzerland.

11   [4] Faculty of Natural Sciences, University of Basel, Basel, Switzerland.

12   [5] Novartis Institutes for BioMedical Research, Novartis Pharma AG, CH-4002 Basel.

13   [6] Department of Chemical Biology and Therapeutics, Novartis Institutes for BioMedical

14   Research, Cambridge, MA, USA.

15

16   [#] Correspondence to:

17   Thomas Welte: thomas.welte@fmi.ch

18   Helge Großhans: helge.grosshans@fmi.ch

19

20

21   **Keywords**

22   TRIM71; LIN-41; RNA-binding protein; stem cell; miRNA; AGO2; UPF1; GW182; miRISC;

23   TNRC6; post-transcriptional gene regulation; congenital hydrocephalus

Highlights

- A genome-wide CRISPR-screen reveals enhanced TRIM71-mediated RNA silencing activity upon miRNA pathway disruption
- The miRISC core component GW182/TNRC6 functions in AGO2-, TRIM71- and UPF1-mediated RNA silencing
- AGO2, TRIM71 and UPF1 recruit TNRC6A to specific sets of target transcripts
- AGO2 antagonizes TRIM71 and UPF1 activity by sequestering GW182/TNRC6

Abstract

The RNA-binding protein TRIM71/LIN-41 is a phylogenetically conserved developmental regulator that functions in mammalian stem cell reprogramming, brain development and cancer. TRIM71 recognizes target mRNAs through hairpin motifs and silences them through molecular mechanisms that await identification. Here, we uncover that TRIM71 silences its targets by recruiting TNRC6/GW182, a core component of the miRNA-induced silencing complex (miRISC). Co-immunoprecipitation reveals interaction of TNRC6A with additional RNA-binding proteins and we demonstrate that AGO2, TRIM71, and UPF1 each recruit TNRC6 to specific, largely distinct sets of transcripts to silence them. As cellular TNRC6 levels are limiting, competition occurs among the silencing pathways, such that loss of AGO2 protein, or of AGO2 binding to TNRC6, enhances the activities of the other pathways. We conclude that a miRNA-like silencing activity is shared among different mRNA silencing pathways and that use of TNRC6 as a central hub provides a means to integrate their activities.

1 Introduction

2 TRIM71/LIN-41 is a phylogenetically conserved RNA-binding protein (RBP) and E3

3 ubiquitin ligase that regulates stem and progenitor cell fates in diverse cell types and

4 organisms (Chen et al., 2012; Ecsedi and Grosshans, 2013; Wang et al., 2019; Worringer

5 et al., 2014). In mice, *Trim71* knock-out causes defects in mouse brain development, an

6 exencephalus phenotype, defects in neural tube formation (Chen et al., 2012; Maller

7 Schulman et al., 2008; Mitschka et al., 2015), germ cell loss (Torres-Fernández et al.,

8 2021a), and death during mid-embryogenesis.

9   In humans, different heterozygous missense mutations in *TRIM71* have been

10 linked to the etiology of congenital hydrocephalus (CH) due to premature differentiation

11 of neuroprogenitor cells (Duy et al., 2022; Furey et al., 2018; Jin et al., 2020; Welte et al.,

12 2019). All these mutations map to the NHL repeat domain through which TRIM71

13 recognizes trinucleotide-loop hairpins with specific sequence features (Kumari et al.,

14 2018; Welte et al., 2019). When binding to mRNAs containing such hairpins in their 3'

15 untranslated regions (UTRs), TRIM71 induces transcript degradation, possibly

16 accompanied by some level of translational repression (Chang et al., 2012; Loedige et

17 al., 2013; Mitschka et al., 2015; Welte et al., 2019).

18   The molecular machinery that mediates TRIM71 silencing is largely unknown. In

19 mouse embryonic stem cells (mESCs), TRIM71 was shown to cooperate with miRNAs to

20 achieve repression of the *Cdkn1a* mRNA (Chang et al., 2012). However, miRNAs do not

21 appear to be generally required for TRIM71 activity (Mitschka et al., 2015; Torres-

22 Fernández et al., 2019; Welte et al., 2019). Indeed, silencing of *CDKN1A* mRNA by

23 TRIM71 is conserved in human HEK293T and HepG2 cells, but does not rely on an intact

3

1   miRNA pathway (Torres-Fernández et al., 2019). Instead, the RNA binding proteins UPF1

2   and SMG1 were reported to promote silencing of *CDKN1A* and possibly other TRIM71

3   targets in these cells (Torres-Fernández et al., 2019). The molecular basis of this

4   apparent cooperation, and the extent to which it is required for TRIM71 activity, have

5   remained unknown.

6   Using a CRISPR-based screen to uncover the molecular mode of action of

7   TRIM71, we find that TNRC6/GW182 is a key mediator of its activity. In mice and humans,

8   TNRC6 comprises a set of three paralogous proteins that function redundantly in the

9   miRNA pathway as a core component of the miRNA silencing complex (miRISC) (Ding

10   and Han, 2007; Eulalio et al., 2008; Jakymiw et al., 2005; Liu et al., 2005). (Throughout

11   this paper, we will generically refer to TNRC6 unless we manipulate experimentally a

12   specific isoform.) Binding to an Argonaute protein (AGO1~4) associated with a miRNA

13   facilitates recruitment of TNRC6 to target transcripts in a sequence-specific manner.

14   Through its interactions with a diversity of general RNA decay and silencing effector

15   proteins, including the CCR4/NOT deadenylase complex, the PAN2/PAN3 deadenylase

16   complex, cytoplasmic poly(A)-binding protein (PABPC) and the RNA helicase DDX6,

17   TNRC6-binding then induces target transcript silencing through degradation or

18   translational repression (Braun et al., 2011; Braun et al., 2013; Chekulaeva et al., 2011;

19   Mathys et al., 2014).

20   We find that TRIM71 recruits TNRC6 to a largely distinct set of transcripts, not

21   targeted by miRISC, to induce their silencing. We observe that TNRC6 levels are limiting

22   for TRIM71 activity. Accordingly, uncoupling TNRC6 from AGO enhances TRIM71

23   activity. This miRISC-independent activity of TNRC6 extends to at least one other RBP,

1 UPF1, identifying TNRC6 as a central hub of post-transcriptional gene regulation. Thus,

2 it can integrate the activities of multiple silencing pathways, exemplified by miRISC's

3 ability to attenuate other RNA silencing pathways through sequestration of TNRC6.

4

5 **Results**

6 **A genome-wide CRISPR/Cas9 sgRNA screen identifies potential co-factors and**

7 **modulators of TRIM71 activity**

8 To identify genes relevant for TRIM71-mediated gene regulation, we performed a

9 genome-wide CRISPR/Cas9 sgRNA screen. Based on our previous studies on TRIM71

10 RNA target recognition (Welte et al., 2019), we constructed a minimal GFP reporter

11 system in mESCs that recapitulates TRIM71-dependent gene regulation. To reduce the

12 likelihood of our reporter being targeted by other endogenous regulatory circuits, we

13 chose to construct a heterologous system based on *C. elegans* 3'UTRs. Using Cas9-

14 expressing mESCs (**Supplemental Figure S1A-C**), we generated the following cell lines:

15   *GFP_Ctrl* cells (negative control): The *C. elegans unc-54* 3' UTR was fused to an

16 *EGFP*-coding sequence. This UTR has no TRIM71-binding motifs and is thus not

17 repressed by TRIM71, resulting in high GFP levels (**Figure 1A**).

18   *GFP_5xT71BS* cells (positive control): A fragment of the *C. elegans mab-10* 3'UTR

19 containing five hairpin motifs recognized by TRIM71(Kumari et al., 2018; Welte et al.,

20 2019) was cloned into the *GFP::unc-54* 3' UTR construct, leading to a marked reduction

21 in GFP levels relative to *GFP_Ctrl* cells (**Figure 1A**). This repression depended on

22 TRIM71, as disruption of *Trim71* in *GFP_5xT71BS* cells caused a shift to high GFP levels,

1   equal to those observed in *GFP_Ctrl* cells. By contrast, *Trim71* disruption in *GFP_Ctrl*

2   cells did not affect the signal (**Figure 1A, Supplemental Figure S1D).**

3   We used the *GFP_5xT71BS* cell line to perform a CRISPR/sgRNA

4   screen(Hoepfner et al., 2019), seeking to identify conditions that would either impair

5   TRIM71 activity, and thus increase GFP signal; or enhance TRIM71 activity, and thus

6   decrease GFP signal. The *GFP_Ctrl* cell line allowed us to control for non-specific effects,

7   not related to modulating TRIM71 activity.

8   Each cell line was separately transduced with two lentiviral libraries comprising in

9   total 91,000 sgRNAs (~5 sgRNAs/gene) at a multiplicity of infection (MOI) of 0.31 and

10   ~700-fold coverage per sgRNA. At day 8, cells were harvested and sorted by

11   fluorescence-activated cell sorting (FACS) to fractions with low and high GFP levels,

12   respectively ('25% low' and '25% high'; **Figure 1B**): DNA from each fraction, as well as

13   an unsorted baseline control was extracted, followed by sequencing of sgRNAs. We

14   aggregated sgRNAs by gene and quantified enrichment in the '25% high' or '25% low'

15   fractions, respectively. We corrected for non-specific effects on gene expression

16   subtracting enrichment values obtained for *GFP_Ctrl* cells from those obtained for

17   *GFP_5xT71BS* cells (see **STAR Methods** for details).

18   Using the top and bottom 985 ranking genes, and 400 unchanged control genes,

19   we performed a validation screen using a lentiviral library with 12,000 new sgRNAs (from

20   (Michlits et al., 2020); **Supplemental Table S1**), transfected at an MOI of 0.1 and ~500-

21   fold coverage. Effects from both screens correlated well (R = 0.481). TRIM71 ranked

22   second and first, respectively, among the '25% high' genes in the two screens, validating

23   the approach (**Figure 1C, D**).

1   Additional genes were reproducibly enriched in the '25% high' and '25% low' set.

2   Strikingly, for the '25% low' set, the top 5 genes were components of the miRNA

3   pathway(Lin and Gregory, 2015), namely *Drosha* and *Dgcr8*, which together form the

4   microprocessor complex that processes pri-miRNAs to pre-miRNAs; *Xpo5*, which

5   mediates export of pre-miRNAs from the nucleus to the cytoplasm; *Dicer1*, which

6   processes pre-miRNAs to generate miRNA duplexes; and *Ago2*, the core miRISC

7   component that binds mature miRNAs (**Figure 1E, F**). This evident pathway enrichment

8   suggested that our screen was close to saturation. It also pointed to a specific connection

9   between the miRNA pathway and TRIM71, which we sought to explore further.

10

11   **The miRNA pathway attenuates TRIM71-dependent gene silencing independent of**

12   **TRIM71 levels.**

13   We validated the effects seen in the screen through sgRNA enrichment by direct

14   assessment of TRIM71 activity, using both the *GFP_5xT71BS* reporter and luciferase-

15   based reporters containing either the *same* 5xT71BS 3'UTR or the 3'UTR of *Plxnb2*, a

16   previously identified TRIM71 target (Mitschka et al., 2015; Welte et al., 2019). Knock-out

17   of *Dicer1*, *Xpo5* or *Ago2* enhanced repression of each of the TRIM71 target reporters

18   without altering expression of control reporters that were not regulated by TRIM71

19   (**Figure 2A-C, Supplemental Figure S2A**). Conversely, transfection of exogenous *Ago2*

20   reverted *GFP_5xT71BS* reporter repression to the wild-type situation (**Figure 2D,**

21   **Supplemental Figure S2B**). The effects were specific to the TRIM71 pathway, as

22   changes in reporter repression only occurred in the presence of *Trim71*. We conclude

1   that attenuation of TRIM71 activity through the miRNA pathway is reproducible and

2   specific, and not limited to the heterologous reporter or GFP signal as a read-out.

3   LIN-41/TRIM71 has been shown to be repressed during development of *C.*

4   *elegans* and mouse by the *let-7* family of miRNAs (Aeschimann et al., 2019; Ecsedi et al.,

5   2015; Rybak et al., 2008; Slack et al., 2000). Although this repression normally occurs in

6   differentiating cells, we wondered if the observed change of TRIM71 silencing activity

7   simply reflected its release from miRNA-mediated repression. This was not the case: RNA

8   sequencing revealed that *Trim71* mRNA levels did not increase in *Ago2*$^{-/-}$ relative to wild-

9   type mESCs (**Figure 2E**), and we failed to observe an increase in TRIM71 protein levels

10   upon knock-out of *Ago2*, *Dicer1*, and *Xpo5* when tested in two independent experiments

11   (**Figure 2F, Supplemental Figure S2A**). By contrast, and as reported previously

12   (Martinez and Gregory, 2013; Wang et al., 2020), Ago2-levels were reduced in *Dicer1*,

13   and *Xpo5* knock-out cells (**Figure 2F, Supplemental Figure S2A**), consistent with the

14   notion that Ago2 requires miRNA binding for stabilization (Smibert et al., 2013). Finally,

15   overexpression of *Homo sapiens TRIM71* (**Supplemental Figure S2A**) complemented

16   *Trim71* knock-out cells to restore silencing of the *GFP_5xT71BS* reporter (**Figure 2A**, row

17   3 vs. row 6), but did not further increase silencing of the reporter in *Trim71* wild-type cells

18   (**Figure 2A**, row 2 vs. row 5).

19   We conclude that TRIM71 is not detectably repressed by miRNAs in mESCs, and

20   that its levels are not limiting for its target silencing activity. Put differently, the modulation

21   of TRIM71 activity through miRNA pathway disruption appears to occur downstream of

22   TRIM71 protein accumulation.

23

1 **TNRC6 contributes to TRIM71-dependent gene silencing.**

2 Our sgRNA screens had identified the major components of miRNA biogenesis and

3 AGO2, a core miRISC component (**Figure 1F**) and the most prominently expressed

4 paralog of the four mammalian *Ago* genes(Boroviak et al., 2018; Lykke-Andersen et al.,

5 2008). However, the second miRISC core component, TNRC6, was not identified in our

6 sgRNA screens.

7 We suspected that TNRC6 was not identified because cells contain three TNRC6

8 isoforms, TNRC6A~C, that are thought to function redundantly (Baillat and Shiekhattar,

9 2009; Johnson et al., 2021; Liu et al., 2019; Meister et al., 2005). Hence, we sought to

10 directly test a possible function of TNRC6 in TRIM71-mediated RNA silencing. Despite

11 extensive attempts, we failed to obtain *Tnrc6* triple-knockout cells, and no such cell line

12 has been described in the literature, suggesting that TNRC6 is essential for mESC

13 survival. By contrast, the miRNA pathway is dispensable for mESC survival (see results

14 above), which implies that TNRC6 may have additional functions beyond their established

15 role in the miRNA pathway.

16 To assess the consequences of TNRC6 deregulation for the TRIM71 pathway, we

17 overexpressed *HsTNRC6A*, *B*, and *C* in the GFP reporter cell lines. This decreased GFP

18 levels in *GFP_5xT71BS* cells (**Figure 3A**, row 5 vs rows 7-9). The effect was TRIM71-

19 dependent, as no silencing was observed in *Trim71$^{-/-}$* cells overexpressing *TNRC6*

20 paralogs (**Figure 3A**). No changes in TRIM71 or AGO2 levels were observed upon

21 *TNRC6* overexpression (**Figure 3B**). Thus, *TNRC6* overexpression is sufficient to

22 recapitulate *Ago2* knock-out phenotypes and enhance TRIM71 activity.

1   We emphasize that the role of TNRC6 is opposite to that of AGO2 and the other

2   miRNA pathway components in these assays, in that increased, rather than decreased

3   TNRC6 levels enhance TRIM71 activity. Combined with our inability to observe protein

4   level regulation of TRIM71 by the miRNA pathway, and the inability of *Trim71*

5   overexpression to enhance TRIM71 activity, these data support a model where TNRC6

6   functions directly in TRIM71-mediated transcript repression. As loss of miRNAs both

7   destabilizes AGO and reduces its affinity to TNRC6n (ref. (Elkayam et al., 2017)), a direct

8   function of TNRC6 in the TRIM71 pathway could also explain why inactivation of miRNA

9   biogenesis enhances TRIM71 activity.

10

11   **TNRC6 proteins coimmunoprecipitate with both AGO2 and TRIM71.**

12   We wondered whether the functional connection between TRIM71 and TNRC6 proteins

13   reflected physical interactions. To test this possibility, we immunoprecipitated

14   endogenously FLAG-AVI-tagged TRIM71 (ref. (Welte et al., 2019)) or endogenously

15   FLAG-tagged AGO2 (ref. (Li et al., 2020)) mESCs. For both proteins, we consistently

16   observed co-precipitation of TNRC6A and TNRC6B. Conversely, when we

17   immunoprecipitated HA-AVI-tagged endogenous TNRC6A, we observed co-precipitation

18   of both AGO2 and TRIM71 (**Figure 4A-C**). Hence, TRIM71 and AGO2 both interact

19   biochemically with TNRC6A/B.

20   We observed reciprocal immunoprecipitation of TRIM71 and AGO2, and both co-

21   immunoprecipitated additional miRNA pathway factors such as DDX6 (**Figure 4A-C**).

22   Moreover, most TRIM71 interactions, including those with AGO2 and TNRC6, were

23   sensitive to treatment with RNase A (**Supplemental Figure S3A, B**). Thus, it seemed

10

1   possible that physical interactions between TNRC6 and TRIM71 could be mediated by

2   shared targets of miRISC and TRIM71. However, *Ago2* knock-out did not compromise

3   co-immunoprecipitation of TNRC6, or of any other protein interactor with TRIM71

4   (**Supplemental Figure S3C-E**). Similarly, interaction of TRIM71 with known target RNAs

5   quantified by RNA immunoprecipitation was not altered in *Ago2* knock-out cells

6   (**Supplemental Figure S3F, G**). In conclusion, although TRIM71 – TNRC6 interactions

7   require RNA for stabilization to be captured by immunoprecipitation, they do not rely on

8   mediation by AGO2.

9

10   **Blocking the interaction of AGO2 and TNRC6 by peptide-based inhibition results in**

11   **improved silencing by TRIM71.**

12   Given the biochemical and functional interactions between TRIM71 and TNRC6,

13   competition of AGO2 and TRIM71 for TNRC6 appeared to provide a possible explanation

14   for why disruption of miRNA biogenesis enhanced TRIM71 activity (**Figure 4D**). Specific

15   disruption of the TNRC6-AGO2 complex without depletion of either component would

16   provide a stringent test of this model. The interaction of TNRC6 with AGO2 is mediated

17   by GW-amino acid motif repeats in the N-terminus of TNRC6 (ref. (Lazzaretti et al., 2009;

18   Lian et al., 2009; Sheu-Gruttadauria and MacRae, 2018; Takimoto et al., 2009; Zipprich

19   et al., 2009)), permitting displacement of endogenous TNRC6 from AGO2, and inhibition

20   of miRNA activity, through expression of a peptide derived from the HsTNRC6B N-

21   terminus (termed T6B$_{WT}$ in the following)(Hauptmann et al., 2015). We verified that a

22   FH::T6B$_{WT}$::mCherry fusion protein (T6B$_{WT}$), but not a mutant derivative thereof,

23   FH::T6B$_{MUT}$::mCherry (T6B$_{Mut}$), co-immunoprecipitated endogenous AGO2 and AGO1

11

1   when stably expressed in mESCs (**Supplemental Figure S4A-D**). However, neither

2   peptide co-immunoprecipitated TRIM71 (**Supplemental Figure S4C, D, Supplemental**

3   **Table S2**). This suggests that TRIM71 binding to TNRC6 differs from binding by AGO2,

4   allowing us to use *T6B* expression to interfere specifically with the TNRC6–AGO2

5   complex (**Figure 4E**).

6   Overexpression of *FH::T6B$_{WT}$::mCherry* but not *FH::T6B$_{MUT}$::mCherry* in the

7   *GFP_5xT71BS* reporter cell line led to a strong and dose-dependent enhancement of

8   repression of the GFP reporter (**Figure 4F**) without changing TRIM71 and AGO2 levels

9   (**Supplemental Figure S4B, E**). This effect was specific, as GFP levels were unaltered

10   in cells lacking TRIM71 or expressing a reporter lacking TRIM71 binding sites **(Figure**

11   **4F)**.

12   In summary, displacing TNRC6 from AGO2 enhances the activity of TRIM71,

13   consistent with competition between AGO2 and TRIM71 for limiting amounts of TNRC6

14   to induce transcript silencing.

15

16   **TRIM71 and AGO2 recruit TNRC6A to transcripts that they repress.**

17   The physical and functional interactions of TRIM71 and TNRC6 support a model of

18   TNRC6 functioning as a silencing factor for TRIM71-mediated repression. This model

19   predicts recruitment of TNRC6 to TRIM71 targets through TRIM71. To test this model,

20   we performed RNA-immunoprecipitations of endogenously HA-tagged TNRC6A (the

21   choice of isoform for tagging was arbitrary), followed by sequencing (RIP-seq) in wild-

22   type, and *Trim71$^{-/-}$* mESCs. We found that pulldown of 229 genes was significantly

23   decreased in the absence of TRIM71 (**Figure 5A**). Consistent with direct recruitment

1   through TRIM71, TRIM71 CRAC-seq data (Welte et al., 2019) revealed that this set of

2   transcripts was enriched for binding by TRIM71 (**Figure 5B**). Supporting functionality,

3   these transcripts were de-silenced in $Trim71^{-/-}$ vs WT cells (**Figure 5C, Supplemental**

4   **Figure S5B**). Finally, an independent set of TRIM71 RIP experiments using RT-qPCR for

5   transcript quantification showed the same trend for the *GFP_5xT71BS* reporter, as well

6   as for the known endogenous TRIM71 target transcripts (*Plxnb2, Mbnl1, Mllt1*;

7   **Supplemental Figure S 5C**). Thus, these data show that TRIM71 recruits TNRC6 to a

8   set of mRNAs that it silences, supporting the notion that TNRC6 is a functional component

9   of a TRIM71-induced silencing complex.

10   To gain more insight into the interplay of TRIM71- and AGO2-mediated gene

11   regulation, we performed TNRC6A RIP-seq experiments on $Ago2^{-/-}$ cells (**Supplemental**

12   **Figure S5A**), along with a repetition of the experiment on wild-type and $Trim71^{-/-}$ cells.

13   The repeat experiment for *HA-Tnrc6a* and *HA-Tnrc6a Trim71$^{-/-}$* cells replicated the earlier

14   experiment well (**Supplemental Figure S5D**). In *Ago2* knock-out cells, binding of 575

15   transcripts by TNRC6A was significantly decreased relative to wild-type cells (**Figure 5D**).

16   This set of transcripts was enriched for AGO2 binding events, quantified by CLIP-seq (Li

17   et al., 2020) (**Figure 5E**), and significantly de-silenced in $Ago2^{-/-}$ relative to wild-type cells

18   (**Figure 5F, Supplemental Figure S5E)**. Most of these transcripts were distinct from

19   those that relied on TRIM71 for TNRC6A binding, *i.e.*, TNRC6A targeting to 43 transcripts

20   depended on both AGO2 and TRIM71, but 532 and 186 target transcripts were unique to

21   AGO2 and TRIM71, respectively (**Supplemental Table S3**). In the following, we will refer

22   to these as 'common', 'AGO2-only' and 'TRIM71-only' targets.

1   Of note, we observe higher correlation of differential TNRC6 targeting (quantified

2   by RIP-seq) with differential gene expression (quantified by RNA-seq), than with methods

3   quantifying direct transcript binding of TNRC6A-recruiting RBPs (*i.e.*, TRIM71 CRAC-seq

4   or AGO2 CLIP-seq experiments; **Supplemental Figure S5B, E-G**). This either indicates

5   a significant amount of non-functionally relevant binding events, or normalization issues

6   in the latter experimental systems. In summary, AGO2 and TRIM71 recruit TNRC6A to

7   their respective target transcripts, and TNRC6A transcript binding correlates well with

8   silencing activity of the respective pathway.

9

10   **Exclusive TRIM71 target transcripts are silenced more efficiently in *Ago2* knock-**

11   **out cells.**

12   The sets of unique and common TRIM71 and AGO2 target transcripts identified above

13   allowed us to ask whether the enhancement of TRIM71 activity upon *Ago2* deletion

14   observed in the genetic reporter screens was true for endogenous TRIM71 targets.

15   Indeed, while 'TRIM71-only' and 'common' targets were de-silenced in *Trim71$^{-/-}$* relative

16   to wild-type cells (**Figure 6A**), we observed increased silencing of 'TRIM71-only' targets

17   in *Ago2$^{-/-}$* relative to wild-type cells (**Figure 6B**). These effects were most pronounced for

18   a subset of transcripts that showed either unchanged, or increased TNRC6A binding in

19   *Ago2$^{-/-}$* relative to WT cells (**Supplemental Figure S6C, D, F, G**). We obtained similar

20   results when comparing gene expression changes between cells expressing *T6B$_{WT}$* and

21   *T6B$_{MUT}$* for these transcript classes (**Figure 6C, Supplemental Figure S6E, H**),

22   consistent with the extensive similarity of gene expression changes introduced by *T6B$_{WT}$*

23   transfection and *Ago2* disruption (**Supplemental Figure S7A**).

14

1   We selected two 'common', two 'AGO2-only' and 10 'TRIM71-only' targets

2   (**Supplemental Figure S7B-G**) to examine their 3'UTR-dependent regulation using

3   luciferase reporters. The 'TRIM71-only' set contains two previously validated TRIM71

4   targets, *Mllt1*, and *Plxnb2* (refs. (Mitschka et al., 2015; Welte et al., 2019)), as well as

5   eight novel reporters. Like the previously validated reporters, all novel TRIM71 target

6   candidates were upregulated in $Trim71^{-/-}$ relative to WT cells. Conversely, the two 'AGO2-

7   only' target candidates were upregulated in $Ago2^{-/-}$ relative to wild-type cells. This

8   validates AGO2- or TRIM71-dependent recruitment of TNRC6A to a transcript as a

9   powerful criterion for identification of target transcripts for the respective pathway. Indeed,

10   and again consistent with our annotation, expression of the two 'common' targets was

11   also increased in $Ago2^{-/-}$ vs WT cells. Confirming specificity, *Ago2* deletion did not cause

12   upregulation of any of the 'TRIM71-only' target reporters. Furthermore, eight of the 10

13   3'UTRs from 'TRIM71-only' targets conferred increased reporter silencing upon *Ago2*

14   knock-out (**Figure 6D, E**), providing additional evidence that miRNA pathway disruption

15   broadly enhances TRIM71-dependent silencing.

16   To further dissect TRIM71- and miRISC-mediated silencing activities, we analyzed

17   the *Mbnl1* 3'UTR, one of the two 'common' 3'UTRs known for both Trim71- and miRNA-

18   mediated silencing (Cerro-Herreros et al., 2018; Welte et al., 2019) (**Figure 6D**). We had

19   previously mapped a functional TRIM71 binding site on this 3'UTR (Welte et al., 2019),

20   allowing us to test whether we could separate the two silencing activities. Indeed, we

21   found that grafting a region ('stretch1') that primarily mediates TRIM71-dependent

22   repression (Welte et al., 2019) into the *Pou5f1* 3'UTR conferred de-silencing in $Trim71^{-/-}$

23   but enhanced silencing in $Ago2^{-/-}$ relative to wild-type cells for the resulting '*Pou5f1::Mbnl1*

15

1   *stretch1* 3'UTR' reporter (**Figure 7F, G**). Conversely, a reporter lacking this TRIM71

2   binding site ('*Mbnl1∆stretch1* 3'UTR') was upregulated in *Ago2$^{-/-}$* relative to *WT* cells

3   (**Figure 7G**). As observed previously (Welte et al., 2019), regulation of the latter reporter

4   by TRIM71 is blunted but not entirely abrogated, which may lead us to underestimate the

5   extent of its miRNA-mediated regulation.

6   In conclusion, AGO2 competes with TRIM71 for TNRC6 as a common silencing

7   pathway, and TRIM71's silencing activity depends on its access to TNRC6.

8

9   **Multiple RNA pathways compete with miRISC for access to TNRC6.**

10   Finally, we wondered if additional RNA silencing pathways depended on TNRC6. We

11   focused on UPF1, an RNA helicase involved in nonsense-mediated RNA decay as well

12   as many other RNA decay processes (Lavysh and Neu-Yilik, 2020), which reproducibly

13   co-immunoprecipitated with TRIM71, AGO2 and TNRC6 (**Figure 4A-C**) (Elbarbary et al.,

14   2017). To test a potential function of UPF1 in TNRC6 recruitment to specific transcripts,

15   we generated *Upf1$^{-/-}$* cells. Neither the levels of TRIM71 (**Supplemental Figure S7A**) nor

16   silencing of the GFP_5xT71BS reporter were altered (**Supplemental Figure S7B**),

17   showing that UPF1 is not required for regulation of TRIM71 levels or silencing activity.

18   We performed HA-TNRC6A RIP-Seq in wild-type, *Upf1$^{-/-}$*, and *Ago2$^{-/-}$* cells. The

19   latter served as a positive control and revealed the expected change in TNRC6A

20   recruitment (**Supplemental Figure S7C**). In *Upf1* knock-out cells, binding of 52

21   transcripts by TNRC6A was significantly decreased relative to wild-type cells (**Figure 7A**).

22   This set of transcripts was significantly de-silenced in *Upf1$^{-/-}$* relative to wild-type cells

23   (**Figure 7B, Supplemental Figure S7D**). Most transcripts were distinct from those that

1   relied on AGO2 for TNRC6A binding, *i.e.*, TNRC6A targeting to only four transcripts

2   depended on both AGO2 and UPF1 ('common' targets), but 571 and 48 target transcripts

3   were unique to AGO2 ('AGO2-only') and UPF1 ('UPF1-only'), respectively

4   (**Supplemental Table S3**). Like 'TRIM71-only' target transcripts, 'UPF1-only' targets

5   displayed increased silencing in $Ago2^{-/-}$ relative to wild-type and $T6B_{WT}$ relative to $T6B_{MUT}$

6   cells (**Figure 7C-E, Supplemental Figure S7E-J**). We conclude that UPF1 recruits

7   TNRC6 to a subset of its targets to achieve silencing, and that this silencing activity is

8   enhanced in the absence of AGO2. In summary, our data reveal that AGO2 can influence

9   transcripts directly, through miRNA-guided silencing, and indirectly, by competing TNRC6

10   away from multiple RNA pathways (*i.e.*, TRIM71 and UPF1), thus constraining their

11   silencing activity.

12

Discussion

14   TNRC6/GW182 has been known as a core component of miRISC (Braun et al., 2011;

15   Chen et al., 2009; Jakymiw et al., 2005; Liu et al., 2005). Our results extend this canonical

16   function by revealing TNRC6 silencing activities in additional pathways, depending on

17   distinct RBPs. A shared dependence on TNRC6 provides a mechanism for cross-

18   regulation among these pathways and allows AGO2 to constrain the activities of

19   additional RNA silencing pathways by sequestering TNRC6. As TRIM71 in turn can

20   repress production of certain miRNAs(Torres-Fernández et al., 2021b; Treiber et al.,

21   2017) and of AGO2 (ref. (Liu et al., 2021)), a cross-regulatory network of interactions

22   among RNA silencing pathways is beginning to emerge.

23

TNRC6 mediates mRNA silencing by TRIM71

Several lines of evidence support the conclusion that TNRC6 has a critical function in mediating TRIM71-dependent RNA silencing: First, over-expression of *TNRC6* paralogs enhances TRIM71 activity. Second, TNRC6 co-immunoprecipitates with TRIM71. Although this interaction is RNA-dependent, it does not simply reflect a coincidental co-occurrence on the same transcript, as third, we find that TRIM71 mediates recruitment of TNRC6 to specific mRNAs. Accordingly, co-immunoprecipitation of TNRC6 with TRIM71 does not depend on the presence of the known TNRC6 binding partner AGO2. Fourth, transcripts that rely on TRIM71 or AGO2 for TNRC6 recruitment are functional targets of each pathway, and largely fall into distinct sets.

Strikingly, loss of TNRC6 binding upon TRIM71 or AGO2 inactivation appears to be a better predictor of each pathway's silencing activity than direct transcript binding of TRIM71 or AGO2 (**Supplemental Figure S5B, E-G**). Thus, the presence of TNRC6 can distinguish productive from non-productive binding events of either RBP. The fact that co-immunoprecipitation of TNRC6 with TRIM71 is sensitive to RNase treatment further suggests that RNA-binding of TRIM71 may support recruitment of, or stabilize the interaction with, TNRC6.

We note that weak predictive power of RNA binding for function is not unique to TRIM71 or AGO2, but a general challenge in experimental systems seeking to quantify direct RBP-RNA interactions (Chen et al., 2019; Vieira-Vieira and Selbach, 2021). Hence, differential recruitment of silencing effectors – TNRC6 as shown here, but potentially also others for other RBPs – appears to be a robust measure to identify functional targets in high throughput and, potentially, diverse contexts.

1

TNRC6 functions outside the miRNA pathway

Although mESCs with deletions of miRNA pathway components *(Ago2, Dicer, Xpo5)* are viable, we were unable to obtain *Tnrc6a-c* triple deletion cells, consistent with functions of TNRC6 beyond miRISC. As cells lacking either *Trim71* or combinations of *Trim71* and miRNA pathway genes are also viable, these 'non-canonical' TNRC6 functions appear not to be restricted to TRIM71. Our demonstration that UPF1 also recruits TNRC6 to specific transcripts for silencing supports this notion. We emphasize that UPF1 causes dysregulation of many transcripts (*n* = 8,074; FDR-cutoff: ≤ 0.05), among which only a small subset exhibit altered TNRC6A recruitment. While we have not investigated which features route specific UPF1 targets to this particular decay pathway, the finding is consistent with the fact that UPF1 employs diverse mechanisms to achieve transcript silencing, including but not limited to its well-established function in NMD(Cho et al., 2015; Choe et al., 2014; Kaygun and Marzluff, 2005; Kim et al., 2005; Kim and Maquat, 2019; Lavysh and Neu-Yilik, 2020; Mino et al., 2015; Park et al., 2016). Irrespectively, our findings demonstrate that TNRC6's function as an RNA silencing factor extends well beyond its canonical role in the miRNA pathway.

The interplay of miRNA, TRIM71 and UPF1 pathways on mRNA silencing

Through various manipulations, we have shown that TRIM71 and UPF1 activity is enhanced when TNRC6 is released from binding by AGO2. The opposite effect, enhanced miRNA activity upon loss of TRIM71 or UPF1, appears weak at best. This may

1   reflect a higher affinity of TNRC6 for AGO2 so that AGO2 can sequester TNRC6 away

2   from other RBPs, while these cannot, or much less efficiently, sequester TNRC6 away

3   from AGO2. Indeed, TNRC6 forms stable complexes with AGO2 in the absence of RNA

4   (Elkayam et al., 2017; Hicks et al., 2017; Sheu-Gruttadauria and MacRae, 2018),

5   distinguishing them from the complexes formed with TRIM71 and UPF1. The fact that the

6   T6B peptide blocks binding of TNRC6 to AGO but enhances TRIM71 and UPF1 activity

7   further indicates that TNRC6 can utilize distinct domains for binding to different RBPs,

8   which future structure-function studies may identify.

9   Although the main effect of miRNA pathway inactivation is an enhancement of

10   TRIM71 and UPF1 silencing activities by increasing TNRC6 availability, more complex

11   responses result for transcripts under simultaneous regulation by AGO2 and either RBP.

12   Incidentally, this validates the benefit of performing a screen with a heterologous 3'UTR

13   to isolate the regulatory phenomenon under investigation from complex cellular regulatory

14   circuits and their confounding effects. Thus, for *Mbnl1*, we showed that its 3'UTR

15   mediates regulation by both AGO2 and TRIM71. This leads to the paradox situation that

16   miRNA pathway inactivation does not promote transcript accumulation, because

17   enhanced TRIM71-dependent silencing compensates for a loss of miRNA-mediated

18   silencing.

19   Additional scenarios are conceivable: Appropriately spaced miRNA-binding sites

20   can cooperatively increase transcript silencing through a mechanism that occurs

21   downstream of target binding by the miRNA (Broderick et al., 2011; de la Mata et al.,

22   2015), possibly at the level of TNRC6 binding (Elkayam et al., 2017). It would thus seem

23   possible that cross-pathway synergy could also occur among appropriately spaced

1   miRNA-, TRIM71-, and UPF1-binding sites. Although not investigated here, support for

2   such a mechanism comes from previous work on the *Cdkn1a* mRNA, which suggested

3   cooperation of TRIM71 with miRNAs and UPF1, to achieve silencing of this particular

4   transcript in mouse and human cells, respectively (Chang et al., 2012; Torres-Fernández

5   et al., 2019). Nonetheless, such cooperative pathway activity - at least in mESCs -

6   appears to be the exception, as we observe little overlap among the target sets of

7   TRIM71, AGO2 and UPF1, respectively.

8   **Acknowledgements**

22

1 **Author Contributions**

2 T.W. conceived the project, performed molecular cloning, genome edited cell lines,

3 designed and performed experiments, computationally analyzed sgRNA screens, RNA-

4 seq, RIP-seq, mass-spectrometry results, and wrote the manuscript. A.N., A.G., C.A., and

5 M.J.L. created plasmid constructs and cell lines, and performed experiments. M.B.S.

6 computationally analyzed sgRNA screens, RNA-seq, and RIP-seq experiments. D.Hess

7 performed and computationally analyzed mass-spectrometry experiments. J.S., and C.S.

8 developed mass-spectrometry analysis software. I.S. performed FACS-sorting for

9 sgRNA-screens. F.N. performed initial bioinformatic analysis of sgRNA screens.

10 D.Hoepfner., D.E., and J.R-H. provided technical support and reagents. H.G. conceived

11 the project, designed and analyzed experiments, and wrote the manuscript.

12

13 **Declaration of interests**

14 Several authors are or were employees of Novartis Pharma AG as listed in their

15 affiliations and may own stock in the company.

16

22
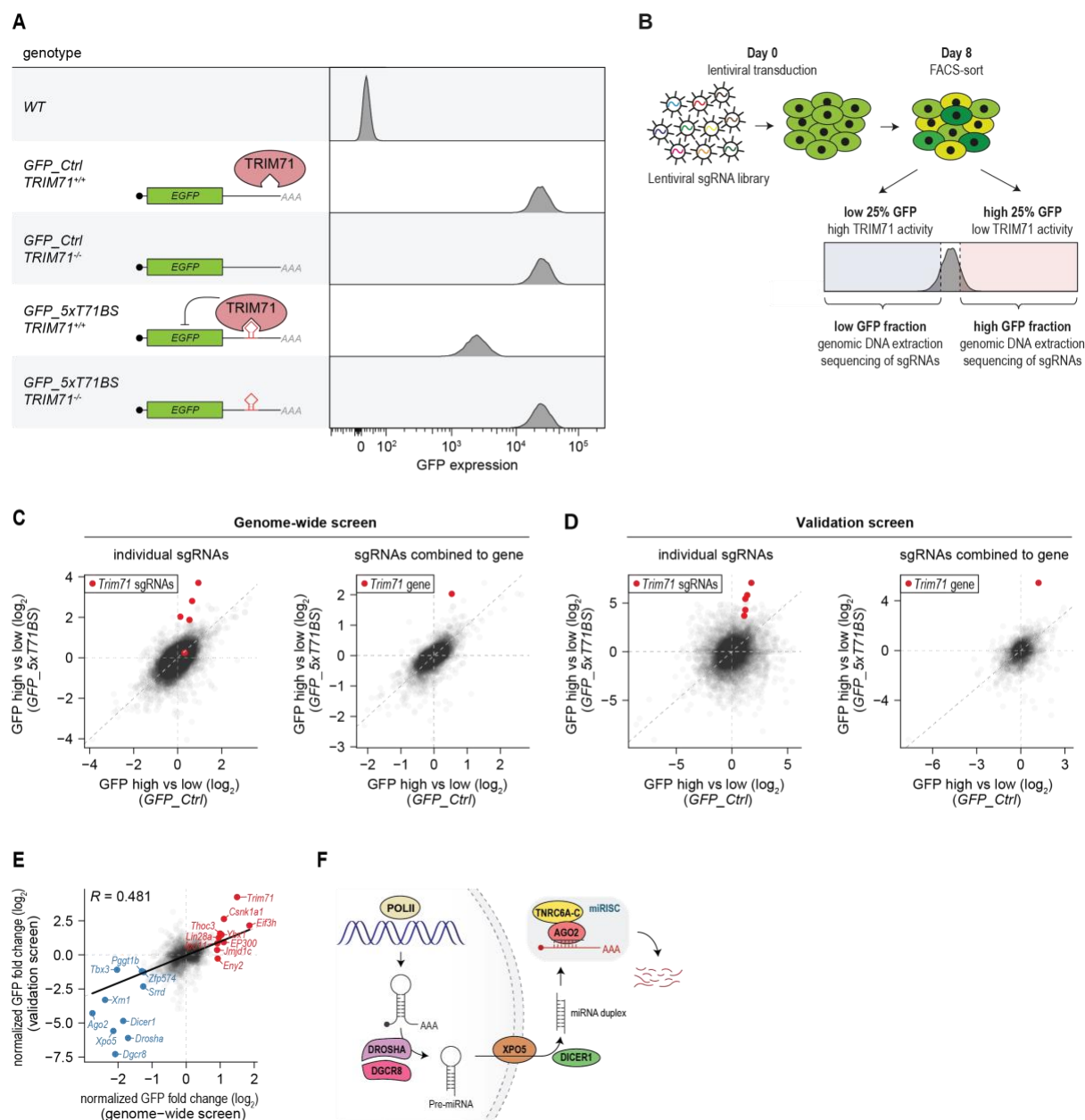
Figures

Figure 1. Two CRISPR/Cas9 sgRNA-screens identify genes involved in miRNA processing and silencing as potent repressors of TRIM71-dependent gene silencing.

(A) Reporter cell lines used in this study (*left*, schematic depiction) and their GFP levels quantified by flow cytometry (*right).* (B) Schematic depiction of the CRISPR/sgRNA

1   screen. **(C), (D)** Scatter plots showing results of a genome-wide **(C)** and a validation

2   CRISPR/sgRNA screen **(D)**, respectively. Enrichment of sgRNAs (left panels) in high vs

3   low GFP fractions are shown for *GFP_Ctrl* cells (x-axis), and *GFP_5xT71BS* (y-axis) cells.

4   *Trim71* sgRNAs are colored in red. The right panels show the aggregated (median) effect

5   of all sgRNAs per gene. *Trim71* is colored in red. **(E)** Scatter plot showing a comparison

6   of effects of genome-wide (x-axis) and validation sgRNA/CRISPR screens (y-axis) on

7   gene-level. Effects of high vs. low GFP fractions in *GFP_5xT71BS* cells are normalized

8   to the same effects in *GFP_Ctrl* cells (from **[C]** and **[D]**). The ten genes with the highest

9   (marked in red) and the lowest (marked in blue) enrichment in the genome-wide

10   CRISPR/sgRNA screen are indicated. A linear regression model was fitted to the data

11   (shown as black line). *R* indicates the Pearson's correlation coefficient. Data source for

12   **(C-E)**: **Supplemental Table S1. (F)** Schematic drawing illustrating the key components
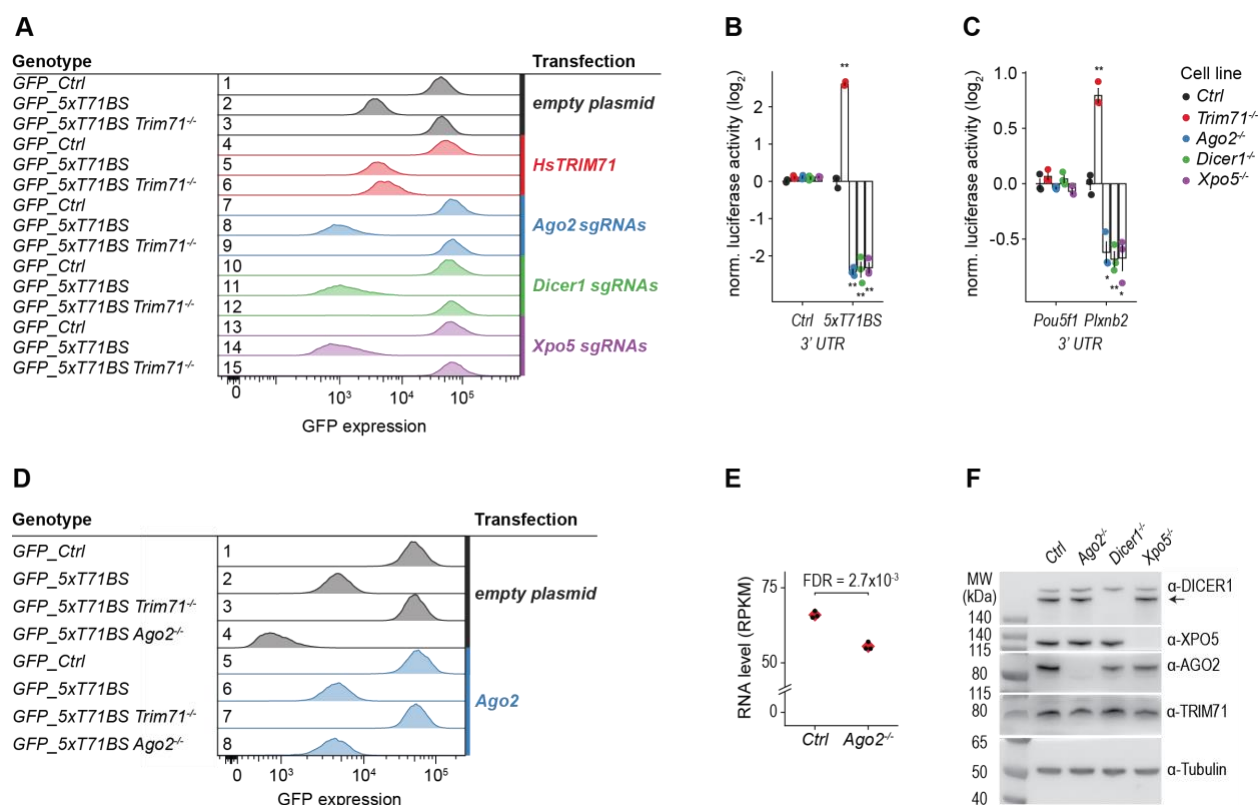
13   of the miRNA pathway.

14

Figure 2. miRNA pathway genes act as repressors of TRIM71-dependent gene silencing.

(A, D) Flow cytometry analysis showing the effect of sgRNAs targeting *Xpo5*, *Dicer1*, *Ago2*, and of transfection with *HsTRIM71* overexpression plasmids as indicated. **(B, C)** Luciferase reporter gene assay with the indicated *Renilla* 3′ UTR-fusion constructs in *WT*, *Trim71*, *Ago2*, *Dicer1*, and *Xpo5* knock-out mESCs. Data were normalized to *WT* and represent mean ± standard error of the mean (SEM). n = 3 biological replicates. Significance was tested using a two-tailed Student's *t*-test. (*) $P < 0.05$; (**) $P < 0.01$; (***) $P < 0.001$; otherwise not significant ($P \geq 0.05$). **(E)** Plot showing levels of *Trim71* mRNA in control, and *Ago2*$^{-/-}$ cells (n = 3 biological replicates; background cell line: *GFP_5xT71BS*). RNA levels are shown as reads per kilobase of transcript per million of mapped reads (RPKM). FDR: Benjamini Hochberg adjusted *P*-value. **(F)** Western blots

1   showing the effect of sgRNAs targeting *Xpo5*, *Dicer1*, *Ago2* as indicated. Parental cell
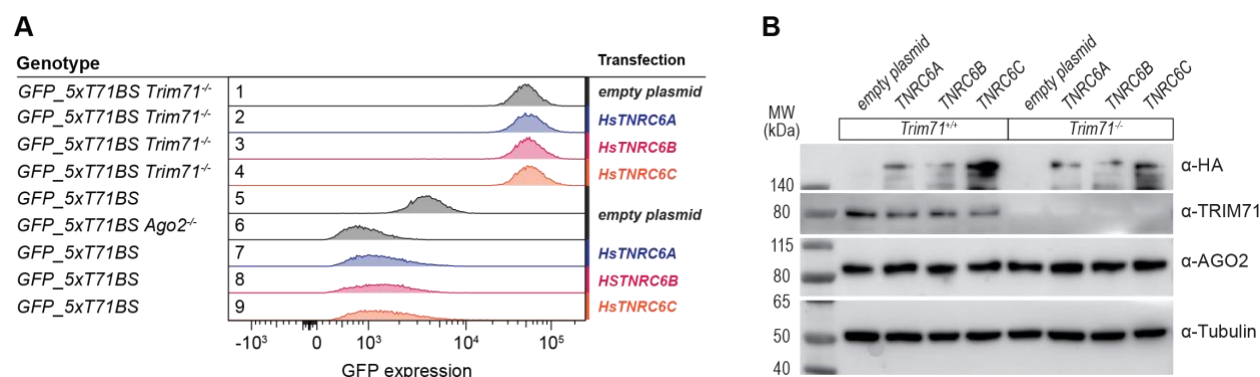
2   line ('*Ctrl*'): *GFP_5xT71BS*.

3

4

5

6   **Figure 3. TNRC6 contributes to TRIM71-dependent gene silencing.**

7   **(A)** Flow cytometry analysis showing the effect of overexpressing *HsTNRC6A*, *B*, and *C*

8   in *Trim71⁺/⁺* and *Trim71⁻/⁻ GFP_5xT71BS* cells, respectively. *GFP_5xT71BS Ago2⁻/⁻* (row

9   6) is included for comparison and replotted from above (**Figure 2D**, row 4). Transfected

10   cells were selected with Puromycin for two days. **(B)** Western blots showing the

11   expression of HA-tagged HsTNRC6A, B, and C (upper panel), and corresponding

12   TRIM71, AGO2, and Tubulin levels of cells used in **(A)**.
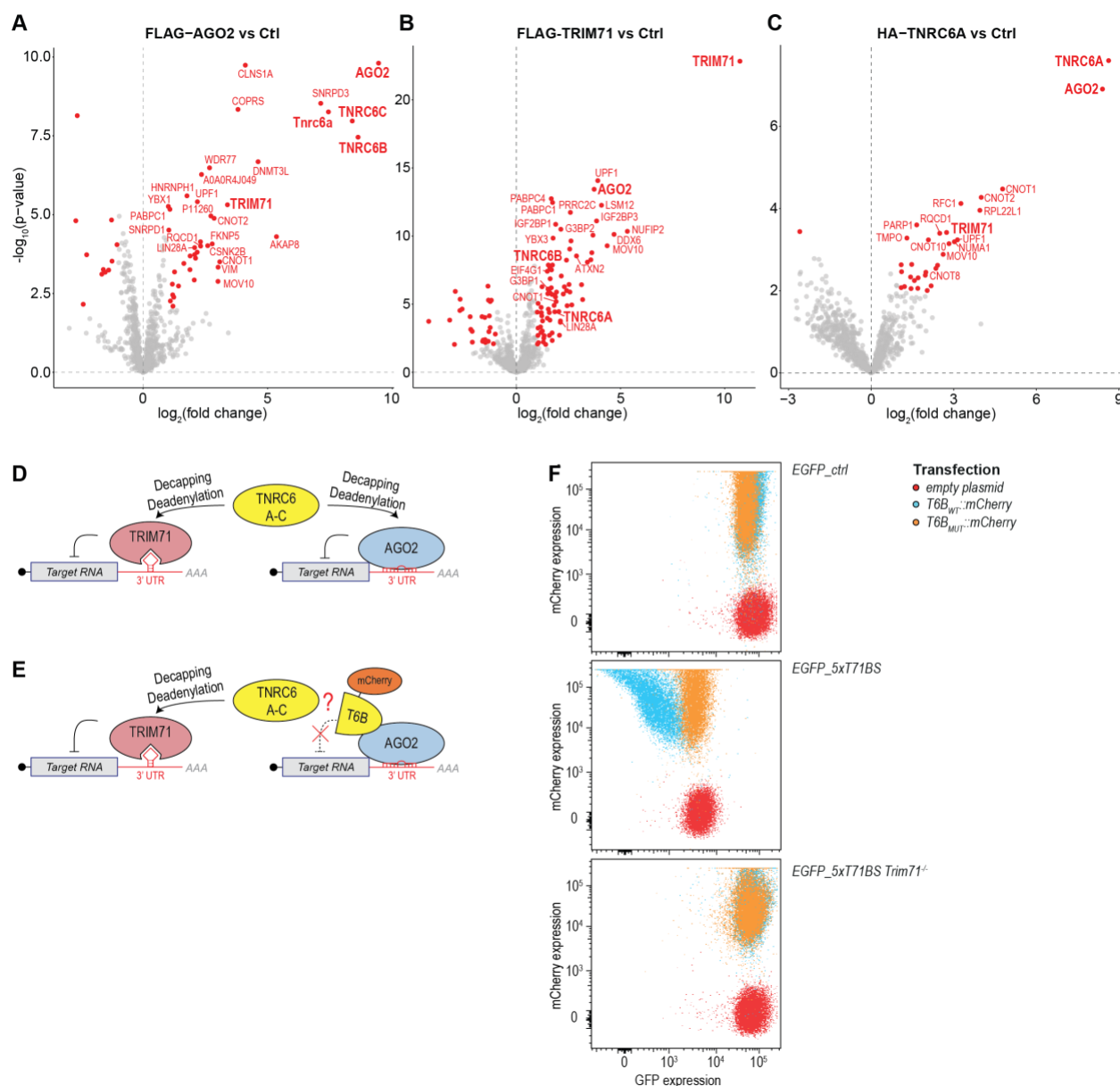
13

26

Figure 4. Blocking the interaction between GW182 and AGO2 increases silencing by TRIM71.

(A-C) Volcano plots showing mass spectrometry results of *FLAG-Ago2* vs untagged control cells ($n = 3$ biological replicates; **[A]**), FLAG-AVI-TRIM71 vs untagged control cells ($n = 9$ biological replicates; **[B]**), and HA-AVI-TNRC6A vs untagged control cells ($n = 3$ biological replicates; **[C]**). Significance was tested using a moderated t-test. Identified proteins with an adjusted *P* value ≤ 0.01 and |log$_2$(fold change)| ≥ 1 are marked in red.

27

1   TNRC6A~C, AGO2, and TRIM71 are marked bold. Data source **A-C**: **Supplemental**

2   **Table S2**. **(D)** Schematic drawing showing the working hypothesis of a competition

3   between miRNA, and TRIM71 pathways for TNRC6 as a common silencing factor. **(E)**

4   Schematic drawing illustrating T6B-peptide based competitive inhibition of TNRC6-AGO2

5   interactions. **(F)** Scatter plots showing FACS results for GFP (x-axis), and mCherry (y-

6   axis) expression in *GFP_Ctrl*, *GFP_5xT71BS*, and *GFP_5xT71BS Trim71$^{-/-}$* reporter cell

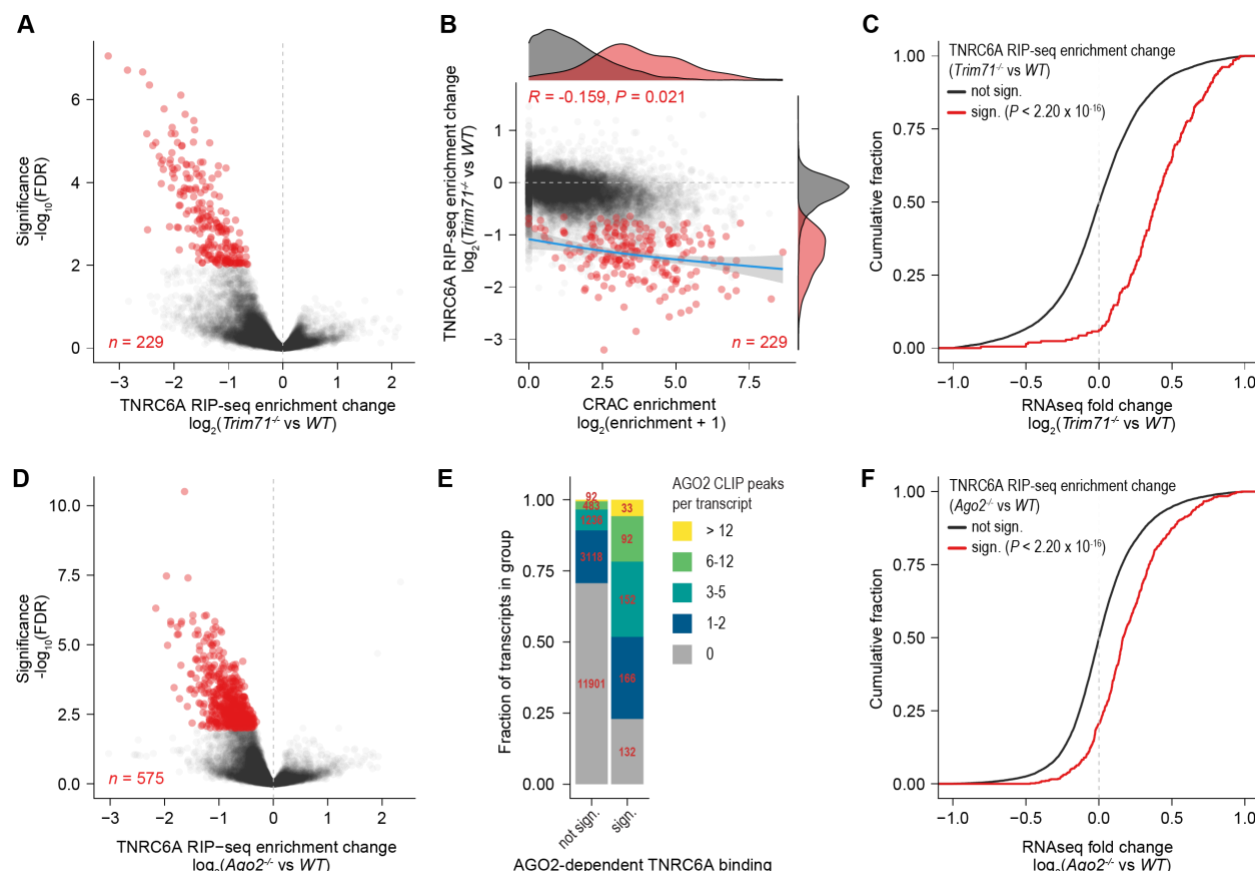7   lines transfected with empty, *T6B$_{WT}$::mCherry*, or *T6B$_{MUT}$::mCherry* plasmids.

8

9

10   **Figure 5. TRIM71 and AGO2 recruit TNRC6A to their respective target RNAs.**

11   **(A)** Volcano plot showing changes of TNRC6A transcript binding in *Trim71$^{-/-}$* vs. *WT* cells

12   as quantified by RIP-seq. Significantly depleted transcripts (FDR ≤ 0.01, log$_2$[TNRC6A

28

1   RIP-seq enrichment change] < 0) are indicated in red. **(B)** Scatter plot showing TRIM71

2   transcript binding assessed by CRAC-seq (x-axis: log$_2$[enrichment + 1](Welte et al.,

3   2019)) and TNRC6A RIP-seq enrichment change in *Trim71*^{-/-} vs *WT* cells (y-axis).

4   Coloring as in **(A)**. The corresponding density distributions are shown on top for CRAC-

5   seq enrichment and to the right for TNRC6A RIP-seq. *R* indicates Pearson's correlation

6   coefficient. *P* value is calculated using a paired, two-sided t test for correlation. **(C)**

7   Cumulative density functions showing de-silencing of transcripts with TRIM71-dependent

8   TNRC6A binding (as defined in **[A]**; red line) vs. all other transcripts (black line).

9   Significance was tested with a two-sided Kolmogorov-Smirnov test. **(D)** Volcano plot

10   showing changes of TNRC6A transcript binding in *Ago2*^{-/-} vs. *WT* cells as quantified by

11   RIP-seq. Significantly depleted transcripts (FDR ≤ 0.01, log$_2$[Tnrc6a RIP-seq enrichment

12   change] < 0) are indicated in red. **(E)** Barplot indicating transcript counts (red numbers)

13   in groups with different numbers of overlapping AGO2 CLIP-seq peaks (Li et al., 2020),

14   as indicated by color labels. Transcripts without (left bar), and with (right bar) significant

15   AGO2-dependent TNRC6A binding (as defined in **[D]**) are separated. **(F)** Cumulative

16   density functions showing de-silencing of transcripts with AGO2-dependent TNRC6A

17   binding (as defined in **[D]**; red line) versus all other transcripts (black line). Significance

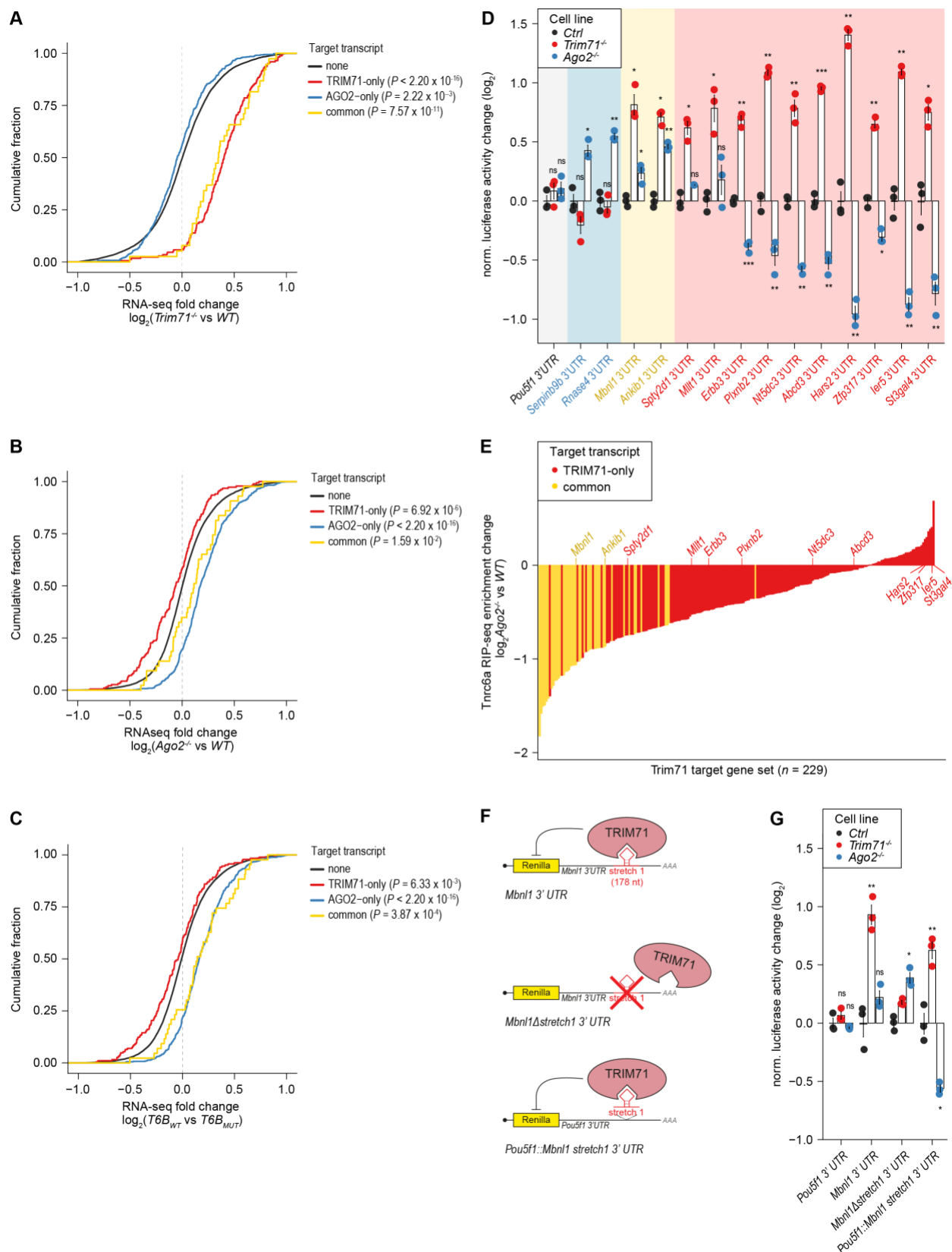18   was tested with a two-sided Kolmogorov-Smirnov test. Data source (**A-F**): **Supplemental**

19   **Table S3**.

20

29

1

1 **Figure 6. Exclusive TRIM71 target transcripts are silenced more effectively in *Ago2***

2 **knock-out cells.**

3 **(A-C)** Cumulative density functions showing global expression changes of transcript

4 groups in *Trim71*$^{-/-}$ vs *WT* cells **(A)**, *Ago2*$^{-/-}$ vs *WT* cells **(B)**, and *T6B$_{WT}$* vs *T6B$_{MUT}$* cells

5 **(C)**. Red color indicates transcripts with significant loss of TNRC6A RIP-seq enrichment

6 in *Trim71*$^{-/-}$ vs *WT* cells (FDR ≤ 0.01, log$_2$(fold change) < 0), but not in *Ago2*$^{-/-}$ vs *WT* cells

7 (*n* = 186). Blue color indicates transcripts with significant loss of RIP-seq enrichment in

8 *Ago2*$^{-/-}$ vs *WT* cells (FDR ≤ 0.01, log$_2$(fold change) < 0), but not in *Trim71*$^{-/-}$ vs *WT* cells

9 (*n* = 532). Yellow color indicates transcripts with significant loss of TNRC6A RIP-seq

10 enrichment in *Trim71*$^{-/-}$ vs *WT* cells≤ 0.01, and in *Ago2*$^{-/-}$ vs *WT* cells (*n* = 43). Black color

11 indicates transcripts with no significant loss of RIP-seq enrichment in *Trim71*$^{-/-}$ vs *WT*

12 cells≤ 0.01, and in *Ago2*$^{-/-}$ vs *WT* cells (*n* = 16,509). Significance was tested with a two-

13 sided Kolmogorov-Smirnov test compared to the group 'none'. **(D, G)** Barplots showing

14 validation experiments with luciferase reporter gene assays with various *Renilla* 3′UTR

15 fusion constructs (selection indicated in **[E** and **Supplemental Figure S7B-G]**) in *WT*,

16 *Trim71* and *Ago2* knock-out mESCs. Background colors indicate grouping of tested

17 transcript, as defined in **(A-C)**. Data were normalized to *WT* and represent mean ± SEM.

18 *n* = 3 biological replicates. Significance was tested using a two-tailed Student's *t*-test. (*)

19 *P* ≤ 0.05; (**) *P* ≤ 0.01; (***) P < 0.001; (ns) not significant (*P* ≥ 0.05). **(E)** Barplot displaying

20 the 'TRIM71 target' gene set as identified in **(Figure 5A)**, ranked by TNRC6A RIP-seq

21 enrichment change in *Ago2*$^{-/-}$ vs *WT* cells. Colors indicate grouping of tested transcripts,

22 as defined in **(A-C)**. Transcripts selected for validation experiments with luciferase

23 reporters **(D)** are indicated. **(F)** Schematic drawing showing the different *Mbnl1* 3'UTR

31

1   reporter constructs used in **(G)**. Background cell line **(A-G)**: *GFP_5xT71BS* mESCs. Data

2   source **(A-C, E)**: **Supplemental Table S3**.

3
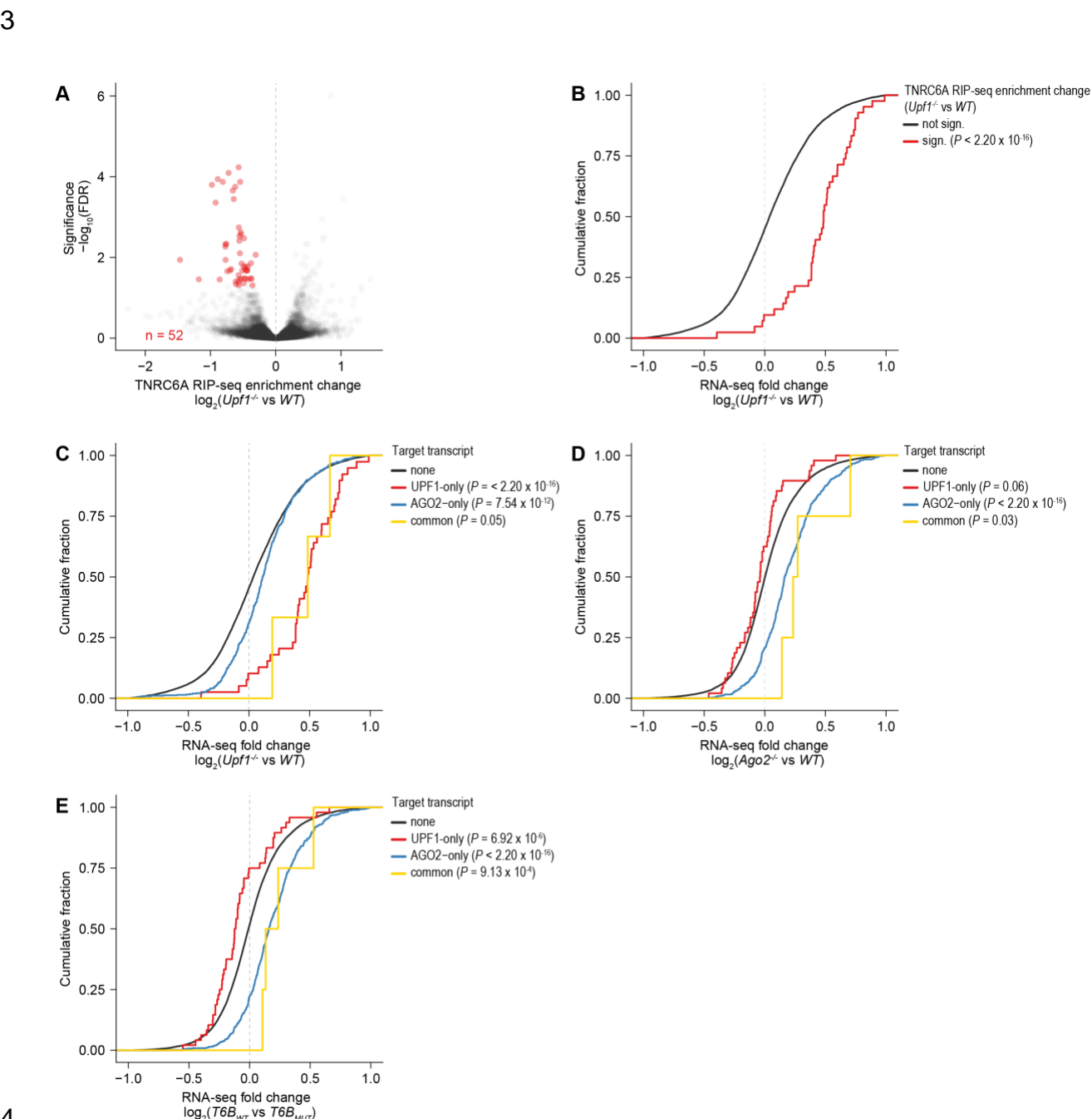
4

5   **Figure 7. UPF1 recruits TNRC6A to its target RNAs. Exclusive UPF1 target**

6   **transcripts are silenced more efficiently in *Ago2* knock-out cells.**

1   **(A)** Volcano plot showing changes of transcript binding by TNRC6A in *Upf1$^{-/-}$* vs. *WT* cells

2   as quantified by RIP-seq. Significantly depleted transcripts (FDR ≤ 0.05, log$_2$[TNRC6A

3   RIP-seq enrichment change] < 0) are indicated in red. **(B)** Cumulative density functions

4   showing de-silencing of transcripts with UPF1-dependent TNRC6A binding (as defined in

5   **[A]**; red line) vs all other transcripts (black line). Significance was tested with a two-sided

6   Kolmogorov-Smirnov test. **(C-E)** Cumulative density functions showing global expression

7   changes of transcript groups in *Upf1$^{-/-}$* vs *WT* cells **(C)**, *Ago2$^{-/-}$* vs *WT* cells **(D)**, and *T6B$_{WT}$*

8   vs *T6B$_{MUT}$* cells **(E)**. Red color indicates transcripts with significant loss of TNRC6A RIP-

9   seq enrichment in *Upf1$^{-/-}$* vs *WT* cells (FDR ≤ 0.05, log$_2$(fold change) < 0), but not in *Ago2^{-}*

10   *$^{/-}$* vs *WT* cells (*n* = 48). Blue color indicates transcripts with significant loss of RIP-seq

11   enrichment in *Ago2$^{-/-}$* vs *WT* cells (FDR ≤ 0.01, log$_2$(fold change) < 0), but not in *Trim71^{-}*

12   *$^{/-}$* vs *WT* cells (*n* = 571). Yellow color indicates transcripts with significant loss of RIP-seq

13   enrichment in *Upf1$^{-/-}$* vs *WT* cells, and in *Ago2$^{-/-}$* vs *WT* cells (*n* = 4). Black color indicates

14   transcripts with no significant loss of RIP-seq enrichment in *Upf1$^{-/-}$* vs *WT* cells, and in

15   *Ago2$^{-/-}$* vs *WT* cells (*n* = 16,648). Significance was tested with a two-sided Kolmogorov-

16   Smirnov test compared to the group 'none'. Data source: **Supplemental Table S3**.

17

18

19

20

21

22

1 **STAR Methods**

2 <u>Materials Availability</u>

3 Helge Großhans, Friedrich Miescher Institute for Biomedical Research,

4 helge.grosshans@fmi.ch, will respond to requests and provide reagents and information.

5 Published research reagents from the FMI are shared with the academic community

6 under a Material Transfer Agreement (MTA) having terms and conditions corresponding

7 to those of the UBMTA (Uniform Biological Material Transfer Agreement).

8

9 <u>Data and Code Availability</u>

10 All the data is included in the manuscript or in the supplementary material. Next-

11 generation sequencing data have been deposited at the Gene Expression Omnibus with

12 accession numbers GSE205968

13 (https://www.ncbi.nlm.nih.gov/geo/query/acc.cgi?acc=GSE205968) and GSE214755

14 (https://www.ncbi.nlm.nih.gov/geo/query/acc.cgi?acc=GSE214755). The mass

15 spectrometry proteomics data have been deposited to the ProteomeXchange Consortium

16 via the PRIDE partner repository (Perez-Riverol et al., 2022) with the dataset identifier

17 PXD034537 (http://www.ebi.ac.uk/pride). The einprot R package (v0.4.4) used for the

18 analysis of mass spectrometry data is deposited online

19 (https://github.com/fmicompbio/einprot).

20

21 **Experimental Model and Subject Details**

34

1   Mouse embryonic stem cells (mESCs)

2   mESCs (TC-1 mouse ES cells (background 129S6/SvEvTac, a gift from D. Schübeler

3   (Lienert et al., 2011) and 129xC57BL/6 *Rosa26*^{*Cre-ERT2/BirA-V5*} [cMB063]) (Ostapcuk et al.,

4   2018) were cultured on gelatin-coated dishes in mESC medium (DMEM [Gibco 21969-

5   035] supplemented with 15% fetal bovine serum [Gibco], 1 × non-essential amino acids

6   [Gibco], 1 mM sodium pyruvate [Gibco], 2 mM L-glutamine [Gibco], 0.1 mM ß-

7   mercaptoethanol [Sigma], 50 µg/ml penicillin, 80 µg/ml streptomycin and home-made

8   LIF) at 37°C in 5% CO_2.

9

10 **Method Details**

11 Generation of cell lines

12 Generated cell lines can be found in **Supplemental Table S5**. Experimental details for

13 the generation of each cell line are given in the **Supplemental Methods** section.

14

15 Molecular cloning

16 Generated plasmids with insert sources and primer sequences can be found in **Tables**

17 **S6 and S7**. Experimental details for the generation of plasmid constructs are given in the

18 **Supplemental Methods** section.

19

20 Genome-wide sgRNA screen

21 Genome-wide sgRNA-screening was performed as described previously (Hoepfner et al.,

22 2019). Briefly, each cell line (mESC *Cas9::BSD*, yGlob [*GFP_Ctrl*; *GFP_5xT71BS*]) was

35

1   expanded to confluency in 8 x 15 cm plates in mESC-medium containing 2.5 μg/ml

2   Blasticidin. Cells were transduced with two separate lentiviral sgRNA libraries (library 1:

3   52,000 unique sgRNAs (~5 per gene); library 2: 39,000 unique sgRNAs (~5 per gene);

4   (Zeng et al., 2018). Cells were transduced at a multiplicity of infection (MOI) of 0.31 using

5   10 μg/ml polybrene at 700x coverage/sgRNA. In total, 126.25×10^6 cells were transduced

6   with library 1 on eight T300 plates [TPP, #90301] and 94.7×10^6 cells were transduced

7   with library 2 on six T300 plates. Transduced cells were selected with Puromycin at 1

8   μg/ml for three days. On day 8, cells were trypsinized, PFA-fixed (4% PFA in PBS, 15 min

9   at room temperature), washed in PBS, and resuspended in FACS-buffer (2% FBS, 2 mM

10   EDTA in PBS), and FACS-sorted to obtain 'high 25%' and 'low 25%' signal fractions per

11   cell line. At day 4 and 8, unsorted fractions (200×10^6 cells per library 1 and 150×10^6 cells

12   per library 2) were collected. Genomic DNA was extracted, followed by library preparation

13   and sequencing as described previously (Hoepfner et al., 2019).

14

15   Validation sgRNA-Screen

16   Using the top 985 enriched and depleted genes (based on a z-score ranking sgRNAs

17   according to their effect on GFP expression specific to the TRIM71 pathway; see

18   bioinformatic methods in the **Supplemental Methods** section), respectively, as well as

19   400 middle-scoring genes from the genome-wide sgRNA screen, we constructed a

20   12,000 sgRNA library (~5 sgRNAs per gene) using a previously published sgRNA library

21   (www.vbc-score.org; (Michlits et al., 2020)). sgRNA sequences can be found in

22   **Supplemental Table S1**. The setup for the validation screen corresponded to the whole-

23   genome screen with appropriately down-scaled cell numbers. Due to low viral titers of the

1   library, cells were transfected at a MOI of 0.1, with a 500-fold coverage.

2

3   Experiments with transiently transfected mESCs

4    $5.0x10^5$ cells were seeded in 6-well plates and transfected with 2 µg of plasmid using

5   Lipofectamine 3000 [Invitrogen; L3000] reagent at 1 µl/µg ratio in OptiMem medium

6   [Gibco; 31985062]. After 24h of transfection, cells transfected with Puromycin-containing

7   constructs were selected with puromycin at 1 µg/ml for two days. For FH-TNRC6A-C

8   constructs, puromycin concentrations were reduced by 50% at day two.

9

10   Luciferase assays

11   Luciferase assays were performed as described previously (Welte et al., 2019). Briefly,

12   25,000 cells were transfected with 100 ng of plasmid DNA in 24-well plates using

13   Lipofectamine 3000 (Invitrogen, L3000001) according to manufacturer's instructions.

14   psiCHECK-2™ (Promega, C8021) luciferase plasmids and primers used can be found in

15   **Supplemental Table S6B** and **Supplemental Table S7C**. Transfections were carried out

16   in triplicates. The following day, cells were washed once with PBS, lysed, and Renilla and

17   Firefly luciferase activities were measured on a luminometer using the Promega dual

18   luciferase kit (Promega, E1910) according to manufacturer's instructions.

19

20   RNA extraction, RT-qPCR and RNA-seq experiments

21   RNA extraction, RT-qPCR, and RNA-seq was done as previously described **(Welte et**

22   **al., 2019)**. Briefly, total RNA was extracted using the Norgen single-cell RNA purification

23   kit (Norgen, 51800) with on-column DNase digestion (Norgen, 25710).

1   For qPCRs, 400 ng of total RNA was transcribed to cDNA using the ImProm-II™ reverse

2   transcription kit (Promega, A3500) with random primers. qPCRs were performed using

3   the SYBR™ Green PCR master mix (Applied Biosystems, 4309155) with standard cycling

4   conditions. Data were normalized to *Gapdh* expression levels. qPCR primer sequences

5   can be found in **Supplemental Table S8**.

6   Sequencing library preparation for RNA-seq was done using the TruSeq™ 2 (Illumina,

7   RS-122-2001) kit, followed by HiSeq2500 (RNA-seq experiments from **Figs. 5-7,**

8   **Extended Data Figs. S5-S7**), or SMART-Seq™ 2 (Illumina, 20040532), followed by

9   NovaSeq (RIP-seq experiments from **Figs. 5-7, Extended Data Figs. S5-S7**).

10

11   <u>Western Blotting</u>

12   Western Blotting was performed as described previously (Welte et al., 2019). Briefly, cells

13   were seeded at equal density in 6-well plates. The following day, cells were lysed with

14   lysis buffer (25 mM Tris-HCl at pH 7.5, 100 mM KCl, 0.5% [v/v] NP-40, 1 mM EDTA,

15   EDTA-free cOmplete mini protease inhibitor [Roche, 1186170001]). 40 µg of protein was

16   loaded onto NuPAGE-Novex Bis-Tris 4%–12% gradient gels (Invitrogen), transferred

17   semidry to PVDF membranes, blocked for 1 h with 5% milk in TBS plus 0.1% Tween 20

18   (TBST), and stained with primary antibodies. Antibodies, dilutions and incubation

19   conditions are summarized in **Supplemental Table S9**.

20

21   <u>Immunoprecipitations with endogenously tagged proteins</u>

22   Immunoprecipitations were performed as described previously (Welte et al., 2019) with

23   the following changes: Cells were grown to confluency in 10-cm dishes. Cells were

1   washed 1x with PBS and lysed with lysis buffer (25 mM Tris-HCl at pH 7.5, 100 mM KCl,

2   0.5% [v/v] NP-40, 1 mM EDTA, EDTA-free cOmplete mini protease inhibitor [Roche,

3   1186170001], PhosSTOP [Roche, PHOSS-RO]. If indicated, RNaseA (250 µg/ml;

4   Quiagen, 19101), or RNase inhibitors [SUPERase•In™ RNase Inhibitor, Invitrogen,

5   AM2694] were added. Lysates were cleared by centrifugation. Equal amounts of protein

6   were incubated with 20 µL of FLAG M2 magnetic beads (Sigma, M8823), or Pierce™ HA

7   magnetic beads (Thermo Scientific, 88836) for 2 h at 4°C. Beads were washed three

8   times with 200 µL of washing buffer (50 mM Tris-HCl at pH 7.5, 150 mM KCl, 5 mM MgCl$_2$,

9   0.05% NP-40, EDTA-free cOmplete mini protease inhibitor [Roche, 11836153001],

10 PhosSTOP [Roche, PHOSS-RO]). If indicated, RNaseA (250 µg/ml; Quiagen, 19101), or

11 RNase inhibitors [SUPERase•In™ RNase Inhibitor, Invitrogen, AM2694] were added. For

12 RIP-seq or qPCR, pulldown RNA was isolated as described above. For mass

13 spectrometry, beads were washed once with 70 µl washing buffer without NP-40.

14

15 <u>Mass Spectrometry</u>

16 On-bead digestion of proteins was performed using 0.2 µg LysC [Wako Chemicals] for 6

17 h at 37 °C in 2.5 M guanidine-HCl, containing 20 mM 3-[4-(2-hydroxyethyl)-1-piperazinyl]-

18 1-propanesulfonic acid (EPPS) pH 8.5, 10 mM chloroacetamide (CAA) and 5 mM Tris(2-

19 carboxyethyl)phosphine hydrochloride (TCEP) in a total volume of 6 µl. Samples were

20 diluted with 18 µl 50mM HEPES pH 8.5 containing 0.2 µg modified porcine trypsin

21 (Promega) and cleaved overnight at 37 °C. Another 0.2 µg trypsin was added and the

22 cleavage was continued for 6 h.

1   The generated peptides were acidified with 0.8% TFA (final concentration) and analyzed

2   by LC–MS/MS on an EASY-nLC 1000 [Thermo Scientific] with a two-column set-up. The

3   peptides were applied onto a peptide µPAC™ trapping column in 0.1% formic acid, 2%

4   acetonitrile in H2O at a constant flow rate of 5 µl/min. Using a flow rate of 500 nl/min,

5   peptides were separated at RT with a linear gradient of 3%–6% buffer B in buffer A in 4

6   min followed by a linear increase from 6 to 22% in 55 min, 22%–40% in 4 min, 40%–80%

7   in 1 min, and the column was finally washed for 13 min at 80% buffer B in buffer A (buffer

8   A: 0.1% formic acid; buffer B: 0.1% formic acid in acetonitrile) on a 50 cm µPAC™ column

9   [PharmaFluidics] mounted on an EASY-Spray™ source [Thermo Scientific] connected to

10   an Orbitrap Fusion LUMOS [Thermo Scientific]. The data were acquired using 120,000

11   resolution for the peptide measurements in the Orbitrap and a top T (3 s) method with

12   HCD fragmentation for each precursor and fragment measurement in the ion trap

13   according the recommendation of the manufacturer (Thermo Scientific).

14

15   <u>Staining of CAS9 for Flow cytometry</u>

16   Staining of FLAG-CAS9 was done as follows: $1.5x10^6$ cells were PFA-fixed in 4% PFA

17   (Pierce™ [Thermo Scientific, 28908]) for 10 min at room temperature. Cells were washed

18   once in PBS, followed by incubation with blocking solution (1% BSA, 3% Donkey Serum

19   [Sigma: D9663], 0.1% (v/v) Tween in PBS) for 1-2 hours at room temperature. Cells were

20   spun down and resuspended in blocking solution with 1:500 anti-FLAG M2 monoclonal

21   antibody (Sigma [F1804]) and incubated over night at 4°C. Cells were washed twice with

22   flow cytometry solubilisation buffer (R&D [FC005]) + 0.1% BSA, followed by incubation

23   for 45 min at room temperature with Goat Anti-Mouse Alexafluor 647 secondary antibody

1   (Thermo Scientific, A-21235) in flow cytometry solubilisation buffer + 0.1% BSA. Cells

2   were washed twice with flow cytometry solubilisation buffer, followed by flow cytometry.

3

4   FLAER assay

5   A FLAER (Fluorescently, Alexa488-labeled, inactive variant of aerolysin) assay to

6   quantify CAS9 editing efficacy was performed as described previously (Hoepfner et al.,

7   2019). At day 7, cells were stained with FLAER reagent (Alexa 488 proaerolysin variant

8   [Cedarlanelabs, FL2S]), and analyzed by flow cytometry.

9

10 Flow cytometry

11 Cells were trypsinized, spun down, and resuspended in PBS. Flow cytometry analysis

12 was done using a BD LSRII SORP analyzer. Unless stated otherwise a stop-gate count

13 of 10,000 events was used. For FACS sorting, resuspended cells were filtered through

14 CellTrics 30 µm filter tubes [Wolflabs; 040042326], followed by sorting using MA900

15 [Sony], FACSAria [BD], or Influx [BD] cell sorters. Analysis of FACS data was performed

16 using FlowJo 10.8.1 software.

17

18 **Quantification and Statistical Analyses**

19 CRISPR-Cas9 screen data analysis, RNA-seq data analysis, mass spectrometry

20 analysis

21 A detailed description is given in the **Supplementary Methods** section.

22

1 <u>RT-qPCR analysis, luciferase assay analysis</u>

2 RT-qPCR and luciferase assays are three biological replicates. The value of each

3 replicate is indicated with a dot. Error bars indicate the mean standard error SEM. *P*-

4 values are calculated using a two-tailed Student's T test.

5

6 **References**

7 Aeschimann, F., Neagu, A., Rausch, M., and Grosshans, H. (2019). let-7 coordinates the

8 transition to adulthood through a single primary and four secondary targets. Life Sci

9 Alliance *2*.

10 Baillat, D., and Shiekhattar, R. (2009). Functional dissection of the human TNRC6

11 (GW182-related) family of proteins. Mol Cell Biol *29*, 4144-4155.

12 Boroviak, T., Stirparo, G.G., Dietmann, S., Hernando-Herraez, I., Mohammed, H., Reik,

13 W., Smith, A., Sasaki, E., Nichols, J., and Bertone, P. (2018). Single cell transcriptome

14 analysis of human, marmoset and mouse embryos reveals common and divergent

15 features of preimplantation development. Development *145*, dev167833.

16 Braun, J.E., Huntzinger, E., Fauser, M., and Izaurralde, E. (2011). GW182 proteins

17 directly recruit cytoplasmic deadenylase complexes to miRNA targets. Mol Cell *44*, 120-

18 133.

19 Braun, J.E., Huntzinger, E., and Izaurralde, E. (2013). The role of GW182 proteins in

20 miRNA-mediated gene silencing. Adv Exp Med Biol *768*, 147-163.

21 Broderick, J.A., Salomon, W.E., Ryder, S.P., Aronin, N., and Zamore, P.D. (2011).

22 Argonaute protein identity and pairing geometry determine cooperativity in mammalian

23 RNA silencing. RNA *17*, 1858-1869.

24 Cerro-Herreros, E., Sabater-Arcis, M., Fernandez-Costa, J.M., Moreno, N., Perez-

25 Alonso, M., Llamusi, B., and Artero, R. (2018). miR-23b and miR-218 silencing increase

26 Muscleblind-like expression and alleviate myotonic dystrophy phenotypes in mammalian

27 models. Nat Commun *9*, 2482.

1   Chang, H.M., Martinez, N.J., Thornton, J.E., Hagan, J.P., Nguyen, K.D., and Gregory,
2   R.I. (2012). Trim71 cooperates with microRNAs to repress Cdkn1a expression and
3   promote embryonic stem cell proliferation. Nat Commun *3*, 923.

4   Chekulaeva, M., Mathys, H., Zipprich, J.T., Attig, J., Colic, M., Parker, R., and Filipowicz,
5   W. (2011). miRNA repression involves GW182-mediated recruitment of CCR4–NOT
6   through conserved W-containing motifs. Nat Struct Mol Biol *18*, 1218-1226.

7   Chen, C.Y.A., Zheng, D.H., Xia, Z.F., and Shyu, A.B. (2009). Ago-TNRC6 triggers
8   microRNA-mediated decay by promoting two deadenylation steps. Nat Struct Mol Biol *16*,
9   1160-U1166.

10 Chen, J., Lai, F., and Niswander, L. (2012). The ubiquitin ligase mLin41 temporally
11 promotes neural progenitor cell maintenance through FGF signaling. Genes Dev *26*, 803-
12 815.

13 Chen, X., Castro, S.A., Liu, Q., Hu, W., and Zhang, S. (2019). Practical considerations on
14 performing and analyzing CLIP-seq experiments to identify transcriptomic-wide RNA-
15 protein interactions. Methods *155*, 49-57.

16 Cho, H., Park, O.H., Park, J., Ryu, I., Kim, J., Ko, J., and Kim, Y.K. (2015). Glucocorticoid
17 receptor interacts with PNRC2 in a ligand-dependent manner to recruit UPF1 for rapid
18 mRNA degradation. Proc Natl Acad Sci U S A *112*, E1540-1549.

19 Choe, J., Ahn, S.H., and Kim, Y.K. (2014). The mRNP remodeling mediated by UPF1
20 promotes rapid degradation of replication-dependent histone mRNA. Nucleic Acids Res
21 *42*, 9334-9349.

22 de la Mata, M., Gaidatzis, D., Vitanescu, M., Stadler, M.B., Wentzel, C., Scheiffele, P.,
23 Filipowicz, W., and Grosshans, H. (2015). Potent degradation of neuronal miRNAs
24 induced by highly complementary targets. EMBO Rep *16*, 500-511.

25 Ding, L., and Han, M. (2007). GW182 family proteins are crucial for microRNA-mediated
26 gene silencing. Trends Cell Biol *17*, 411-416.

27 Duy, P.Q., Weise, S.C., Marini, C., Li, X.J., Liang, D., Dahl, P.J., Ma, S., Spajic, A., Dong,
28 W., Juusola, J.*, et al.* (2022). Impaired neurogenesis alters brain biomechanics in a
29 neuroprogenitor-based genetic subtype of congenital hydrocephalus. Nat Neurosci *25*,
30 458-473.

1   Ecsedi, M., and Grosshans, H. (2013). LIN-41/TRIM71: emancipation of a miRNA target.
2   Genes Dev *27*, 581-589.

3   Ecsedi, M., Rausch, M., and Grosshans, H. (2015). The let-7 microRNA directs vulval
4   development through a single target. Dev Cell *32*, 335-344.

5   Elbarbary, R.A., Miyoshi, K., Hedaya, O., Myers, J.R., and Maquat, L.E. (2017). UPF1
6   helicase promotes TSN-mediated miRNA decay. Genes Dev *31*, 1483-1493.

7   Elkayam, E., Faehnle, C.R., Morales, M., Sun, J., Li, H., and Joshua-Tor, L. (2017).
8   Multivalent Recruitment of Human Argonaute by GW182. Mol Cell *67*, 646-658 e643.

9   Eulalio, A., Huntzinger, E., and Izaurralde, E. (2008). GW182 interaction with Argonaute
10   is essential for miRNA-mediated translational repression and mRNA decay. Nat Struct
11   Mol Biol *15*, 346-353.

12   Furey, C.G., Choi, J., Jin, S.C., Zeng, X., Timberlake, A.T., Nelson-Williams, C., Mansuri,
13   M.S., Lu, Q., Duran, D., Panchagnula, S.*, et al.* (2018). De Novo Mutation in Genes
14   Regulating Neural Stem Cell Fate in Human Congenital Hydrocephalus. Neuron *99*, 302-
15   314 e304.

16   Hauptmann, J., Schraivogel, D., Bruckmann, A., Manickavel, S., Jakob, L., Eichner, N.,
17   Pfaff, J., Urban, M., Sprunck, S., Hafner, M.*, et al.* (2015). Biochemical isolation of
18   Argonaute protein complexes by Ago-APP. Proc Natl Acad Sci U S A *112*, 11841-11845.

19   Hicks, J.A., Li, L., Matsui, M., Chu, Y., Volkov, O., Johnson, K.C., and Corey, D.R. (2017).
20   Human GW182 Paralogs Are the Central Organizers for RNA-Mediated Control of
21   Transcription. Cell Rep *20*, 1543-1552.

22   Hoepfner, D., McAllister, G., and Hoffman, G.R. (2019). CRISPR/Cas9-Based
23   Chemogenomic Profiling in Mammalian Cells. Methods Mol Biol *1888*, 153-174.

24   Jakymiw, A., Lian, S., Eystathioy, T., Li, S., Satoh, M., Hamel, J.C., Fritzler, M.J., and
25   Chan, E.K. (2005). Disruption of GW bodies impairs mammalian RNA interference. Nat
26   Cell Biol *7*, 1267-1274.

27   Jin, S.C., Dong, W., Kundishora, A.J., Panchagnula, S., Moreno-De-Luca, A., Furey,
28   C.G., Allocco, A.A., Walker, R.L., Nelson-Williams, C., Smith, H.*, et al.* (2020). Exome
29   sequencing implicates genetic disruption of prenatal neuro-gliogenesis in sporadic
30   congenital hydrocephalus. Nat Med *26*, 1754-1765.

1 Johnson, S.T., Chu, Y., Liu, J., and Corey, D.R. (2021). Impact of scaffolding protein
2 TNRC6 paralogs on gene expression and splicing. RNA *27*, 1004-1016.

3 Kaygun, H., and Marzluff, W.F. (2005). Regulated degradation of replication-dependent
4 histone mRNAs requires both ATR and Upf1. Nat Struct Mol Biol *12*, 794-800.

5 Kim, Y.K., Furic, L., DesGroseillers, L., and Maquat, L.E. (2005). Mammalian Staufen1
6 recruits Upf1 to specific mRNA 3′ UTRs so as to elicit mRNA decay. Cell *120*, 195-208.

7 Kim, Y.K., and Maquat, L.E. (2019). UPFront and center in RNA decay: UPF1 in
8 nonsense-mediated mRNA decay and beyond. RNA *25*, 407-422.

9 Kumari, P., Aeschimann, F., Gaidatzis, D., Keusch, J.J., Ghosh, P., Neagu, A.,
10 Pachulska-Wieczorek, K., Bujnicki, J.M., Gut, H., Grosshans, H.*, et al.* (2018).
11 Evolutionary plasticity of the NHL domain underlies distinct solutions to RNA recognition.
12 Nat Commun *9*, 1549.

13 Lavysh, D., and Neu-Yilik, G. (2020). UPF1-Mediated RNA Decay-Danse Macabre in a
14 Cloud. Biomolecules *10*, 999.

15 Lazzaretti, D., Tournier, I., and Izaurralde, E. (2009). The C-terminal domains of human
16 TNRC6A, TNRC6B, and TNRC6C silence bound transcripts independently of Argonaute
17 proteins. RNA *15*, 1059-1066.

18 Li, X., Pritykin, Y., Concepcion, C.P., Lu, Y., La Rocca, G., Zhang, M., King, B., Cook,
19 P.J., Au, Y.W., Popow, O.*, et al.* (2020). High-Resolution In Vivo Identification of miRNA
20 Targets by Halo-Enhanced Ago2 Pull-Down. Mol Cell *79*, 167-179 e111.

21 Lian, S.L., Li, S., Abadal, G.X., Pauley, B.A., Fritzler, M.J., and Chan, E.K. (2009). The
22 C-terminal half of human Ago2 binds to multiple GW-rich regions of GW182 and requires
23 GW182 to mediate silencing. RNA *15*, 804-813.

24 Lienert, F., Wirbelauer, C., Som, I., Dean, A., Mohn, F., and Schubeler, D. (2011).
25 Identification of genetic elements that autonomously determine DNA methylation states.
26 Nat Genet *43*, 1091-U1078.

27 Lin, S., and Gregory, R.I. (2015). MicroRNA biogenesis pathways in cancer. Nat Rev
28 Cancer *15*, 321-333.

29 Liu, J., Rivas, F.V., Wohlschlegel, J., Yates, J.R., 3rd, Parker, R., and Hannon, G.J.
30 (2005). A role for the P-body component GW182 in microRNA function. Nat Cell Biol *7*,
31 1261-1266.

1   Liu, Q.Y., Chen, X.L., Novak, M.K., Zhang, S.J., and Hu, W.Q. (2021). Repressing Ago2

2   mRNA translation by Trim71 maintains pluripotency through inhibiting let-7 microRNAs.

3   Elife *10*, e66288.

4   Liu, Z., Johnson, S.T., Zhang, Z., and Corey, D.R. (2019). Expression of TNRC6 (GW182)

5   proteins Is not necessary for gene silencing by fully complementary RNA duplexes.

6   Nucleic Acid Ther *29*, 323-334.

7   Loedige, I., Gaidatzis, D., Sack, R., Meister, G., and Filipowicz, W. (2013). The

8   mammalian TRIM-NHL protein TRIM71/LIN-41 is a repressor of mRNA function. Nucleic

9   Acids Res *41*, 518-532.

10 Lykke-Andersen, K., Gilchrist, M.J., Grabarek, J.B., Das, P., Miska, E., and Zernicka-

11 Goetz, M. (2008). Maternal Argonaute 2 Is Essential for Early Mouse Development at the

12 Maternal-Zygotic Transition. Mol Biol Cell *19*, 4383-4392.

13 Maller Schulman, B.R., Liang, X., Stahlhut, C., DelConte, C., Stefani, G., and Slack, F.J.

14 (2008). The let-7 microRNA target gene, Mlin41/Trim71 is required for mouse embryonic

15 survival and neural tube closure. Cell Cycle *7*, 3935-3942.

16 Martinez, N.J., and Gregory, R.I. (2013). Argonaute2 expression is post-transcriptionally

17 coupled to microRNA abundance. RNA *19*, 605-612.

18 Mathys, H., Basquin, J., Ozgur, S., Czarnocki-Cieciura, M., Bonneau, F., Aartse, A.,

19 Dziembowski, A., Nowotny, M., Conti, E., and Filipowicz, W. (2014). Structural and

20 biochemical insights to the role of the CCR4-NOT complex and DDX6 ATPase in

21 microRNA repression. Mol Cell *54*, 751-765.

22 Meister, G., Landthaler, M., Peters, L., Chen, P.Y., Urlaub, H., Luhrmann, R., and Tuschl,

23 T. (2005). Identification of novel argonaute-associated proteins. Curr Biol *15*, 2149-2155.

24 Michlits, G., Jude, J., Hinterndorfer, M., de Almeida, M., Vainorius, G., Hubmann, M.,

25 Neumann, T., Schleiffer, A., Burkard, T.R., Fellner, M.*, et al.* (2020). Multilayered VBC

26 score predicts sgRNAs that efficiently generate loss-of-function alleles. Nat Methods *17*,

27 708-716.

28 Mino, T., Murakawa, Y., Fukao, A., Vandenbon, A., Wessels, H.H., Ori, D., Uehata, T.,

29 Tartey, S., Akira, S., Suzuki, Y.*, et al.* (2015). Regnase-1 and Roquin Regulate a Common

30 Element in Inflammatory mRNAs by Spatiotemporally Distinct Mechanisms. Cell *161*,

31 1058-1073.

1   Mitschka, S., Ulas, T., Goller, T., Schneider, K., Egert, A., Mertens, J., Brustle, O.,
2   Schorle, H., Beyer, M., Klee, K.*, et al.* (2015). Co-existence of intact stemness and priming
3   of neural differentiation programs in mES cells lacking Trim71. Sci Rep *5*, 11126.
4   Ostapcuk, V., Mohn, F., Carl, S.H., Basters, A., Hess, D., Iesmantavicius, V.,
5   Lampersberger, L., Flemr, M., Pandey, A., Thoma, N.H.*, et al.* (2018). Activity-dependent
6   neuroprotective protein recruits HP1 and CHD4 to control lineage-specifying genes.
7   Nature *557*, 739-743.
8   Park, O.H., Park, J., Yu, M., An, H.T., Ko, J., and Kim, Y.K. (2016). Identification and
9   molecular characterization of cellular factors required for glucocorticoid receptor-
10 mediated mRNA decay. Genes Dev *30*, 2093-2105.
11 Perez-Riverol, Y., Bai, J., Bandla, C., Garcia-Seisdedos, D., Hewapathirana, S.,
12 Kamatchinathan, S., Kundu, D.J., Prakash, A., Frericks-Zipper, A., Eisenacher, M.*, et al.*
13 (2022). The PRIDE database resources in 2022: a hub for mass spectrometry-based
14 proteomics evidences. Nucleic Acids Res *50*, D543-D552.
15 Rybak, A., Fuchs, H., Smirnova, L., Brandt, C., Pohl, E.E., Nitsch, R., and Wulczyn, F.G.
16 (2008). A feedback loop comprising lin-28 and let-7 controls pre-let-7 maturation during
17 neural stem-cell commitment. Nat Cell Biol *10*, 987-993.
18 Sheu-Gruttadauria, J., and MacRae, I.J. (2018). Phase Transitions in the Assembly and
19 Function of Human miRISC. Cell *173*, 946-957 e916.
20 Slack, F.J., Basson, M., Liu, Z., Ambros, V., Horvitz, H.R., and Ruvkun, G. (2000). The
21 lin-41 RBCC gene acts in the C. elegans heterochronic pathway between the let-7
22 regulatory RNA and the LIN-29 transcription factor. Mol Cell *5*, 659-669.
23 Smibert, P., Yang, J.S., Azzam, G., Liu, J.L., and Lai, E.C. (2013). Homeostatic control
24 of Argonaute stability by microRNA availability. Nat Struct Mol Biol *20*, 789-795.
25 Takimoto, K., Wakiyama, M., and Yokoyama, S. (2009). Mammalian GW182 contains
26 multiple Argonaute-binding sites and functions in microRNA-mediated translational
27 repression. RNA *15*, 1078-1089.
28 Torres-Fernández, L.A., Emich, J., Port, Y., Mitschka, S., Wöste, M., Schneider, S., Fietz,
29 D., Oud, M.S., Di Persio, S., and Neuhaus, N. (2021a). TRIM71 deficiency causes germ
30 cell loss during mouse embryogenesis and is associated with human male infertility. Front
31 Cell Dev Biol *9*, 970.

1 Torres-Fernández, L.A., Jux, B., Bille, M., Port, Y., Schneider, K., Geyer, M., Mayer, G., and Kolanus, W. (2019). The mRNA repressor TRIM71 cooperates with Nonsense-Mediated Decay factors to destabilize the mRNA of CDKN1A/p21. Nucleic Acids Res *47*, 11861-11879.

5 Torres-Fernández, L.A., Mitschka, S., Ulas, T., Weise, S., Dahm, K., Becker, M., Händler, K., Beyer, M., Windhausen, J., and Schultze, J.L. (2021b). The stem cell–specific protein TRIM71 inhibits maturation and activity of the prodifferentiation miRNA let-7 via two independent molecular mechanisms. RNA *27*, 805-828.

9 Treiber, T., Treiber, N., Plessmann, U., Harlander, S., Daiss, J.L., Eichner, N., Lehmann, G., Schall, K., Urlaub, H., and Meister, G. (2017). A Compendium of RNA-Binding Proteins that Regulate MicroRNA Biogenesis. Mol Cell *66*, 270-284 e213.

12 Vieira-Vieira, C.H., and Selbach, M. (2021). Opportunities and Challenges in Global Quantification of RNA-Protein Interaction via UV Cross-Linking. Front Mol Biosci *8*, 669939.

15 Wang, J., Lee, J.E., Riemondy, K., Yu, Y., Marquez, S.M., Lai, E.C., and Yi, R. (2020). XPO5 promotes primary miRNA processing independently of RanGTP. Nat Commun *11*, 1845.

18 Wang, L., Su, Y., Huang, C., Yin, Y., Chu, A., Knupp, A., and Tang, Y. (2019). NANOG and LIN28 dramatically improve human cell reprogramming by modulating LIN41 and canonical WNT activities. Biol Open *8*.

21 Welte, T., Tuck, A.C., Papasaikas, P., Carl, S.H., Flemr, M., Knuckles, P., Rankova, A., Buhler, M., and Grosshans, H. (2019). The RNA hairpin binder TRIM71 modulates alternative splicing by repressing MBNL1. Genes Dev *33*, 1221-1235.

24 Worringer, K.A., Rand, T.A., Hayashi, Y., Sami, S., Takahashi, K., Tanabe, K., Narita, M., Srivastava, D., and Yamanaka, S. (2014). The let-7/LIN-41 pathway regulates reprogramming to human induced pluripotent stem cells by controlling expression of prodifferentiation genes. Cell Stem Cell *14*, 40-52.

28 Zeng, H., Lu, B., Zamponi, R., Yang, Z., Wetzel, K., Loureiro, J., Mohammadi, S., Beibel, M., Bergling, S., and Reece-Hoyes, J. (2018). mTORC1 signaling suppresses Wnt/β-catenin signaling through DVL-dependent regulation of Wnt receptor FZD level. Proc Natl Acad Sci U S A *115*, E10362-E10369.

1   Zipprich, J.T., Bhattacharyya, S., Mathys, H., and Filipowicz, W. (2009). Importance of

2   the C-terminal domain of the human GW182 protein TNRC6C for translational repression.

3   RNA *15*, 781-793.

4

5

1   **Convergence of distinct RNA-silencing pathways on GW182/TNRC6**

2

3   Thomas Welte, Alison Goulois, Michael B. Stadler, Daniel Hess, Charlotte Soneson,

4   Anca Neagu, Chiara Azzi, Marlena J. Lübke, Jan Seebacher, Isabel Schmidt, David

5   Estoppey, Florian Nigsch, John Reece-Hoyes, Dominic Hoepfner, Helge Großhans

6

7

8

9

10   **Supplemental Material**

11   Supplemental Methods

12   Supplemental Figure S1 – 10

13   Legends for Supplemental Table S1 – 3 (Excel files not included in this document)

14   Supplemental Table S4 – 9

15   Supplemental References

16

17

18

19

1   **Supplemental Methods**

2   **Generation of cell lines:**

3   *mESC Cas9::BSD:*
4   3×10^6 TC-1 mESCs (background 129S6/SvEvTac, gift from D. Schübeler with a
5   recombinase-mediated cassette exchange (RMCE) site located in the gamma-globin
6   gene locus(Lienert et al., 2011) were transfected with 3 µg of pC2P *Cas9::BSD* (pTW71,
7   see **Supplemental Table S6A**), followed by Blasticidin selection. Transfections were
8   carried out using Lipofectamine 2000 [Invitrogen; L2000] reagent at 3.3 µl/µg ratio in Opti-
9   MEM medium [Gibco; 31985062]. Single clones were isolated and tested for Cas9
10   expression by Western Blot and Cas9 staining. The optimal titer for viral transfection was
11   determined using a reference virus expressing RFP. Cas9 editing capability verified via a
12   FLAER-Assay according to manufacturers' instructions(Brodsky, 2009) Briefly, 50,000
13   cells were plated, infected with either gRNA targeting the PIG-A gene or control virus in
14   ESC media containing 10 µg/ml polybrene on day one, and were selected with Puromycin
15   at 1 µg/ml for three days from day two. On day seven, 200,000 suspended cells were
16   stained with 1:100 FLAER reagent in 3 % BSA, fixed in 4% fomaldehyde in PBS, and the
17   ratio of FLAER-negative cells was determined by FACS direcly correlating with Cas9
18   mediated editing (**Supplemental Figure S1A-C**).
19
20   *mESC Cas9::BSD, yGlob (GFP_Ctrl & GFP_5xT71BS):*
21   These cell lines were generated using RMCE as described previously(Lienert et al., 2011;
22   Yang et al., 2006), using pL1_1L_pCAG_GFP::unc54 3UTR (*'GFP_Ctrl'*; pTW97) &
23   pL1_1L_pCAG_GFP::unc54::mab10$_{condensed}$ 3UTR (*'GFP_5xT71BS'*; pTW98).
24
25   *mESC Cas9::BSD, yGlob (GFP_Ctrl & GFP_5xT71BS) Trim71$^{-/-}$, Ago$^{-/-}$, Dicer$^{-/-}$, Xpo5$^{-/-}$:*
26   5×10^5 *mESC Cas9::BSD, yGlob (GFP_Ctrl & GFP_5xT71BS)* were seeded per well in 6-
27   well plates. Cells were transfected with 2 µg of respective pC2P sgRNA plasmids
28   (sgRNAs: see **Supplemental Table S4**). After 24 h of transfection, cells were selected
29   with Puromycin at 1 µg/ml for 50 hours. Knockout was confirmed by Western Blotting.
30
31   *mESC Cas9::BSD, yGlob (GFP_5xT71BS), HA-AVI-Tnrc6a:*
32   5×10^5 cells were transfected with 1 µg each of pC2P Tnrc6a_sgRNA-Nterm and
33   ssODN_Tnrc6a_HAAVI (see **Supplemental Table S5**). Transfected cells were selected
34   by Puromycin at 1 µg/ml 24 h after transfection, followed by clonal selection and
35   genotyping (Primers: see **Supplemental Table S7A**).
36
37   *mESC Cas9::BSD, yGlob (GFP_5xT71BS), HA-AVI-Tnrc6a Trim71$^{-/-}$, Ago$^{-/-}$:*
38   5×10^5 *mESC Cas9::BSD, yGlob (GFP_5xT71BS), HA-AVI-Tnrc6a* were seeded per well
39   in 6-well plates. Cells were transfected with 2 µg of respective pC2P sgRNA plasmids
40   (sgRNAs: see **Supplemental Table S4**). After 24 h of transfection, cells were selected
41   with Puromycin at 1 µg/ml for 50 hours. Knockout was confirmed by Western Blotting.
42

1 *mESC Cas9::BSD, yGlob (GFP_5xT71BS) FLAG-HA-T6B$_{WT}$::mCherry, mESC*
2 *Cas9::BSD, yGlob (GFP_5xT71BS) FLAG-HA-T6B$_{MUT}$::mCherry:*
3 5×10^5 cells were transfected with 2 µg each of pCIP FH-T6B$_{WT}$::mCherry (pTW114), pCIP
4 FH-T6B$_{MUT}$::mCherry (pTW115). Transfected cells were selected by Puromycin at 1 µg/ml
5 24 h after transfection for 7 days, followed by one round of FACS-sorting (for mCherry
6 fusion proteins) to exclude mCherry-negative cells. Expression of constructs was
7 evaluated by Western Blot.
8

9

10 **Molecular cloning:**

11 Primer sequences for the generation of the respective plasmid number can be found in

12 **Supplemental Table S7B, S7C**.

13 *Generation of pC2P Cas9::BSD (pTW71):*
14 pC2P *Cas9::BSD* (pTW71) was created from pTW42(Welte et al., 2019). Deletion of the
15 U6 promoter plus sgRNA scaffold was achieved by digestion with *Pcl*I, *Kpn*I, blunting and
16 ligation. Exchange of Puromycin to Blasticidin was achieved by digestion with *Spe*I, *Not*I.
17 Blasticidin was amplified from pEF1-B (Matyas Flemr). BGHPA was amplified from pC2P
18 (pTW71). Fragments were assembled by Gibson assembly.
19
20 *Generation of pL1_1L_CAG_GFP::unc54 3UTR ('GFP_Ctrl', pTW97) and*
21 *pL1_1L_CAG_GFP::unc54::mab10$_{condensed}$ 3UTR ('GFP_5xT71BS', pTW98):*
22 pTW47 (*GFP_Ctrl*) and pTW48 (*GFP_5xT71BS*)(Welte et al., 2019) were digested with
23 *Spe*I/*Pac*I to cut out the expression cassette (Promoter, GFP, 3UTR, poly-A sequence).
24 pL1_1L was amplified from pL1_LPP-1_1L(Lienert et al., 2011). Fragments were
25 assembled by Gibson assembly.
26
27 *pC2P Ago2, Dicer1, Xpo5, Tnrc6a sgRNA plasmids:*
28 Plasmids were generated by cloning sgRNAs into pC2P as described previously(Welte
29 et al., 2019). A list of sgRNAs can be found in **Supplemental Table S4**.
30
31 *Generation of pCIP Ago2 (pTW110), pCIP FH-HsTNRC6A (pTW111), pCIP FH-*
32 *HsTNRC6C (pTW113):*
33 MmuAgo2, FH-HsTNRC6A, and FH-HsTNR6C were amplified from Addgene plasmids
34 #73538, #19883, #19885, respectively. Fragments were Gibson-assembled into the
35 *BamHI* site of pCIP (Addgene #79009).
36
37 *Generation of pCIP HA-HsTNRC6B (pTW112)*:

1   HsTNRC6B was amplified from Addgene plasmid #10979. The FH-Tag was amplified
2   from pCIP FH-HsTNRC6A (pTW111). Fragments were Gibson-assembled into the
3   *BamHI* site of pCIP (Addgene #79009).
4
5   *Generation of pCIP FH_T6B_{WT}_mCherry and pCIP FH_T6B_{MUT}_mCherry (pTW114,*
6   *pTW115):*
7   Plasmids   were   generated   by   cloning   FH_T6B_eYFP   and
8   FH_T6B_mut_eYFP(Hauptmann et al., 2015) into the BamHI restriction site of pCIP by
9   Gibson assembly. EYFP from FH_T6B_eYFP and FH_T6B_mut_eYFP was replaced
10 with mCherry by digestion with *Pac*I and *Not*I. mCherry was amplified from pTW51(Welte
11 et al., 2019). Fragments were Gibson-assembled.
12
13 *Luciferase reporter gene constructs:*
14 *psiCHECK-2 Abcd3_3'UTR (pTW132), Nt5cd3_3'UTR (pTW133), Spty2d1_3'UTR*
15 *(pTW134), Ankib1_3'UTR (pTW135), Hars2_3'UTR (pTW136), St3gal4_3'UTR*
16 *(pTW137), Ier5_3'UTR (pTW138), Erbb3_3'UTR (pTW139):* 3' UTRs were amplified from
17 mESC genomic DNA and Gibson-assembled into the NotI-site of psiCHECK-2.
18

19 **Bioinformatic analyses**

20 Bioinformatic analyses and data visualization were performed in R v4.1.1. and v.4.1.2 (R

21 Core Team, 2021).

22 *sgRNA screens*

23 SgRNA counts were generated by aligning raw sequences to the reference libraries using

24 Bowtie(Langmead et al., 2009), allowing for no mismatches. Normalization and

25 differential fold change estimates between samples for each sgRNA were generated

26 using edgeR(Robinson et al., 2010), version 3.28.0, using the functions *calcNormFactors*

27 with raw sgRNA counts and default parameters as inputs and *cpm* with parameters "log

28 = TRUE, prior.count = 4.0". Log$_2$ fold changes for contrasts of interest were then

29 calculated by subtracting the normalized log-transformed counts return by *cpm*.

30 *Genome-wide screen:* SgRNAs with TRIM71-specific effects were filtered, using the

31 following contrasts:

1 *Contrast 1:* Unsorted cell lines (*GFP_Ctrl* vs *GFP_5xT71BS*) for differences between the

2 genotypes that are unrelated to GFP expression:

3 *Contrast 2:* Sorted negative control cell lines (*GFP_Ctrl* positive vs negative) for effects

4 on GFP expression that are unrelated to the TRIM71 pathway.

5 *Contrast 3:* Sorted positive control cell lines (*GFP_5xT71BS* positive vs negative) for

6 effects on GFP expression that are both related and unrelated to the TRIM71 pathway.

7 *Contrast 4:* Contrast 3 - │Contrast 1│ for removing unwanted genotype effects in any

8 direction.

9 *Contrast 5:* Contrast 3 – Contrast 2 for removing TRIM71-unrelated effects on GFP

10 expression.

11 A z-score ('score.up') was calculated for contrasts 4 and 5, by subtracting the mean and

12 dividing by the standard deviation over all sgRNAs, resulting in a ranking of sgRNAs

13 according to their effect on GFP expression specific to the TRIM71 pathway. Effects of

14 sgRNAs per gene were summarized by calculating the median of fold changes for all

15 sgRNAs per gene. **Genes for the validation screen were chosen based on this z-**

16 **score.**

17

18 *Validation screen and comparison of screens:* As no unsorted samples were obtained,

19 only contrasts 2, 3, and 5 were calculated (see genome-wide screen). These contrasts

20 were used for comparing genome-wide and validation screens.

21

1   *Visualisation of sgRNA screens:* (**Figure 1C, D**) were plotted using *Contrast 3* for negative

2   control ('logFC.GFP.neg.control'; x-axis) and positive control cells

3   ('logFC.GFP.pos.control'; y-axis) for genome-wide (**Figure 1C**) and validation (**Figure**

4   **1D**) screens. (**Figure 1E**) was plotted using *Contrast 5* ('logFC.GFP.pathwayControlled')

5   for the genome-wide (x-axis) and the validation screen (y-axis). Data source:

6   **Supplemental Table S1**.

7

8   *RNA-seq and RIP-seq analysis*

9   Alignment and differential gene expression analysis for RNA-seq experiments was

10 performed as follows: Samples were aligned against the GRCm38 mouse genome

11 assembly from GENCODE(Frankish et al., 2021), primary assembly from release M24).

12 Alignments were performed using STAR version 2.7.3a with settings --outFilterType

13 BySJout --outFilterMultimapNmax 20 --outMultimapperOrder Random --

14 alignSJoverhangMin 8 --alignSJDBoverhangMin 1 --outFilterMismatchNmax 999 --

15 alignIntronMin 20 --alignIntronMax 1000000 --alignMatesGapMax 1000000 --

16 outSAMmultNmax 1 (Gaidatzis et al., 2015). These settings follow ENCODE guidelines

17 and report a single randomly selected alignment for reads that map to the genome no

18 more than 20 times(Langmead et al., 2009). Gene annotations were also obtained from

19 GENCODE release M24, transforming the gtf file into a Bioconductor TxDb object using

20 the makeTxDbFromGFF function from the GenomicFeatures package (version

21 1.44.0(Lawrence et al., 2013)). Gene-level read counts were obtained by summing the

22 counts from the union of all exons per gene, using the qCount function from the QuasR

23 package (v1.32.0(Gaidatzis et al., 2015)) with the created TxDb and parameters

1. orientation = 'opposite'. EdgeR (v3.34.1(Robinson et al., 2010)) was used to test for

2. differentially enriched genes in different conditions, using a likelihood ratio test with

3. Benjamini-Hochberg multiple hypothesis testing correction.

4.

5. *RIP-seq normalization and identification of TRIM71, Ago2, and Upf1-dependent TNRC6A*

6. *binding*

7. Alignment and differential enrichment analysis for RIP-seq experiments was performed as
8. described for RNA-seq samples(Robinson et al., 2010), with the following modifications: As we
9. observed increased levels of most features (> 50%) in RNA IP versus input contrasts, library sizes
10. could not be estimated using the calcNormFactors function which assumes that less than half of
11. the features are differential. We therefore first identified features that are depleted in IP
12. versus input (have a $\log_2$ fold-change less than zero) using a default normalization approach,
13. assuming that these features can be safely assumed to correspond to non-enriched features.
14. Next, we used the raw counts of these features (at least 3,700) for estimation of library sizes and
15. calculation of normalization factors using calcNormFactors. The resulting normalization factors
16. were then applied to the analysis of all features. TRIM71 and AGO2 targets were identified as
17. transcripts with significantly reduced IP versus input TNRC6A enrichment (FDR ≤ 0.01 and log2
18. fold-change < 0) in $Trim71^{-/-}$, or $Ago2^{-/-}$ compared to *wildtype* conditions, using the double contrast
19. [(IP_Trim71$^{-/-}$ - input_Trim71$^{-/-}$) - (IP_wildtype – input_wildtype)], or [(IP_Ago2$^{-/-}$ - input_Ago2$^{-/-}$) -
20. (IP_wildtype – input_wildtype)]. UPF1 targets were identified as transcripts with significantly
21. reduced IP versus input TNRC6A enrichment (FDR ≤ 0.05 and log2 fold-change < 0) in $Upf1^{-/-}$,
22. compared to *wildtype* conditions, using the double contrast [(IP_Upf1$^{-/-}$ - input_Upf1$^{-/-}$) -
23. (IP_wildtype – input_wildtype)].

24.

25. *Calculation of AGO2-bound hairpins, and Ago2 transcript enrichment*

26. *AGO2 peak counts*: A file (GSE_mESC_peaks.csv.gz; GSE139345) with annotations for AGO2
27. peaks was downloaded from GEO(Li et al., 2020). Peaks with an adj. *P*-value of ≤ 0.05 were
28. chosen, and peaks per gene were counted. Whole-gene AGO2 enrichments were calculated by
29. summing all peak enrichments per gene.

30.

31. *RNA-seq heatmap*

32. For the RNA-seq heatmap, we included transcripts with significant expression change
33. (FDR ≤ 0.01, $|\log_2$(fold change)| > 1.0 in at least one condition. Expression changes were
34. normalized to control samples (data not shown: *GFP_5xT71BS* - experiment 1;
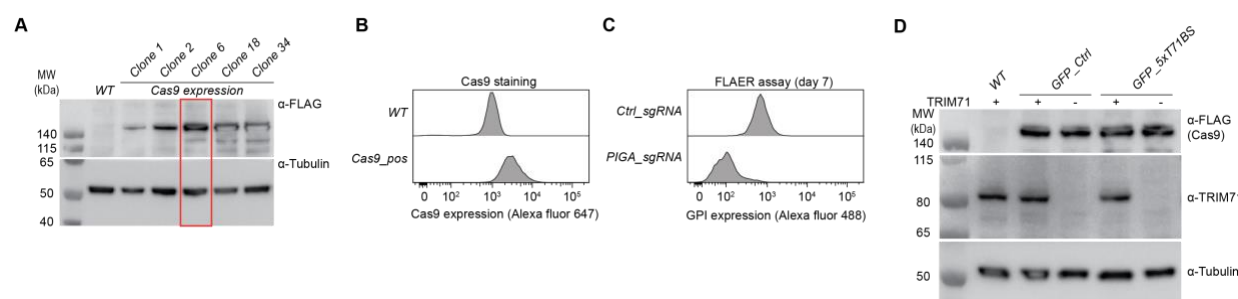35. *GFP_5xT71BS* expressing *T6B$_{MUT}$* - experiment 2).

36. *Mass spectrometry analysis*

56

1   Protein identification and relative quantification of the proteins was performed with

2   MaxQuant v.1.5.3.8 using Andromeda as search engine(Cox et al., 2011), and label-free

3   quantification (LFQ)(Cox et al., 2014; Hubner et al., 2010). The mouse subset of the

4   UniProt v.2021_05 combined with the contaminant database from MaxQuant was

5   searched and the protein and peptide FDR were set to 0.01.

6   The LFQ intensities estimated by MaxQuant were analyzed with the einprot R package

7   (https://github.com/fmicompbio/einprot) v0.4.4. Features classified by MaxQuant as

8   potential contaminants or reverse (decoy) hits or identified only by site, as well as features

9   identified based on a single peptide or with a score below 10, were filtered out. The LFQ

10   intensities were $\log_2$ transformed and missing values were imputed using the 'MinProb'

11   method from the imputeLCMD R package v2.0(Lazar, 2015) with default settings.

12   Pairwise comparisons were performed using limma v3.50.0(Ritchie et al., 2015),

13   considering only features with at least 2 non-imputed values across all the samples in the

14   comparison. Estimated $\log_2$-fold changes and *P*-values (moderated t-test(Smyth, 2004))

15   from limma were used to construct volcano plots.

16

17

18

19

20

21

1

2
3
4
5
6
7
8
9
10
11
12
13
14
15
16
17
18
19
20

21 **Supplemental Figures**

22
23

24 **Supplemental Figure S1. Generation of reporter cell lines for CRISPR-sgRNA-**
25 **screens.**
26 **(A)** Western Blot showing Cas9 levels in different mESC clones. Clone 6 was used for
27 further experiments (**B-D**). **(B)** Cas9 staining showing homogeneous Cas9 expression in
28 Cas9 positive cells in comparison to *WT* cells. **(C)** FLAER assay showing high Cas9
29 editing efficacy in the Cas9-expressing cell line. The assay was quantified after seven
30 days. **(D)** Western Blot showing Cas9 and TRIM71 expression levels in the generated
31 cell lines from **Figure 1A**.

32
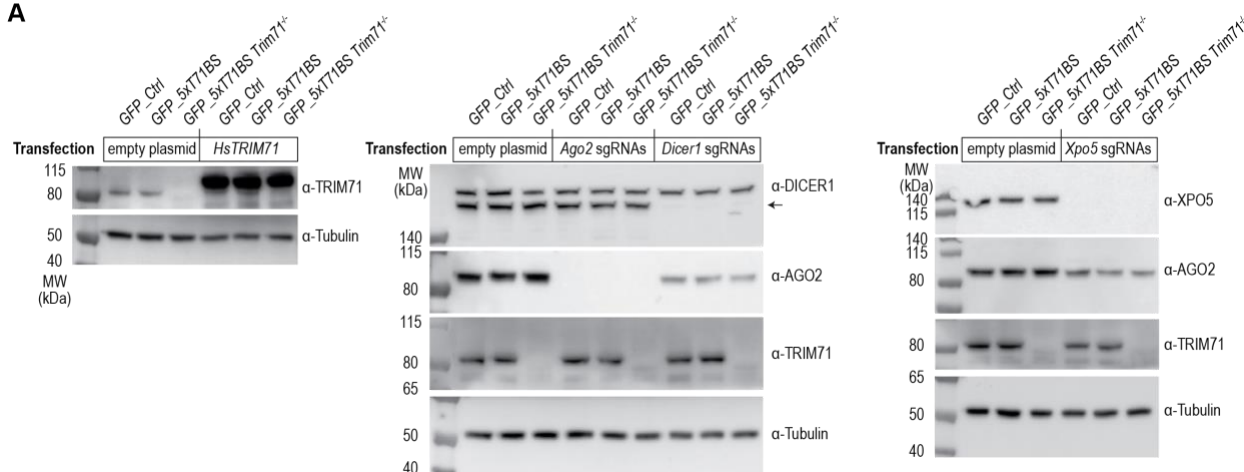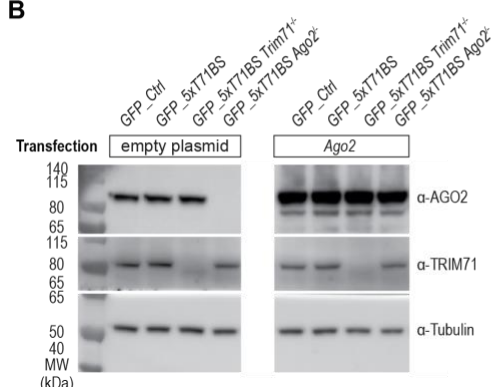
Supplemental Figure S2. Western Blots related to Figure 2.

(A, B) Western Blots showing the effect of transfection with *HsTRIM71* and *Ago2* overexpression plasmids, as well as sgRNAs targeting *Xpo5*, *Dicer1*, *Ago2*. Transfected cell lines are indicated. DICER1 antibodies detect two high-molecular bands. The lower one corresponding to DICER1 is marked with an arrowhead. In (**B**), white space separates lanes spliced together from the same blot (see **Supplemental Figure S8B**).

59
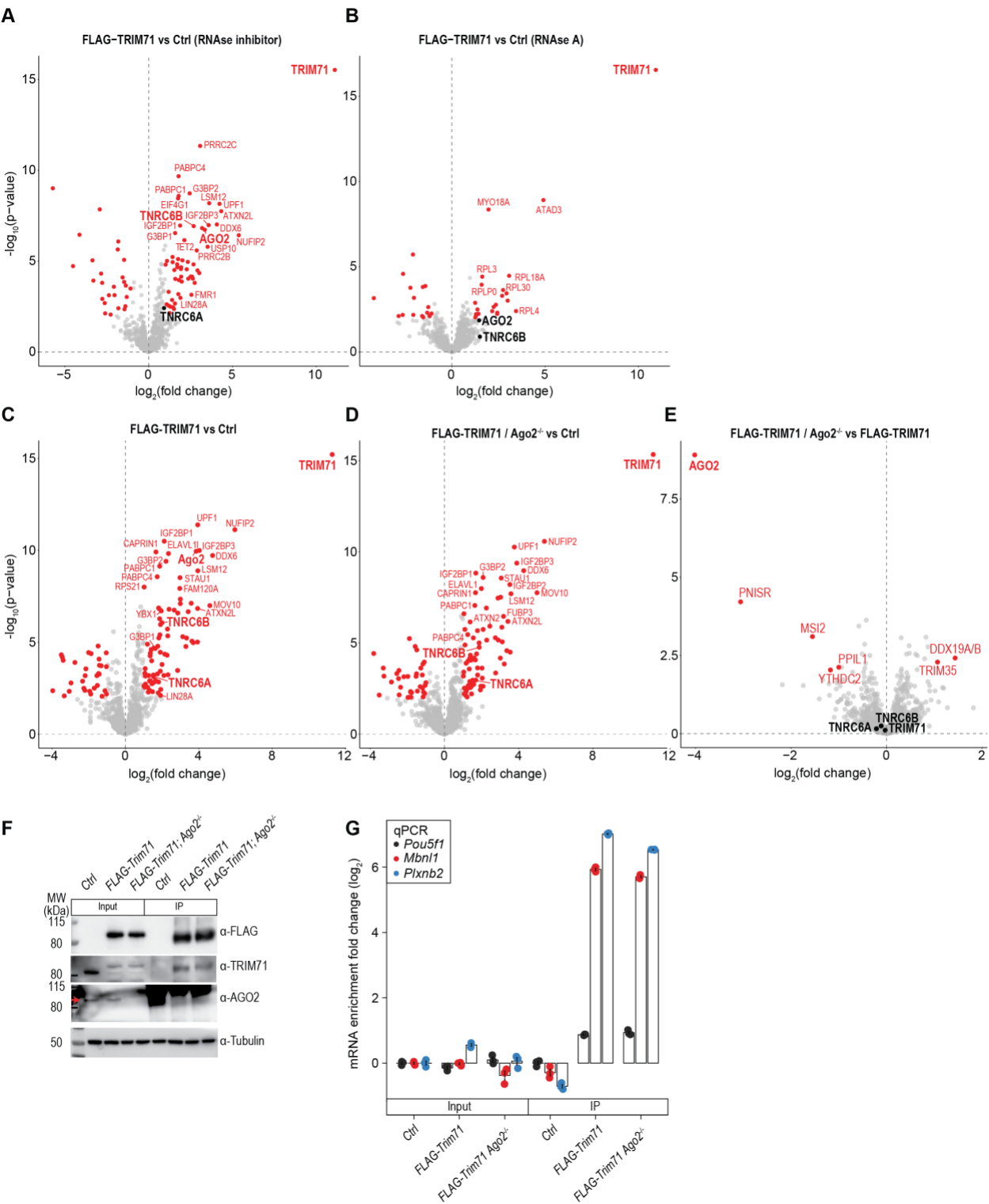
Supplemental Figure S3. TRIM71 interactions are RNA-dependent and independent of AGO2.

(A, B) Volcano plots showing mass spectrometry results of FLAG-AVI-TRIM71 vs untagged control cells in absence **(A)**, and presence **(B)** of RNase A (n = 6 biological

60

1   replicates), FLAG-AVI-TRIM71 $Ago2^{-/-}$ cells vs FLAG-AVI-TRIM71 cells (n = 6 biological
2   replicates; **[C-E]**). Significance was tested using a moderated t-test. Identified proteins
3   with an adjusted P value ≤ 0.01 and |log$_2$(fold change)|≥ 1 are marked in red. Proteins of
4   interest not meeting the significance cutoff are marked in black. Data source:
5   **Supplemental Table S2**. **(F)** Western Blot showing TRIM71, AGO2, and Tubulin
6   expression levels for cells used **in (C-E, G).** Strong background signal from antibody
7   chains was observed in immunoprecipitations with AGO2. AGO2 bands in input fractions
8   are indicated with a red arrow. **(G)** Quantification of RNA immunoprecipitating with FLAG-
9   AVI-TRIM71 by RT-qPCR in presence and absence of AGO2. Data were normalized to
10 WT mESC input levels and represent mean ± SEM. n = 3 biological replicates.
11 Background cell line (**A-G**): 'Ctrl'; mES (129xC57BL/6) $Rosa26^{Cre-ERT2/BirA-V}$.
12
13
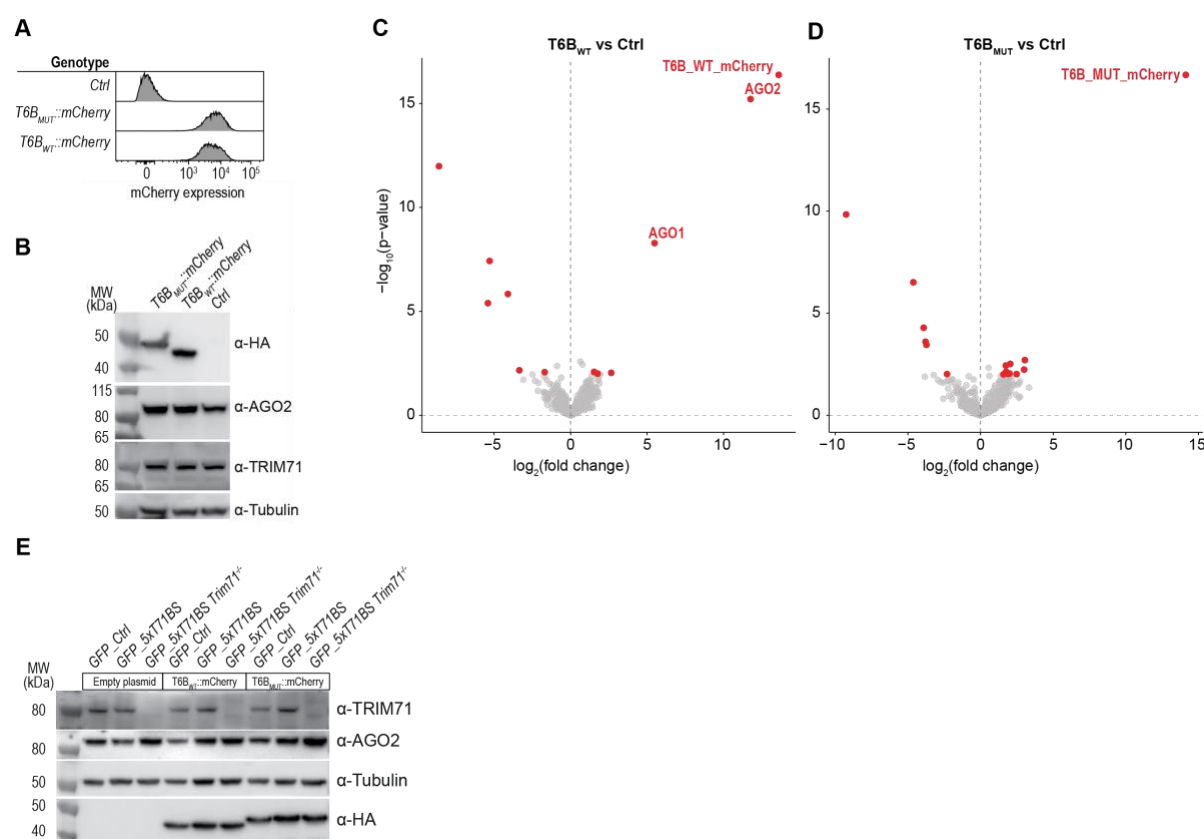
14
15
16 **Supplemental Figure S4. Competition of TRIM71 with AGO2 for TNRC6s.**
17 Flow cytometry plots **(A)** and Western Blot **(B)**, showing expression of untagged control
18 cells, cells stably expressing $HA\text{-}T6B_{WT}::mCherry$, and $HA\text{-}T6B_{MUT}::mCherry$. **(C, D)**
19 Volcano plots showing mass spectrometry results of HA-T6B$_{WT}$::mCherry and HA-
20 T6B$_{MUT}$::mCherry immunoprecipitations (n = 6 biological replicates per condition).
21 Significance was tested using a moderated t-test. Identified proteins with an adjusted P
22 value ≤ 0.01 and |log$_2$(fold change)|≥ 1 are marked in red. Data source: **Supplemental**
23 **Table S2**. Background 'Ctrl' cell line (**A-D**): $GFP\_5xT71BS$ mESCs). **(E)** Western Blots
24 showing overexpression of HA-T6B$_{WT}$::mCherry and HA-T6B$_{MUT}$::mCherry (lowest

61

1 panel), and corresponding TRIM71, AGO2, and Tubulin levels of cells used in (**Figure**
2 **4F**).
3
4
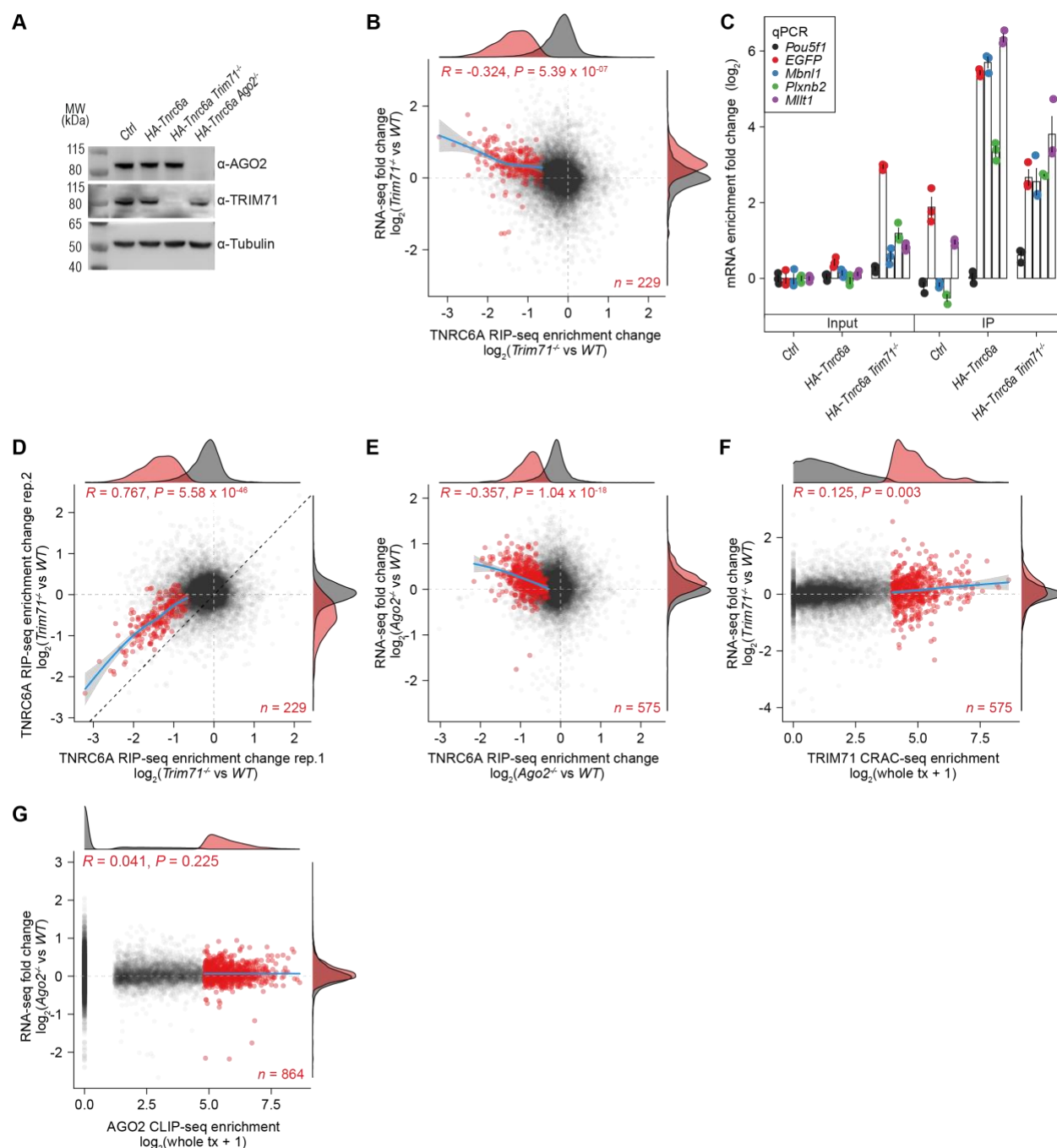
5
6 **Supplemental Figure S5. TNRC6A binds to TRIM71 target transcripts in the**
7 **presence of TRIM71.**
8 **(A)** Western Blot showing TRIM71, AGO2, and Tubulin expression levels in cell lines used

9 for RNA-immunoprecipitation experiments. **(B)** Scatter plot showing changes of TNRC6A

1   transcript enrichment in $Trim71^{-/-}$ vs WT cells as quantified by RIP-seq (x-axis), and

2   changes in transcript level in $Trim71^{-/-}$ vs WT cells as quantified by RNA-seq (y axis). Red

3   color indicates transcripts with significant loss of RIP-seq enrichment (FDR ≤ 0.01,

4   log_2[fold change] < 0). A generalized additive model was fitted to these transcripts (blue

5   line, 95% confidence interval: grey shadow). R indicates Pearson's correlation coefficient

6   calculated for transcripts with significant loss of enrichment. **(C)** Bar plot showing results

7   of an RNA-immunoprecipitation experiment using untagged control cells, ('*Ctrl*'), *HA-AVI-*

8   *Tnrc6a* cells, *HA-AVI-Tnrc6a* cells lacking *Trim71* (*HA-Tnrc6a Trim71$^{-/-}$*). Data were

9   normalized to input *Ctrl* cells and represent mean ± SEM. n = 3 biological replicates. **(D)**

10 Scatter plot showing changes of TNRC6A transcript enrichment in $Trim71^{-/-}$ vs WT cells

11 as quantified by RIP-seq in rep. 1 (x-axis), and rep. 2 (y-axis). Red color indicates

12 transcripts with significant TNRC6A enrichment change in rep. 1. R indicates Pearson's

13 correlation coefficient for transcripts with significant TNRC6A enrichment change in rep.

14 1. **(E)** Scatter plot showing changes of TNRC6A transcript enrichment in $Ago2^{-/-}$ vs WT

15 cells as quantified by RIP-seq (x-axis), and changes in transcript level in $Ago2^{-/-}$ vs WT

16 cells as quantified by RNA-seq (y axis). Red color indicates transcripts with significant

17 loss of RIP-seq enrichment in $Ago2^{-/-}$ vs WT cells (FDR ≤ 0.01, log_2[fold change] < 0). A

18 generalized additive model was fitted to these transcripts (blue line, 95% confidence

19 interval: grey shadow). R is Pearson's correlation coefficient calculated for transcripts with

20 significant loss of enrichment. The corresponding density distributions for (**B, D, E**) are

21 shown on top (x-axis), and to the right (y-axis). P values in (**B, D, E**) are calculated using

22 a paired, two-sided t test for correlation. Background cell line (**B-E**): *GFP_5xT71BS*

23 mESCs. (**F**) Scatter plot showing TRIM71 transcript binding assessed by CRAC-seq (x-

1   axis: $\log_2$[enrichment + 1]; (Welte et al., 2019)) and changes in transcript levels in *Trim71*$^-$

2    $^{/-}$ vs *WT* cells as quantified by RNA-seq (y axis). Red color indicates the 5% most strongly

3   bound transcripts. (**G**) Scatter plot showing AGO2 transcript binding assessed by CLIP-

4   seq (x-axis: $\log_2$[enrichment + 1]; (Li et al., 2020)) and changes in transcript levels in

5   *Ago2*$^{-/-}$ vs *WT* cells as quantified by RNA-seq (y axis). Red color indicates the 5% most

6   strongly bound transcripts. Data source (**A-G**): **Supplemental Table S3**.

7
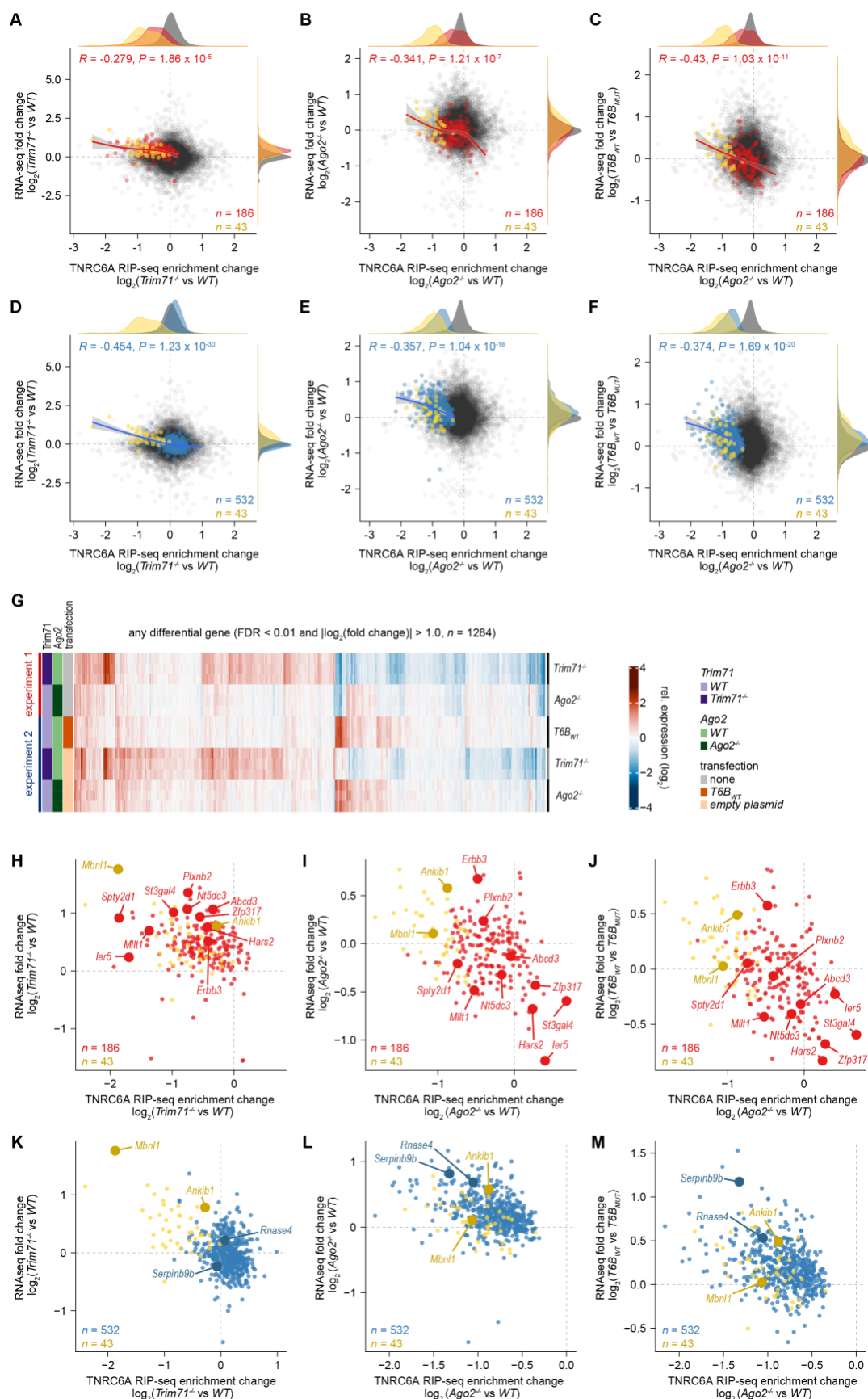
1 **Supplemental Figure S6. TNRC6A RIP-seq identifies TRIM71 and AGO2 target**

2 **transcripts with high precision. Exclusive TRIM71 target transcripts are silenced**

3 **more efficiently in *Ago2* knock-out cells.**

4 **(A, D)** Scatter plots showing changes of TNRC6A transcript enrichment in *Trim71*$^{-/-}$ vs
5 *WT* cells as quantified by RIP-seq (x-axis), and changes in transcript level in *Trim71*$^{-/-}$ vs
6 *WT* cells as quantified by RNA-seq (y axis). **(B, E)** Scatter plots showing changes of
7 TNRC6A transcript enrichment in *Ago2*$^{-/-}$ vs *WT* cells as quantified by RIP-seq (x-axis),
8 and changes in transcript level in *Ago2*$^{-/-}$ vs *WT* cells as quantified by RNA-seq (y axis).
9 **(C, F)** Scatter plots showing changes of TNRC6A transcript enrichment in *Ago2*$^{-/-}$ vs *WT*
10 cells as quantified by RIP-seq (x-axis), and changes in transcript level in *T6B$_{WT}$* vs *T6B$_{MUT}$*
11 cells as quantified by RNA-seq (y axis). Red color indicates transcripts with significant
12 loss of RIP-seq enrichment in *Trim71*$^{-/-}$ vs *WT* cells (FDR ≤ 0.01, log$_2$[fold change] < 0),
13 but not in *Ago2*$^{-/-}$ vs *WT* cells. Blue color indicates transcripts with significant loss of RIP-
14 seq enrichment in *Ago2*$^{-/-}$ vs *WT* cells (FDR ≤ 0.01, log$_2$[fold change) < 0], but not in
15 *Trim71*$^{-/-}$ vs *WT* cells. Yellow color indicates transcripts with significant loss of RIP-seq
16 enrichment in *Trim71*$^{-/-}$ vs *WT* cells, and in *Ago2*$^{-/-}$ vs *WT* cells. **(G)** Heatmap showing
17 gene expression fold changes of differentially expressed genes (FDR ≤ 0.01, |log$_2$(fold
18 change)| > 1 in *Trim71*$^{-/-}$, *Ago2*$^{-/-}$ (experiment 1), and *T6B$_{WT}$*, *Trim71*$^{-/-}$, and *Ago2*$^{-/-}$ cells
19 (experiment 2). Cells in experiment 2 were transfected with either *T6B$_{WT}$*, *T6B$_{MUT}$* or
20 empty plasmid (for *Trim71*$^{-/-}$, and *Ago2*$^{-/-}$ cells), and selected with 1 µg/ml Puromycin for
21 two days, followed by RNA extraction and sequencing. Individual replicates are
22 normalized to the mean of three *WT* cells (for experiment 1), and T6B$_{MUT}$ expressing cells
23 (experiment 2), respectively. **(H-M)** Scatter plots showing transcripts chosen for luciferase
24 assay validation experiments. Coloring as in **(A-F)**. *R* values are Pearson's correlation
25 coefficients, calculated for red and yellow (**A-C**), or blue and yellow (**D-F**) data points. *P*
26 values are calculated using a paired, two-sided t test for correlation. Data source **(A-F, H-**
27 **M)**: **Supplemental Table S3**. Background cell line: *GFP_5xT71BS* mESCs.
28
29
30

31

32
33

66
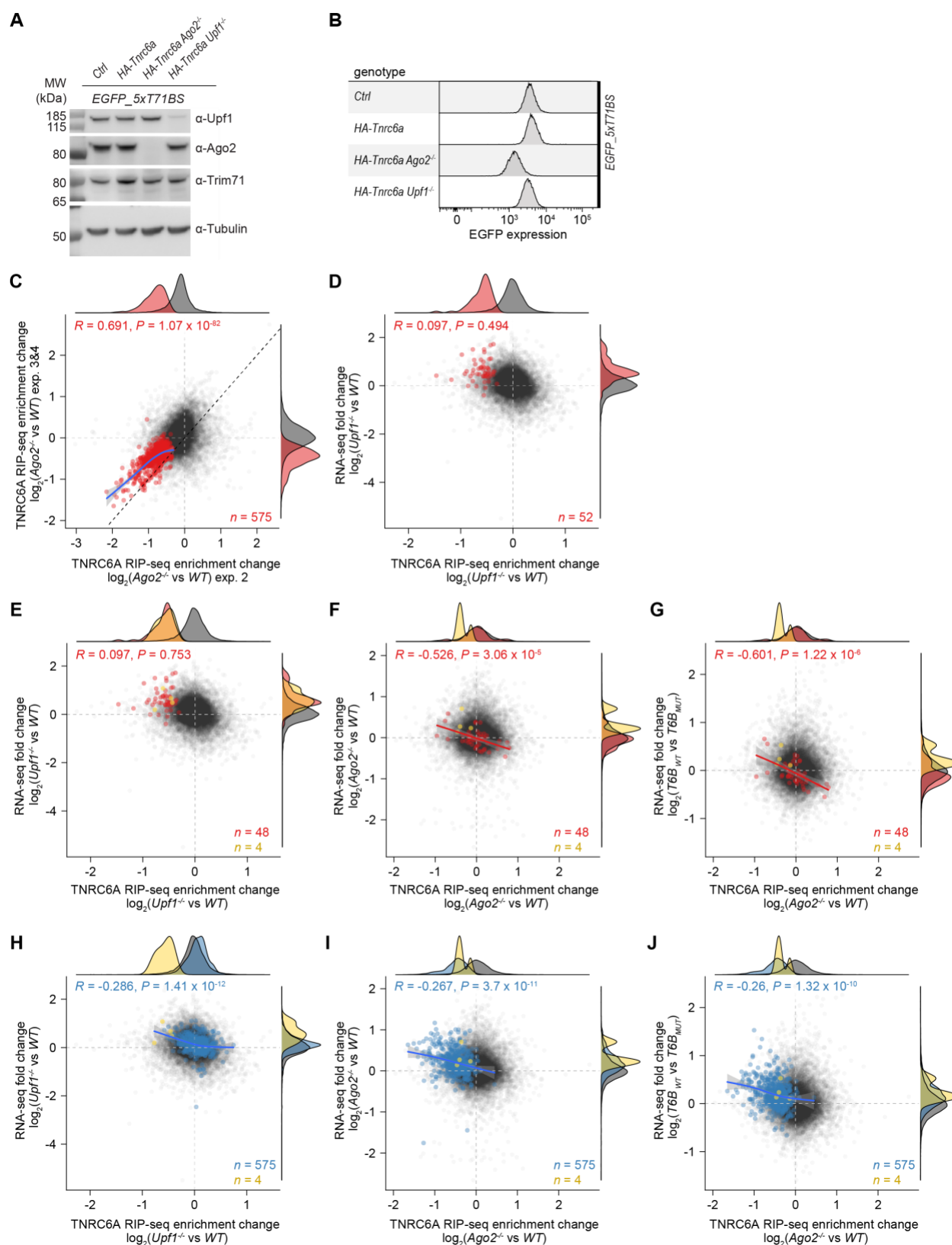
1 **Supplemental Figure S7. TNRC6A RIP-seq identifies UPF1 target transcripts.**

2 **Exclusive UPF1 target transcripts are silenced more efficiently in *Ago2* knock-out**

3 **cells.**

4 **(A)** Western Blot showing UPF1, AGO2, and Tubulin expression levels in cell lines used
5 for RIP-seq experiments. **(B)** Flow cytometry analysis, showing expression of
6 GFP_5xT71BS in cells used for RIP-seq. **(C)** Scatter plot showing changes of TNRC6A
7 transcript enrichment in *Ago2$^{-/-}$* vs *WT* cells as quantified by RIP-seq in exp. 2 (x-axis),
8 and exp. 3&4 (y-axis). Red color indicates transcripts with significant TNRC6A enrichment
9 change in *Ago2$^{-/-}$* vs *WT* cells (FDR ≤ 0.01, log$_2$[fold change] < 0) in exp. 2. *R* indicates
10 Pearson's correlation coefficient for transcripts with significant loss of TNRC6A
11 enrichment in exp. 2. **(D)** Scatter plot showing changes of TNRC6A transcript enrichment
12 in *Upf1$^{-/-}$* vs *WT* cells as quantified by RIP-seq (x-axis), and changes in transcript level in
13 *Upf1$^{-/-}$* vs *WT* cells as quantified by RNA-seq (y axis). Red color indicates transcripts with
14 significant loss of RIP-seq enrichment (FDR ≤ 0.05, log$_2$[fold change] < 0. *R* indicates
15 Pearson's correlation coefficient calculated for transcripts with significant loss of
16 enrichment. **(E, H)** Scatter plots showing changes of TNRC6A transcript enrichment in
17 *Upf1$^{-/-}$* vs *WT* cells as quantified by RIP-seq (x-axis), and changes in transcript level in
18 *Upf1$^{-/-}$* vs *WT* cells as quantified by RNA-seq (y axis). **(F, I)** Scatter plots showing changes
19 of TNRC6A transcript enrichment in *Ago2$^{-/-}$* vs *WT* cells as quantified by RIP-seq (x-axis),
20 and changes in transcript level in *Ago2$^{-/-}$* vs *WT* cells as quantified by RNA-seq (y axis).
21 **(G, J)** Scatter plots showing changes of TNRC6A transcript enrichment in *Ago2$^{-/-}$* vs *WT*
22 cells as quantified by RIP-seq (x-axis), and changes in transcript level in *T6B$_{WT}$* vs *T6B$_{MUT}$*
23 cells as quantified by RNA-seq (y axis). Red color indicates transcripts with significant
24 loss of TNRC6A RIP-seq enrichment in *Upf1$^{-/-}$* vs *WT* cells (FDR ≤ 0.05, log$_2$[fold change]
25 < 0), but not in *Ago2$^{-/-}$* vs *WT* cells. Blue color indicates transcripts with significant loss of
26 RIP-seq enrichment in *Ago2$^{-/-}$* vs *WT* cells (FDR ≤ 0.01, log$_2$[fold change) < 0], but not in
27 *Upf1$^{-/-}$* vs *WT* cells. Yellow color indicates transcripts with significant loss of RIP-seq
28 enrichment in *Upf1$^{-/-}$* vs *WT* cells, and in *Ago2$^{-/-}$* vs *WT* cells. R values are Pearson's
29 correlation coefficients. *P* values are calculated using a paired, two-sided t test for
30 correlation. Data source **(C-J)**: **Supplemental Table S3**. Background cell line:
31 *GFP_5xT71BS* mESCs.
32
33
34
35
36
37
38
39
40
41
42
43

1
2
3
4
5
6
7
8
9
10
11
12
13 **Supplemental uncropped gels.**
14 **Black boxed areas are shown in corresponding figures.**
15
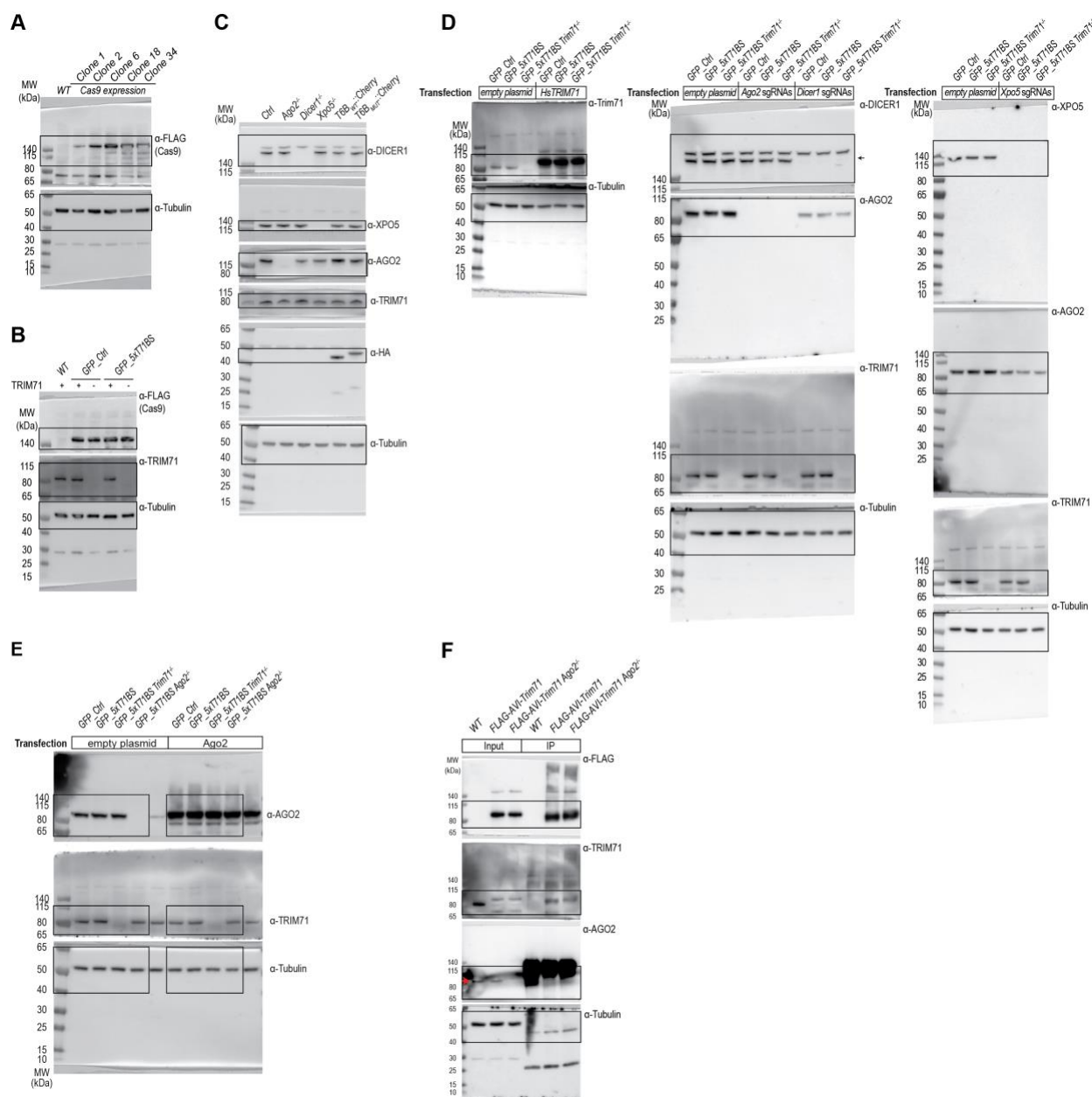
1
2 **Supplemental uncropped gels Figure 1.**
3 **(A)** Gels from **Supplemental Figure S1A**. **(B)** Gels from **Supplemental Figure S1D**. **(C)**
4 Gels from **Figure 2A**. **(D)** Gels from **Supplemental Figure S2A**. **(E)** Gels from
5 **Supplemental Figure S2B**. **(F)** Gels from **Supplemental Figure S3F**.
6
7
8
9
10

1
2
3 **Supplemental uncropped gels Figure 2.**
4 **(A)** Gels from **Figure 3B**.
5
6
7
8
9
10
11

Supplemental uncropped gels Figure 3.
(A) Gels from **Supplemental Figure S4B**. **(B)** Gels from **Supplemental Figure S4E**. **(C)** Gels from **Supplemental Figure S5A**. **(D)** Gels from **Supplemental Figure S7A**.

1

2

3   **Extended Data Tables**

4   **Supplemental Table S1. SgRNA screen results. Related to Figure 1B-D.**

5   Tab 1: genome-wide screen results by sgRNA. Tab 2: genome-wide screen results by

6   gene. Tab 3: validation screen results by sgRNA. Tab 4: validation screen results by gene.

7   Tab 5: comparison of genome-wide and validation screens. Results by gene. Tab 6:

8   SgRNA library used for the validation screen. Legend Tab 1-6: logFC = $\log_2$ fold change

9   between groups; logFC.genotype.unspecific: *GFP_5xT71BS* day 8 unsorted vs *GFP_Ctrl*

10 day 8 unsorted. logFC.GFP.neg.control: *GFP_Ctrl* day 8 (GFP high) – *GFP_Ctrl* day 8

11 (GFP low). logFC.GFP.pos.control: *GFP_5xT71BS* day 8 (GFP high) – *GFP_5xT71BS*

12 day 8 (GFP low). logFC.GFP.genotypeControlled: logFC.GFP.pos.control -

13 │logFC.genotype.unspecific│. logFC.GFP.pathwayControlled: logFC.GFP.pos.control -

14 logFC.GFP.neg.control. score.up: z-score of logFC.GFP.genotypeControlled and

15 logFC.GFP.pathwayControlled.   score.down: negative   z-score   of

16 logFC.GFP.genotypeControlled and logFC.GFP.pathwayControlled. p.value = two-sided

17 *P*-value; FDR = Benjamini Hochberg adjusted *P*-value). Tab 7, 8: Raw read counts for

18 each sgRNA in genome-wide (Tab 7), and validation (Tab 8) sgRNA screens. Legend

19 Tab 7, 8:   column 'sample_type': mESCs = count data generated from sequencing

20 screened mESCs, plasmid = count data generated from sequencing input sgRNA library;

21 column 'genotype': genotype of mESCs; column 'sorting_status': sorted_GFP_high =

22 25% high GFP FACS-sorted mESCs, sorted_GFP_low = 25% low GFP FACS-sorted

23 mESCs, unsorted = unsorted mESCs; column 'timepoint': day_8 = DNA extraction at day

24 8; day_4 = DNA extraction at day 4.

25

1 **Supplemental Table S2. Mass spectrometry results. Related to Figure 3a-c and**
2 **Supplemental Figure S4A-E, Supplemental Figure S4C, D.**
3 Legend: Protein.IDs: UniProt protein IDs, Protein.names: Protein names, Gene.names:
4 Gene names, logFC: Log2 fold change, AveExpr: Average expression, P.Value: two-
5 sided P-value (moderated t-test), adj.P.Val: Benjamini Hochberg adjusted P-value,
6 mlog10p: $-\log_{10}$(adj.P.val), iBAQ.avg: average IBAQ value, iBAQ.sd: standard deviation
7 IBAQ value.
8
9
10 **Supplemental Table S3. RNA-seq and RIP-seq results. Related to Figure 5-7,**
11 **Supplemental Figure S5-7.**
12 Legend: LFC, $\log_2$ fold change; FDR, Benjamini Hochberg adjusted *P*-value. Blue

13 columns: Differential gene expression analysis with EdgeR of $Trim71^{-/-}$ vs *WT* mESCs

14 (Trim71_KO_vs_WT), $Ago2^{-/-}$ vs *WT* mESCs (AGO2_KO_vs_WT), $Upf1^{-/-}$ vs *WT* mESCs

15 (UPF1_KO_vs_WT), and $T6B_{WT}$ vs $T6B_{MUT}$ mESCs (T6B_WT_vs_MUT; *n* = 3 biological

16 replicates). Yellow column: Trim71.CRAC.enrichment.vs.RNA: Whole transcript CRAC

17 enrichment. **Data source:** (Welte et al., 2019). Orange column: Ago2_CLIP_peaks: Ago2

18 CLIP peaks per gene. Ago2_CLIP_enrichment: Sum of Ago2 CLIP peaks per gene. **Data**

19 **source:** (Li et al., 2020). Green columns: RIP-seq results: *n* = 4 independent experiments,

20 3 replicates per experiment: RIP_1, RIP_2, RIP_3&4. LFC_IP-enrichment HA-Tnrc6a:

21 $\log_2$(IP vs input [Tnrc6a_IP_input]). Dependent_Tnrc6a_IP_input: TRUE, if

22 FDR_Tnrc6a_IP_input ≤ 0.01. LFC_Tnrc6a_RIP_enr.change_Trim71_KO_vs_WT:

23 $\log_2$(enrichment difference of HA-Tnrc6a IP vs input in $Trim71^{-/-}$ vs WT mESCs).

24 Dependent_enr.change_Trim71_KO_vs_WT: TRUE, if

25 FDR_Tnrc6a_RIP_enr.change_Trim71_KO_vs_WT ≤ 0.01.

26 LFC_Tnrc6a_RIP_enr.change_Ago2_KO_vs_WT: $\log_2$(enrichment difference of HA-

27 Tnrc6a IP vs input in $Ago2^{-/-}$ vs WT mESCs). Dependent_enr.change_Ago2_vs_WT:

28 TRUE, if FDR_Tnrc6a_RIP_enr.change_Ago2_KO_vs_WT ≤ 0.01.

29 LFC_Tnrc6a_RIP_enr.change_Upf1_KO_vs_WT: $\log_2$(enrichment difference of HA-

1   Tnrc6a IP vs input in Upf1$^{-/-}$ vs WT mESCs). Dependent_enr.change_Upf1_KO_vs_WT:

2   TRUE,   if   FDR_Tnrc6a_RIP_enr.change_Upf1_KO_vs_WT   ≤   0.05.

3   target_to_pathway_TRIM71_AGO2:   none,

4   RIP_1_dependent_enr.change_Trim71_KO_vs_WT   *and*

5   RIP_2_dependent_enr.change_Ago2_KO_vs_WT   FALSE.   Trim71-only:

6   RIP_1_dependent_enr.change_Trim71_KO_vs_WT: TRUE   *and*

7   RIP_2_dependent_enr.change_Ago2_KO_vs_WT: FALSE.   Ago2-only:

8   RIP_2_dependent_enr.change_Ago2_KO_vs_WT: TRUE   *and*

9   RIP_1_dependent_enr.change_Trim71_KO_vs_WT: FALSE.   Common:

10 RIP_1_dependent_enr.change_Trim71_KO_vs_WT   *and*

11 RIP_2_dependent_enr.change_Ago2_KO_vs_WT   TRUE.

12 target_to_pathway_UPF1_AGO2: none, RIP_dependent_enr.change_Upf1_KO_vs_WT

13 *and*   RIP_2_dependent_enr.change_Ago2_KO_vs_WT   FALSE.   Upf1-only:

14 RIP_3&4_dependent_enr.change_Upf1_KO_vs_WT: TRUE   *and*

15 RIP_2_dependent_enr.change_Ago2_KO_vs_WT: FALSE.   Ago2-only:

16 RIP_2_dependent_enr.change_Ago2_KO_vs_WT: TRUE   *and*

17 RIP_3&4_dependent_enr.change_Upf1_KO_vs_WT: FALSE.   Common:

18 RIP_3&4_dependent_enr.change_Upf1_KO_vs_WT   *and*

19 RIP_2_dependent_enr.change_Ago2_KO_vs_WT TRUE.

20

21

22 **Supplemental Table S4. sgRNA sequences and ssODNs. Asterisks in ssODN**

23 **sequences indicate phosporothioate bonds.**

Gene/ locus	Purpose	Name	Target Sequence	Source
Trim71	Deletion *Trim71*	TRIM71_Nterm_sgRNA TRIM71_RING_sgRNA1 TRIM71_RING_sgRNA2	CCGGGAACGAAGCCATTTGC ACTTCCAGATCTGCCTGCTG CTGCTGTGCAAGGAGATGTG	(Welte et al., 2019)
Ago2	Deletion *Ago2*	Ago2_sgRNA1 Ago2_sgRNA2 Ago2_sgRNA3 Ago2_sgRNA4	AAGGTGGAGATAACGCACTG CTTTAAAACTCAGATCTTCG CCTGTCCGACTTGTAAACAC CGTTACACGATGCACTTTCG	Addgene #73633 sgRNA library
Dicer1	Deletion *Dicer1*	Dicer1_sgRNA1 Dicer1_sgRNA2 Dicer1_sgRNA3 Dicer1_sgRNA4	TGGAAAGTTGTTCCATTCAA CTCACGCATGGCATCTTACA AGAGCTGGACTTACATGACG AGGTACGTATTACTCAGTAG	(Doench et al., 2016)
Xpo5	Deletion *Xpo5*	Xpo5_sgRNA1 Xpo5_sgRNA2 Xpo5_sgRNA3 Xpo5_sgRNA4	TCTAGCCGGCTACATTGACT AGAGCGCTGAGACATTAGTG GTGGTGGGCTACACACCCAG AAGGCCAAAATGTCTGACGA	
Upf1	Deletion *Upf1*	Upf1_sgRNA1 Upf1_sgRNA2	AGGTGAGTGTTTGCGAGCTG CACTTGTGCGTCGAGCTGGC	this study
Tnrc6a	*Tnrc6a* N-terminal HA-Tag	Tnrc6a_sgRNA_Nterm ssODN_Tnrc6a_HAAVI	TAGTGCACTTTACACACATG G*C*TTGAGGCTCGCGAGCCTCGTTCCCCGCGCCTCA CGCGCTAGTGCACTTTACACACATGTACCCATACGAT GTTCCAGATTACGCTGCTGGCCTGAACGACATCTTCG AGGCTCAGAAAATCGAATGGCACGAAGGTCCTAGGTG AGCGGACCGGAGGGGAGGCTCGCTCGGGGGGCCAG GAGCCAGCCTCCGGCGC*T*G	this study

1
2
3
4
5
6
7

Supplemental Table S5. Cell lines.

Cell line No.	Genotype	Description	Source
1	mES (129xC57BL/6) *Rosa26*$^{Cre-ERT2/BirA-V5}$	Untagged control cell line for Trim71-immunoprecipitations	(Ostapcuk et al., 2018)
4	mES (129xC57BL/6) *Rosa26*$^{Cre-ERT2/BirA-V5}$ *Trim71*$^{FlagAvi/FlagAvi}$	N terminal 3xFLAG-AVI-tagged *Trim71*	(Welte et al., 2019)
20	mES (V6.5), *Ago2*$^{Halo-LSL/+}$	N-terminal FLAG-tagged *Ago2*	(Li et al., 2020)
21	mES (129S6/SvEvTac)	Parental cell line for Cas9 integration	(Lienert et al., 2011)
22	mES (129S6/SvEvTac), stable transfection *Cas9::T2A::Blasticidin*	Overexpression of *Cas9*, parental cell line for GFP reporter gene integration	this study
23	mES (129S6/SvEvTac), *yGlob (GFP_Ctrl),* stable transfection *Cas9::T2A::Blasticidin*	Overexpression of *Cas9*, overexpression of *GFP_Ctrl*	this study
24	mES (129S6/SvEvTac), *yGlob (GFP_5xT71BS),* stable transfection *Cas9::T2A::Blasticidin*	Overexpression of *Cas9*, overexpression of *GFP_5xT71BS*	this study
25	mES (129S6/SvEvTac), *yGlob (GFP_Ctrl), Trim71*$^{-/-}$, stable transfection *Cas9::T2A::Blasticidin*	Overexpression of *Cas9*, overexpression of *GFP_Ctrl,* deletion of Trim71	this study
26	mES (129S6/SvEvTac), *yGlob (GFP_5xT71BS), Trim71*$^{-/-}$, stable transfection *Cas9::T2A::Blasticidin*	Overexpression of *Cas9*, overexpression of *GFP_5xT71BS*, deletion of *Trim71*	this study
27	mES (129S6/SvEvTac), *yGlob (GFP_5xT71BS),* Ago2$^{-/-}$, stable transfection *Cas9::T2A::Blasticidin*	Overexpression of *Cas9*, overexpression of *GFP_5xT71BS*, Deletion of *Ago2*	this study
28	mES (129S6/SvEvTac), *yGlob (GFP_5xT71BS), Dicer1*$^{-/-}$, stable transfection *Cas9::T2A::Blasticidin*	Overexpression of *Cas9*, overexpression of *GFP_5xT71BS*, deletion of *Dicer1*	this study
29	mES (129S6/SvEvTac), *yGlob (GFP_5xT71BS),* Xpo5$^{-/-}$,	Overexpression of *Cas9*, overexpression of *GFP_5xT71BS*,	this study

	stable transfection *Cas9::T2A::Blasticidin*	deletion of *Xpo5*	
34	mES (129S6/SvEvTac)*, yGlob (GFP_5xT71BS), HA-AVI-Tnrc6a,* stable transfection *Cas9::T2A::Blasticidin*	Overexpression of *Cas9*, overexpression of *GFP_5xT71BS*, N-terminal HA-AVI-tag of *Tnrc6a*	this study
35	mES (129S6/SvEvTac)*, yGlob (GFP_5xT71BS), HA-AVI-Tnrc6a, Trim71*^{-/-}, stable transfection *Cas9::T2A::Blasticidin*	Overexpression of *Cas9*, overexpression of *GFP_5xT71BS*, N-terminal HA-AVI-tag of *Tnrc6a*, deletion of *Trim71*	this study
36	mES (129S6/SvEvTac)*, yGlob (GFP_5xT71BS), HA-AVI-Tnrc6a, Ago2*^{-/-}, stable transfection *Cas9::T2A::Blasticidin*	Overexpression of *Cas9*, overexpression of *GFP_5xT71BS*, N-terminal HA-AVI-tag of *Tnrc6a*, deletion of *Ago2*	this study
37	mES (129S6/SvEvTac)*, yGlob (GFP_5xT71BS),* stable transfection *FH-T6B$_{WT}$::mCherry*, stable transfection *Cas9::T2A::Blasticidin*	Overexpression of *Cas9*, overexpression of *GFP_5xT71BS*, Overexpression of *FH-T6B$_{WT}$::mCherry*	this study
38	mES (129S6/SvEvTac)*, yGlob (GFP_5xT71BS),* stable transfection *FH-T6B$_{MUT}$::mCherry*, stable transfection *Cas9::T2A::Blasticidin*	Overexpression of *Cas9*, overexpression of *GFP_5xT71BS*, Overexpression of *FH-T6B$_{MUT}$::mCherry*	this study
39	mES (129S6/SvEvTac)*, yGlob (GFP_5xT71BS), HA-AVI-Tnrc6a, Upf1*^{-/-}, stable transfection *Cas9::T2A::Blasticidin*	Overexpression of *Cas9*, overexpression of *GFP_5xT71BS*, N-terminal HA-AVI-tag of *Tnrc6a*, deletion of *Upf1*	this study

1
2
3
4
5
6
7
8
9

Supplemental Table S6A. Overexpression plasmids.

Name	Backbone	Resistence	Insert	Backbone reference	Insert reference	Primers used
pTW71	pC2P	AMP	*Cas9::BSD*	pTW42 (Welte et al., 2019)	pEF1-B; Matyas Flemr, Marc Bühler	225-228
pTW97	pL1_1L	AMP	*GFP_Ctrl* (*EGFP::unc-54* 3'UTR)	pL1_1L; (Lienert et al., 2011)	pTW47; (Welte et al., 2019)	406, 407
pTW98	pL1_1L	AMP	*GFP_5xT71BS* (*EGFP::mab-10$_{condensed}$*)	pL1_1L; (Lienert et al., 2011)	pTW48; (Welte et al., 2019)	406, 407
pTW110	pCIP	AMP	*mmuAgo2 IRES2 Puro*	Addgene #79009 (Young et al., 2016)	Addgene #73538 (Ngondo et al., 2018)	745, 746
pTW111	pCIP	AMP	*HsTNRC6A IRES2 Puro*	Addgene #79009 (Young et al., 2016)	Addgene #19883 (Landthaler et al., 2008)	747, 748
pTW112	pCIP	AMP	*HsTNRC6B IRES2 Puro*	Addgene #79009 (Young et al., 2016)	Addgene #10979 (Meister et al., 2005)	747, 750, 780, 781
pTW113	pCIP	AMP	*HsTNRC6C IRES2 Puro*	Addgene #79009 (Young et al., 2016)	Addgene #19885 (Landthaler et al., 2008)	751, 752
pTW114	pCIP	AMP	*FH_T6B$_{WT}$ ::mCherry IRES2 Puro*	Addgene #79009	pIRESneo FLAG/HA-T6B_WT-	764, 765, 768, 769

77

				(Young et al., 2016)	eYFP; (Hauptmann et al., 2015) ; pTW51; (Welte et al., 2019)	
pTW115	pCIP	AMP	*FH_T6B~MUT::~mCherry IRES2 Puro*	Addgene #79009 (Young et al., 2016)	pIRESneo FLAG/HA-T6B_MUT-eYFP; (Hauptmann et al., 2015); pTW51; (Welte et al., 2019)	764, 765, 768, 769

1
2
3
4
5
6
7
8
9
10
11
12
13
14
15

Supplemental Table S6B. Luciferase reporter gene constructs.

name	backbone	resistence	insert	Reference	insert reference	used primers
pTW1	psiCHECK-2	AMP	*unc-54* 3' UTR ('*Ctrl*' 3'UTR **Figure 2B**)	(Welte et al., 2019)	see reference	see reference
pTW5	psiCHECK-2	AMP	*Pou5f1* 3' UTR	(Welte et al., 2019)	see reference	see reference
pTW6	psiCHECK-2	AMP	*unc-54::mab-10~condensed~* ('*5xT71BS*' 3'UTR **Figure 2B**)	(Welte et al., 2019)	see reference	see reference
pTW7	psiCHECK-2	AMP	*Mbnl1* 3' UTR	(Welte et al., 2019)	see reference	see reference
pTW8	psiCHECK-2	AMP	*Plxnb2* 3' UTR	(Welte et al., 2019)	see reference	see reference
pTW9	psiCHECK-2	AMP	*Mllt1* 3' UTR	(Welte et al., 2019)	see reference	see reference
pTW22	psiCHECK-2	AMP	*Mbnl1 3UTR deletion CRAC stretch1*	(Welte et al., 2019)	see reference	see reference
pTW26	psiCHECK-2	AMP	*Pou5f1::Mbnl1 narrow stretch*	(Welte et al., 2019)	see reference	see reference
pTW132	psiCHECK-2	AMP	*Abcd3* 3'UTR	this study	genomic DNA	816, 817
pTW133	psiCHECK-2	AMP	*Nt5cd3* 3'UTR	this study	genomic DNA	814, 815
pTW134	psiCHECK-2	AMP	*Spty2d1* 3'UTR	this study	genomic DNA	818, 819
pTW135	psiCHECK-2	AMP	*Ankib1* 3'UTR	this study	genomic DNA	888, 889
pTW136	psiCHECK-2	AMP	*Hars2* 3'UTR	this study	genomic DNA	898, 899
pTW137	psiCHECK-2	AMP	*St3gal4* 3'UTR	this study	genomic DNA	902, 903
pTW138	psiCHECK-2	AMP	*Ier5* 3'UTR	this study	genomic DNA	904, 905
pTW139	psiCHECK-2	AMP	*Erbb3* 3'UTR	this study	genomic DNA	890, 891
pTW140	psiCHECK-2	AMP	*Serpinb9b* 3'UTR	this study	genomic DNA	918, 919
pTW141	psiCHECK-2	AMP	*Rnase4* 3'UTR	this study	genomic DNA	920, 921

16
17

1 **Supplemental Table S7A Genotyping primers.**

Cell line	Orientation	Primer ID	Sequence	Description
mES (129S6/SvEvTac), *yGlob (GFP_5xT71BS), HA-AVI-Tnrc6a,* stable transfection *Cas9::T2A::Blasticidin*	For	772	GGCCTAGTTGCTAGGACCTCCATC	*Tnrc6a* Nterm HA-AVI-tag genotyping
	Rev	773	GCCGGAGGCTGGCTCCT	
	Rev_insert	774	AGGACCTTCGTGCCATTCGA	
mES (129S6/SvEvTac), *yGlob (GFP_5xT71BS), HA-AVI-Tnrc6a, Upf1$^{-/-}$,* stable transfection *Cas9::T2A::Blasticidin*	UPF1_GT_F	961	GGCAACTCAGAGCTCAGAACCG	*Upf1* deletion genotyping
	UPF1_GT_R	962	GCAGGTAGACCTGGAAGAGGTAGTTG	
	UPF1_GT_insert_R	963	GGGTGAAGTCGGTGAATTCGAACTC	

2
3
4
5
6
7
8
9
10
11
12
13
14
15
16
17
18
19
20 **Supplemental Table S7B. Primers for cloning of overexpression constructs.**

Name	Orienta-tion	Primer ID	Sequence	Description
BSDII	For	225	GGAGGAGAACCCTGGACCTACTAGTGCCAAGCCTTTGTCTCAAGAAGAATCC	Amplification of BSD from pEF1-B for creation of pTW71
BSDII	Rev	226	GAGCTCTAGGAATTTATCGATTAGCCCTCCCACACATAACCAGAG	
BGHPA	For	227	CGATAAATTCCTAGAGCTCGCTGATCAGC	Amplification BGHPA from pTW71 for creation of pTW71
BGHPA	Rev	228	CACTAGGGGTTCCTGCGGCC	
Reporter_re_clone_3	For	406	TGATTACTATTAATAACTAGTCAATAATCAATGTCGAGGCCGCCACCGGGATATCGATATTTAAATGCTCATCATT	Amplification of *CAG-GFP::unc54* (from pTW47)/*CAG-GFP::unc54::mab10$_{condensed}$* (pTW48) for creation of pTW97 and pTW98
Reporter_re_clone_3	Rev	407	CTTGGATCCCTCGAGTTAATGGGACGCGTATTTAAATTCATCATT	
pCIP_mmuAgo2	For	745	GCTAGCGCCATCAGCAATTGCCACCATGTACCCATACGA	Amplification of *mmuAgo2* for creation of pTW110
pCIP_mmuAgo2	Rev	746	AACTCGATCTAGATCGGATCTCAAGCAAAGTACATGGTGC	
pCIP_HsTnrc6a	For	747	GCTAGCGCCATCAGCAATTGCCACCATGGACTACAAGGACGACG	Amplification of HsTNRC6A and HsTNRC6B for creation of pTW111 and pTW112
pCIP_HsTnrc6a	Rev	748	AACTCGATCTAGATCGGATCTTACATGGACTCTCCACCC	Amplification of HsTNRC6A for creation of pTW111
pCIP_HsTnrc6b	Rev	750	AACTCGATCTAGATCGGATCTCAGATTGAATCCGACCC	Amplification of HsTNRC6A for creation of pTW112
pCIP_HsTnrc6c	For	751	GCTAGCGCCATCAGCAATTGCCACCATGGACTACAAGG	Amplification of HsTNRC6C for creation of pTW113

79

pCIP_HsTnrc6c	Rev	752	AACTCGATCTAGATCGGATCCTACAGGGACTCCCCG	
pCIP_Tnrc6b_FH	For	780	CAGGCTCCACCATGGGAACCAGAGAGAAGGAGCAAGAAAG	Amplification of FH-tag for creation of pTW112
pCIP_Tnrc6b_FH	Rev	781	GGTTCCCATGGTGGAGCCTGCTTTTTTG	
pCIP_FH-T6B-eYFP	For	764	GCTAGCGCCATCAGCAATTGATGGACTACAAGGACGAC	Amplification of FH-T6B$_{WT}$ and FH-T6B$_{MUT}$ for creation of pTW114 and pTW115
pCIP_FH-T6B-eYFP	Rev	765	AACTCGATCTAGATCGGATCTTAAAGCTTCTTGTACAGCTC	
pCIP_FH-T6B-mCherry	For	768	GGGGGAGCTCGTCGCCACCGGATCCGTGAGCAAGGGCGAG	Amplification of *mCherry* for creation of pTW114 and pTW115
pCIP_FH-T6B-mCherry	Rev	769	GGGGGGGGGCGGAATTCTTATTACTTGTACAGCTCGTCCAT	Amplification of *mCherry* for creation of pTW114, pTW115

1
2
3
4
5
6
7
8
9
10
11
12
13
14
15
16
17

18 **Supplemental Table S7C. Primers for cloning of luciferase reporter gene**
19 **constructs.**

Name	Orientation	Primer ID	Sequence	Description
Abcd3_3_UTR	For	816	AATTCGTTTAAACCTAGAGCAGACCATCTCAAGAACTTCAT	Amplification of *Abcd3* 3'UTR from genomic DNA
	Rev	817	TTTTATTGCGGCCAGCGGCCTGCCTAGAAATATAAAACAAAATCTTT	
Nt5dc3_3_UTR	For	814	AATTCGTTTAAACCTAGAGCTCCTGTGTTTGCCTGAG	Amplification of *Nt5dc3* 3' UTR from genomic DNA
	Rev	815	TTTTATTGCGGCCAGCGGCCCCCAGGAGATACAACTCAAGC	
Spty2d1_3_UTR	For	818	AATTCGTTTAAACCTAGAGCCTGCTGCTACTGTAGATTCT	Amplification of *Spty2dl1* 3' UTR from genomic DNA
	Rev	819	TTTTATTGCGGCCAGCGGCCTATCAATAAAATATTTTAATGCCTACAATT	
Erbb3_3_UTR	For	890	TTTTATTGCGGCCAGCGGCCAACAAAAAAACTCTGACATT	Amplification of *Erbb3* 3' UTR from genomic DNA
	Rev	891	AATTCGTTTAAACCTAGAGCCCTCGGTTCCTTGAGA	
Ankib1_3_UTR	For	888	TTTTATTGCGGCCAGCGGCCGGTGTGAAGCACGACATTT	Amplification of *Ankib1* 3' UTR from genomic DNA
	Rev	889	AATTCGTTTAAACCTAGAGCACTGCACACATTTGCTCTC	
Hars2_3_UTR	For	898	AATTCGTTTAAACCTAGAGCTTAGTGCCTGATTTCCATCTG	Amplification of *Hars2* 3' UTR from genomic DNA

	Rev	899	TTTTATTGCGGCCAGCGGCCTTTTG TTTTGTTTTGTTTTATTGAGAGA	
Zfp317_3_UTR	For	900	AATTCGTTTAAACCTAGAGCGTCTT CCATGACCTTCCATG	Amplification of *Zfp317* 3' UTR from genomic DNA
	Rev	901	TTTTATTGCGGCCAGCGGCCTAAT CTTGTAATCAATTTTATTGTTTTCTC A	
St3gal4_3_UTR	For	902	AATTCGTTTAAACCTAGAGCCTTGG ATGGGAGCTGTAA	Amplification of *St3gal4* 3' UTR from genomic DNA
	Rev	903	TTTTATTGCGGCCAGCGGCCTTCC ATTTTAGAAAAAAAAATATTTTAATG G	
Ier5_3_UTR	For	904	AATTCGTTTAAACCTAGAGCGCCCC CGGGACC	Amplification of *Ier5* 3' UTR from genomic DNA
	Rev	905	TTTTATTGCGGCCAGCGGCCTAAC AATCTGATTAAAGCATGTTTT	
Serpinb9b_3_U TR	For	918	AATTCGTTTAAACCTAGAGCAGGCA CATTACTATGTGG	Amplification of *Serpinb9b* 3' UTR from genomic DNA
	Rev	919	TTTTATTGCGGCCAGCGGCCACCA TTCCACATATGGAATT	
Rnase4_3_UTR	For	920	AATTCGTTTAAACCTAGAGCATGCT GTCCTGCAGCTG	Amplification of *Rnase4* 3' UTR from genomic DNA
	Rev	921	TTTTATTGCGGCCAGCGGCCCAGA TGGCTCAACATACAGC	

1

Supplemental Table S8. qPCR Primers.

Target	Orientation	Primer ID	Sequence	Description
Gapdh	For	43	AAGGTCATCCCAGAGCTGAA	qPCR *Gapdh*
	Rev	44	CTGCTTCACCACCTTCTTGA	
Plxnb2	For	333	CTAGACATCCCTGAGTCACG	qPCR *Plxnb2*
	Rev	334	AGTCAGCAGTGATGCAAAGT	
Mllt1	For	345	GGCTCCAAGGATGCCAACAAG	qPCR *Mllt1*
	Rev	346	GACAGGCTCTCCAGCTTGGT	
Mbnl1	For	278	CACTGAAAGGTCGTTGCTCCA	qPCR *Mbnl1*
	Rev	279	CGCCCATTTATCTCTAACTGTGT	
Pou5f1	For	n.a.	GTTGGAGAAGGTGGAACCAA	qPCR *Pou5f1*
	Rev	n.a.	CTCCTTCTGCAGGGCTTTC	

3
4

Supplemental Table S9. Antibodies for Western Blotting.

Antibody	Dilution	Incubation	Company	Catalog No.
α-TRIM71	1:500	4 °C overnight	R&D Systems	AF5104
α-Sheep-HRP	1:5,000	1h room temperature	Abcam	ab97130
α-Tubulin	1:10,000	1h room temperature	Abcam	ab6160
α-Rat-HRP	1:15,000	1h room temperature	Jackson ImmunoResearch	112035175
α-AGO2	1:1,000	1h room temperature	Abcam	ab156870
α-DICER1	1:1,000	1h room temperature	Abcam	ab227518
α-XPO5	1:1,000	1h room temperature	Abcam	ab168844
α-HA	1:500	1h room temperature	MerckMillipore	11867423001
α-Rabbit-HRP	1:5,000	1h room temperature	GE Healthcare	LNA934V
α-FLAG-HRP	1:500	1h room temperature	Sigma	A8592
α-UPF1	1:2,000	1h room temperature	Abcam	ab86057

6
7

Supplemental References

Aeschimann, F., Neagu, A., Rausch, M., and Grosshans, H. (2019). let-7 coordinates the transition to adulthood through a single primary and four secondary targets. Life Sci Alliance *2*.

81

Baillat, D., and Shiekhattar, R. (2009). Functional dissection of the human TNRC6 (GW182-related) family of proteins. Mol Cell Biol *29*, 4144-4155.

Boroviak, T., Stirparo, G.G., Dietmann, S., Hernando-Herraez, I., Mohammed, H., Reik, W., Smith, A., Sasaki, E., Nichols, J., and Bertone, P. (2018). Single cell transcriptome analysis of human, marmoset and mouse embryos reveals common and divergent features of preimplantation development. Development *145*, dev167833.

Braun, J.E., Huntzinger, E., Fauser, M., and Izaurralde, E. (2011). GW182 proteins directly recruit cytoplasmic deadenylase complexes to miRNA targets. Mol Cell *44*, 120-133.

Braun, J.E., Huntzinger, E., and Izaurralde, E. (2013). The role of GW182 proteins in miRNA-mediated gene silencing. Adv Exp Med Biol *768*, 147-163.

Broderick, J.A., Salomon, W.E., Ryder, S.P., Aronin, N., and Zamore, P.D. (2011). Argonaute protein identity and pairing geometry determine cooperativity in mammalian RNA silencing. RNA *17*, 1858-1869.

Brodsky, R.A. (2009). How I treat paroxysmal nocturnal hemoglobinuria. Blood *113*, 6522-6527.

Cerro-Herreros, E., Sabater-Arcis, M., Fernandez-Costa, J.M., Moreno, N., Perez-Alonso, M., Llamusi, B., and Artero, R. (2018). miR-23b and miR-218 silencing increase Muscleblind-like expression and alleviate myotonic dystrophy phenotypes in mammalian models. Nat Commun *9*, 2482.

Chang, H.M., Martinez, N.J., Thornton, J.E., Hagan, J.P., Nguyen, K.D., and Gregory, R.I. (2012). Trim71 cooperates with microRNAs to repress Cdkn1a expression and promote embryonic stem cell proliferation. Nat Commun *3*, 923.

Chekulaeva, M., Mathys, H., Zipprich, J.T., Attig, J., Colic, M., Parker, R., and Filipowicz, W. (2011). miRNA repression involves GW182-mediated recruitment of CCR4–NOT through conserved W-containing motifs. Nat Struct Mol Biol *18*, 1218-1226.

Chen, C.Y.A., Zheng, D.H., Xia, Z.F., and Shyu, A.B. (2009). Ago-TNRC6 triggers microRNA-mediated decay by promoting two deadenylation steps. Nat Struct Mol Biol *16*, 1160-U1166.

Chen, J., Lai, F., and Niswander, L. (2012). The ubiquitin ligase mLin41 temporally promotes neural progenitor cell maintenance through FGF signaling. Genes Dev *26*, 803-815.

Chen, X., Castro, S.A., Liu, Q., Hu, W., and Zhang, S. (2019). Practical considerations on performing and analyzing CLIP-seq experiments to identify transcriptomic-wide RNA-protein interactions. Methods *155*, 49-57.

Cho, H., Park, O.H., Park, J., Ryu, I., Kim, J., Ko, J., and Kim, Y.K. (2015). Glucocorticoid receptor interacts with PNRC2 in a ligand-dependent manner to recruit UPF1 for rapid mRNA degradation. Proc Natl Acad Sci U S A *112*, E1540-1549.

Choe, J., Ahn, S.H., and Kim, Y.K. (2014). The mRNP remodeling mediated by UPF1 promotes rapid degradation of replication-dependent histone mRNA. Nucleic Acids Res *42*, 9334-9349.

Cox, J., Hein, M.Y., Luber, C.A., Paron, I., Nagaraj, N., and Mann, M. (2014). Accurate proteome-wide label-free quantification by delayed normalization and maximal peptide ratio extraction, termed MaxLFQ. Mol Cell Proteomics *13*, 2513-2526.

Cox, J., Neuhauser, N., Michalski, A., Scheltema, R.A., Olsen, J.V., and Mann, M. (2011). Andromeda: A Peptide Search Engine Integrated into the MaxQuant Environment. J Proteome Res *10*, 1794-1805.

de la Mata, M., Gaidatzis, D., Vitanescu, M., Stadler, M.B., Wentzel, C., Scheiffele, P., Filipowicz, W., and Grosshans, H. (2015). Potent degradation of neuronal miRNAs induced by highly complementary targets. EMBO Rep *16*, 500-511.

Ding, L., and Han, M. (2007). GW182 family proteins are crucial for microRNA-mediated gene silencing. Trends Cell Biol *17*, 411-416.

Doench, J.G., Fusi, N., Sullender, M., Hegde, M., Vaimberg, E.W., Donovan, K.F., Smith, I., Tothova, Z., Wilen, C., Orchard, R.*, et al.* (2016). Optimized sgRNA design to maximize activity and minimize off-target effects of CRISPR-Cas9. Nat Biotechnol *34*, 184-191.

Duy, P.Q., Weise, S.C., Marini, C., Li, X.J., Liang, D., Dahl, P.J., Ma, S., Spajic, A., Dong, W., Juusola, J., *et al.* (2022). Impaired neurogenesis alters brain biomechanics in a neuroprogenitor-based genetic subtype of congenital hydrocephalus. Nat Neurosci *25*, 458-473.

Ecsedi, M., and Grosshans, H. (2013). LIN-41/TRIM71: emancipation of a miRNA target. Genes Dev *27*, 581-589.

Ecsedi, M., Rausch, M., and Grosshans, H. (2015). The let-7 microRNA directs vulval development through a single target. Dev Cell *32*, 335-344.

Elbarbary, R.A., Miyoshi, K., Hedaya, O., Myers, J.R., and Maquat, L.E. (2017). UPF1 helicase promotes TSN-mediated miRNA decay. Genes Dev *31*, 1483-1493.

Elkayam, E., Faehnle, C.R., Morales, M., Sun, J., Li, H., and Joshua-Tor, L. (2017). Multivalent Recruitment of Human Argonaute by GW182. Mol Cell *67*, 646-658 e643.

Eulalio, A., Huntzinger, E., and Izaurralde, E. (2008). GW182 interaction with Argonaute is essential for miRNA-mediated translational repression and mRNA decay. Nat Struct Mol Biol *15*, 346-353.

Frankish, A., Diekhans, M., Jungreis, I., Lagarde, J., Loveland, J.E., Mudge, J.M., Sisu, C., Wright, J.C., Armstrong, J., Barnes, I., *et al.* (2021). Gencode 2021. Nucleic Acids Res *49*, D916-D923.

Furey, C.G., Choi, J., Jin, S.C., Zeng, X., Timberlake, A.T., Nelson-Williams, C., Mansuri, M.S., Lu, Q., Duran, D., Panchagnula, S., *et al.* (2018). De Novo Mutation in Genes Regulating Neural Stem Cell Fate in Human Congenital Hydrocephalus. Neuron *99*, 302-314 e304.

Gaidatzis, D., Lerch, A., Hahne, F., and Stadler, M.B. (2015). QuasR: quantification and annotation of short reads in R. Bioinformatics *31*, 1130-1132.

Hauptmann, J., Schraivogel, D., Bruckmann, A., Manickavel, S., Jakob, L., Eichner, N., Pfaff, J., Urban, M., Sprunck, S., Hafner, M., *et al.* (2015). Biochemical isolation of Argonaute protein complexes by Ago-APP. Proc Natl Acad Sci U S A *112*, 11841-11845.

Hicks, J.A., Li, L., Matsui, M., Chu, Y., Volkov, O., Johnson, K.C., and Corey, D.R. (2017). Human GW182 Paralogs Are the Central Organizers for RNA-Mediated Control of Transcription. Cell Rep *20*, 1543-1552.

Hoepfner, D., McAllister, G., and Hoffman, G.R. (2019). CRISPR/Cas9-Based Chemogenomic Profiling in Mammalian Cells. Methods Mol Biol *1888*, 153-174.

Hubner, N.C., Bird, A.W., Cox, J., Splettstoesser, B., Bandilla, P., Poser, I., Hyman, A., and Mann, M. (2010). Quantitative proteomics combined with BAC TransgeneOmics reveals in vivo protein interactions. J Cell Biol *189*, 739-754.

Jakymiw, A., Lian, S., Eystathioy, T., Li, S., Satoh, M., Hamel, J.C., Fritzler, M.J., and Chan, E.K. (2005). Disruption of GW bodies impairs mammalian RNA interference. Nat Cell Biol *7*, 1267-1274.

Jin, S.C., Dong, W., Kundishora, A.J., Panchagnula, S., Moreno-De-Luca, A., Furey, C.G., Allocco, A.A., Walker, R.L., Nelson-Williams, C., Smith, H., *et al.* (2020). Exome sequencing implicates genetic disruption of prenatal neuro-gliogenesis in sporadic congenital hydrocephalus. Nat Med *26*, 1754-1765.

Johnson, S.T., Chu, Y., Liu, J., and Corey, D.R. (2021). Impact of scaffolding protein TNRC6 paralogs on gene expression and splicing. RNA *27*, 1004-1016.

Kaygun, H., and Marzluff, W.F. (2005). Regulated degradation of replication-dependent histone mRNAs requires both ATR and Upf1. Nat Struct Mol Biol *12*, 794-800.

Kim, Y.K., Furic, L., DesGroseillers, L., and Maquat, L.E. (2005). Mammalian Staufen1 recruits Upf1 to specific mRNA 3' UTRs so as to elicit mRNA decay. Cell *120*, 195-208.

Kim, Y.K., and Maquat, L.E. (2019). UPFront and center in RNA decay: UPF1 in nonsense-mediated mRNA decay and beyond. RNA *25*, 407-422.

Kumari, P., Aeschimann, F., Gaidatzis, D., Keusch, J.J., Ghosh, P., Neagu, A., Pachulska-Wieczorek, K., Bujnicki, J.M., Gut, H., Grosshans, H., *et al.* (2018). Evolutionary plasticity of the NHL domain underlies distinct solutions to RNA recognition. Nat Commun *9*, 1549.

Landthaler, M., Gaidatzis, D., Rothballer, A., Chen, P.Y., Soll, S.J., Dinic, L., Ojo, T., Hafner, M., Zavolan, M., and Tuschl, T. (2008). Molecular characterization of human Argonaute-containing ribonucleoprotein complexes and their bound target mRNAs. RNA *14*, 2580-2596.

Langmead, B., Trapnell, C., Pop, M., and Salzberg, S.L. (2009). Ultrafast and memory-efficient alignment of short DNA sequences to the human genome. Genome Biol *10*, R25.

Lavysh, D., and Neu-Yilik, G. (2020). UPF1-Mediated RNA Decay-Danse Macabre in a Cloud. Biomolecules *10*, 999.

Lawrence, M., Huber, W., Pages, H., Aboyoun, P., Carlson, M., Gentleman, R., Morgan, M.T., and Carey, V.J. (2013). Software for computing and annotating genomic ranges. PLoS Comput Biol *9*, e1003118.

Lazar, C. (2015). imputeLCMD: a collection of methods for left-censored missing data imputation. R package, version *2*.

Lazzaretti, D., Tournier, I., and Izaurralde, E. (2009). The C-terminal domains of human TNRC6A, TNRC6B, and TNRC6C silence bound transcripts independently of Argonaute proteins. RNA *15*, 1059-1066.

Li, X., Pritykin, Y., Concepcion, C.P., Lu, Y., La Rocca, G., Zhang, M., King, B., Cook, P.J., Au, Y.W., Popow, O.*, et al.* (2020). High-Resolution In Vivo Identification of miRNA Targets by Halo-Enhanced Ago2 Pull-Down. Mol Cell *79*, 167-179 e111.

Lian, S.L., Li, S., Abadal, G.X., Pauley, B.A., Fritzler, M.J., and Chan, E.K. (2009). The C-terminal half of human Ago2 binds to multiple GW-rich regions of GW182 and requires GW182 to mediate silencing. RNA *15*, 804-813.

Lienert, F., Wirbelauer, C., Som, I., Dean, A., Mohn, F., and Schubeler, D. (2011). Identification of genetic elements that autonomously determine DNA methylation states. Nat Genet *43*, 1091-U1078.

Lin, S., and Gregory, R.I. (2015). MicroRNA biogenesis pathways in cancer. Nat Rev Cancer *15*, 321-333.

Liu, J., Rivas, F.V., Wohlschlegel, J., Yates, J.R., 3rd, Parker, R., and Hannon, G.J. (2005). A role for the P-body component GW182 in microRNA function. Nat Cell Biol *7*, 1261-1266.

Liu, Q.Y., Chen, X.L., Novak, M.K., Zhang, S.J., and Hu, W.Q. (2021). Repressing Ago2 mRNA translation by Trim71 maintains pluripotency through inhibiting let-7 microRNAs. Elife *10*, e66288.

Liu, Z., Johnson, S.T., Zhang, Z., and Corey, D.R. (2019). Expression of TNRC6 (GW182) proteins Is not necessary for gene silencing by fully complementary RNA duplexes. Nucleic Acid Ther *29*, 323-334.

Loedige, I., Gaidatzis, D., Sack, R., Meister, G., and Filipowicz, W. (2013). The mammalian TRIM-NHL protein TRIM71/LIN-41 is a repressor of mRNA function. Nucleic Acids Res *41*, 518-532.

Lykke-Andersen, K., Gilchrist, M.J., Grabarek, J.B., Das, P., Miska, E., and Zernicka-Goetz, M. (2008). Maternal Argonaute 2 Is Essential for Early Mouse Development at the Maternal-Zygotic Transition. Mol Biol Cell *19*, 4383-4392.

Maller Schulman, B.R., Liang, X., Stahlhut, C., DelConte, C., Stefani, G., and Slack, F.J. (2008). The let-7 microRNA target gene, Mlin41/Trim71 is required for mouse embryonic survival and neural tube closure. Cell Cycle *7*, 3935-3942.

Martinez, N.J., and Gregory, R.I. (2013). Argonaute2 expression is post-transcriptionally coupled to microRNA abundance. RNA *19*, 605-612.

Mathys, H., Basquin, J., Ozgur, S., Czarnocki-Cieciura, M., Bonneau, F., Aartse, A., Dziembowski, A., Nowotny, M., Conti, E., and Filipowicz, W. (2014). Structural and biochemical insights to the role of the CCR4-NOT complex and DDX6 ATPase in microRNA repression. Mol Cell *54*, 751-765.

Meister, G., Landthaler, M., Peters, L., Chen, P.Y., Urlaub, H., Luhrmann, R., and Tuschl, T. (2005). Identification of novel argonaute-associated proteins. Curr Biol *15*, 2149-2155.

Michlits, G., Jude, J., Hinterndorfer, M., de Almeida, M., Vainorius, G., Hubmann, M., Neumann, T., Schleiffer, A., Burkard, T.R., Fellner, M.*, et al.* (2020). Multilayered VBC score predicts sgRNAs that efficiently generate loss-of-function alleles. Nat Methods *17*, 708-716.

1 Mino, T., Murakawa, Y., Fukao, A., Vandenbon, A., Wessels, H.H., Ori, D., Uehata, T., Tartey, S., Akira, S.,
2 Suzuki, Y., *et al.* (2015). Regnase-1 and Roquin Regulate a Common Element in Inflammatory mRNAs by
3 Spatiotemporally Distinct Mechanisms. Cell *161*, 1058-1073.
4 Mitschka, S., Ulas, T., Goller, T., Schneider, K., Egert, A., Mertens, J., Brustle, O., Schorle, H., Beyer, M.,
5 Klee, K., *et al.* (2015). Co-existence of intact stemness and priming of neural differentiation programs in
6 mES cells lacking Trim71. Sci Rep *5*, 11126.
7 Ngondo, R.P., Cirera-Salinas, D., Yu, J., Wischnewski, H., Bodak, M., Vandormael-Pournin, S., Geiselmann,
8 A., Wettstein, R., Luitz, J., Cohen-Tannoudji, M., *et al.* (2018). Argonaute 2 Is Required for Extra-
9 embryonic Endoderm Differentiation of Mouse Embryonic Stem Cells. Stem Cell Rep *10*, 461-476.
10 Ostapcuk, V., Mohn, F., Carl, S.H., Basters, A., Hess, D., Iesmantavicius, V., Lampersberger, L., Flemr, M.,
11 Pandey, A., Thoma, N.H., *et al.* (2018). Activity-dependent neuroprotective protein recruits HP1 and
12 CHD4 to control lineage-specifying genes. Nature *557*, 739-743.
13 Park, O.H., Park, J., Yu, M., An, H.T., Ko, J., and Kim, Y.K. (2016). Identification and molecular
14 characterization of cellular factors required for glucocorticoid receptor-mediated mRNA decay. Genes
15 Dev *30*, 2093-2105.
16 Perez-Riverol, Y., Bai, J., Bandla, C., Garcia-Seisdedos, D., Hewapathirana, S., Kamatchinathan, S., Kundu,
17 D.J., Prakash, A., Frericks-Zipper, A., Eisenacher, M., *et al.* (2022). The PRIDE database resources in 2022:
18 a hub for mass spectrometry-based proteomics evidences. Nucleic Acids Res *50*, D543-D552.
19 Ritchie, M.E., Phipson, B., Wu, D., Hu, Y., Law, C.W., Shi, W., and Smyth, G.K. (2015). limma powers
20 differential expression analyses for RNA-sequencing and microarray studies. Nucleic Acids Res *43*, e47.
21 Robinson, M.D., McCarthy, D.J., and Smyth, G.K. (2010). edgeR: a Bioconductor package for differential
22 expression analysis of digital gene expression data. Bioinformatics *26*, 139-140.
23 Rybak, A., Fuchs, H., Smirnova, L., Brandt, C., Pohl, E.E., Nitsch, R., and Wulczyn, F.G. (2008). A feedback
24 loop comprising lin-28 and let-7 controls pre-let-7 maturation during neural stem-cell commitment. Nat
25 Cell Biol *10*, 987-993.
26 Sheu-Gruttadauria, J., and MacRae, I.J. (2018). Phase Transitions in the Assembly and Function of Human
27 miRISC. Cell *173*, 946-957 e916.
28 Slack, F.J., Basson, M., Liu, Z., Ambros, V., Horvitz, H.R., and Ruvkun, G. (2000). The lin-41 RBCC gene acts
29 in the C. elegans heterochronic pathway between the let-7 regulatory RNA and the LIN-29 transcription
30 factor. Mol Cell *5*, 659-669.
31 Smibert, P., Yang, J.S., Azzam, G., Liu, J.L., and Lai, E.C. (2013). Homeostatic control of Argonaute stability
32 by microRNA availability. Nat Struct Mol Biol *20*, 789-795.
33 Smyth, G.K. (2004). Linear models and empirical bayes methods for assessing differential expression in
34 microarray experiments. Stat Appl Genet Mol Biol *3*, Article3.
35 Takimoto, K., Wakiyama, M., and Yokoyama, S. (2009). Mammalian GW182 contains multiple
36 Argonaute-binding sites and functions in microRNA-mediated translational repression. RNA *15*, 1078-
37 1089.
38 Torres-Fernández, L.A., Emich, J., Port, Y., Mitschka, S., Wöste, M., Schneider, S., Fietz, D., Oud, M.S., Di
39 Persio, S., and Neuhaus, N. (2021a). TRIM71 deficiency causes germ cell loss during mouse
40 embryogenesis and is associated with human male infertility. Front Cell Dev Biol *9*, 970.
41 Torres-Fernández, L.A., Jux, B., Bille, M., Port, Y., Schneider, K., Geyer, M., Mayer, G., and Kolanus, W.
42 (2019). The mRNA repressor TRIM71 cooperates with Nonsense-Mediated Decay factors to destabilize
43 the mRNA of CDKN1A/p21. Nucleic Acids Res *47*, 11861-11879.
44 Torres-Fernández, L.A., Mitschka, S., Ulas, T., Weise, S., Dahm, K., Becker, M., Händler, K., Beyer, M.,
45 Windhausen, J., and Schultze, J.L. (2021b). The stem cell–specific protein TRIM71 inhibits maturation
46 and activity of the prodifferentiation miRNA let-7 via two independent molecular mechanisms. RNA *27*,
47 805-828.

Treiber, T., Treiber, N., Plessmann, U., Harlander, S., Daiss, J.L., Eichner, N., Lehmann, G., Schall, K., Urlaub, H., and Meister, G. (2017). A Compendium of RNA-Binding Proteins that Regulate MicroRNA Biogenesis. Mol Cell *66*, 270-284 e213.

Vieira-Vieira, C.H., and Selbach, M. (2021). Opportunities and Challenges in Global Quantification of RNA-Protein Interaction via UV Cross-Linking. Front Mol Biosci *8*, 669939.

Wang, J., Lee, J.E., Riemondy, K., Yu, Y., Marquez, S.M., Lai, E.C., and Yi, R. (2020). XPO5 promotes primary miRNA processing independently of RanGTP. Nat Commun *11*, 1845.

Wang, L., Su, Y., Huang, C., Yin, Y., Chu, A., Knupp, A., and Tang, Y. (2019). NANOG and LIN28 dramatically improve human cell reprogramming by modulating LIN41 and canonical WNT activities. Biol Open *8*.

Welte, T., Tuck, A.C., Papasaikas, P., Carl, S.H., Flemr, M., Knuckles, P., Rankova, A., Buhler, M., and Grosshans, H. (2019). The RNA hairpin binder TRIM71 modulates alternative splicing by repressing MBNL1. Genes Dev *33*, 1221-1235.

Worringer, K.A., Rand, T.A., Hayashi, Y., Sami, S., Takahashi, K., Tanabe, K., Narita, M., Srivastava, D., and Yamanaka, S. (2014). The let-7/LIN-41 pathway regulates reprogramming to human induced pluripotent stem cells by controlling expression of prodifferentiation genes. Cell Stem Cell *14*, 40-52.

Yang, J.G., Madrid, T.S., Sevastopoulos, E., and Narlikar, G.J. (2006). The chromatin-remodeling enzyme ACF is an ATP-dependent DNA length sensor that regulates nucleosome spacing. Nat Struct Mol Biol *13*, 1078-1083.

Young, N.P., Kamireddy, A., Van Nostrand, J.L., Eichner, L.J., Shokhirev, M.N., Dayn, Y., and Shaw, R.J. (2016). AMPK governs lineage specification through Tfeb-dependent regulation of lysosomes. Gene Dev *30*, 535-552.

Zeng, H., Lu, B., Zamponi, R., Yang, Z., Wetzel, K., Loureiro, J., Mohammadi, S., Beibel, M., Bergling, S., and Reece-Hoyes, J. (2018). mTORC1 signaling suppresses Wnt/β-catenin signaling through DVL-dependent regulation of Wnt receptor FZD level. Proc Natl Acad Sci U S A *115*, E10362-E10369.

Zipprich, J.T., Bhattacharyya, S., Mathys, H., and Filipowicz, W. (2009). Importance of the C-terminal domain of the human GW182 protein TNRC6C for translational repression. RNA *15*, 781-793.